AFRL-AFOSR-UK-TR-2011-0057

Magnetic Nozzles for Plasma Thrusters: Acceleration, Thrust, and Detachment Mechanisms

Eduardo A. Ahedo

Universidad Politécnica de Madrid
Aeronautics Engineering School
ETSI Aeronauticos
Plaza Cardenal Cisneros
Madrid, Spain 28040

EOARD GRANT 10-3085

October 2011

Final Report for 25 August 2010 to 25 August 2011

Air Force Research Laboratory
Air Force Office of Scientific Research
European Office of Aerospace Research and Development
Unit 4515 Box 14, APO AE 09421

REPORT DOCUMENTATION PAGE

Form Approved OMB No. 0704-0188

1. REPORT DATE *(DD-MM-YYYY)*	2. REPORT TYPE	3. DATES COVERED *(From – To)*
06-10-2011	Final Report	25 August 2010 – 25 August 2011

4. TITLE AND SUBTITLE

Magnetic Nozzles for Plasma Thrusters: Acceleration, Thrust, and Detachment Mechanisms

5a. CONTRACT NUMBER

FA8655-10-1-3085

5b. GRANT NUMBER

Grant 10-3085

5c. PROGRAM ELEMENT NUMBER

6. AUTHOR(S)

Professor Eduardo A. Ahedo

5d. PROJECT NUMBER

5d. TASK NUMBER

5e. WORK UNIT NUMBER

7. PERFORMING ORGANIZATION NAME(S) AND ADDRESS(ES)

Universidad Politécnica de Madrid
Aeronautics Engineering School
ETSI Aeronauticos
Plaza Cardenal Cisneros
Madrid, Spain 28040

8. PERFORMING ORGANIZATION REPORT NUMBER

N/A

9. SPONSORING/MONITORING AGENCY NAME(S) AND ADDRESS(ES)

EOARD
Unit 4515 BOX 14
APO AE 09421

10. SPONSOR/MONITOR'S ACRONYM(S)

AFRL/AFOSR/RSW (EOARD)

11. SPONSOR/MONITOR'S REPORT NUMBER(S)

AFRL-AFOSR-UK-TR-2011-0057

12. DISTRIBUTION/AVAILABILITY STATEMENT

Approved for public release; distribution is unlimited. (approval given by local Public Affairs Office)

13. SUPPLEMENTARY NOTES

Government Purpose Rights - The U.S Government is authorized to reproduce and distribute reprints for Governmental purpose notwithstanding any copyright notation thereon.

14. ABSTRACT

Significant achievements have been made on the understanding of the 2D plasma expansion and detachment on a magnetic nozzle. An advanced fluid model and code have been built. Key clarifications of main processes have been unveiled, which dispute some previous theories. The subject will benefit greatly from continuing the research along the following lines:
1. Analysis of the effect of an adiabatic model for electrons. The issue is whether the vanishing of pressure can modify qualitatively the far beam behaviour.
2. Extension of the study to more general conditions on ion flow at the entrance, such as ion swirl and hot ions, of interest for plasma sources
3. Completion of the study of plasma detachment via demagnetization. The aim is to confirm present results, to solve the issue of formation of magnetic singularities, and to match with nonzero-beta plasma from the source.
4. Extension of plasma model beyond turning point of the magnetic nozzle. It is needed to analyze the far beam. It requires a more sophisticated integration technique.
5. Plasma detachment via non-neutral separation. this is a proposed mechanism whose analysis requires completing the previous task.
6. Development of the hybrid code, which, beyond supporting the fluid code, will allow consideration of new aspects and effects, such as plasma resistivity, ion gyroradius effects, the matching with the internal source, and probably the transition to an unmagnetized plume.

15. SUBJECT TERMS

EOARD, Modeling & Simulation, Electric Propulsion, Model Checking, Electromagnetic Fields, Electromagnetics, pulsed plasma thrusters

16. SECURITY CLASSIFICATION OF:			17. LIMITATION OF ABSTRACT	18, NUMBER OF PAGES	19a. NAME OF RESPONSIBLE PERSON
a. REPORT	b. ABSTRACT	c. THIS PAGE			Brad Thompson
UNCLAS	UNCLAS	UNCLAS	SAR	98	19b. TELEPHONE NUMBER *(Include area code)* +44 (0)1895 616163

FINAL REPORT

Magnetic nozzles for plasma thrusters: acceleration, thrust, and detachment mechanisms

Eduardo Ahedo
Mario Merino

Plasmas and Space Propulsion Team,
Universidad Politécnica de Madrid, Spain

Award FA8655-10-1-3085

August 25, 2011

SUMMARY

The work carried out within this project can be divided in two parts: 1) plasma acceleration and thrust in a magnetic nozzle, and 2) plasma detachment mechanisms. Results are presented in 9 annexed papers. The project departed from the 2D model and associated code DIMAGNO we had just published ['Two-dimensional supersonic plasma acceleration in a magnetic nozzle', E. Ahedo and M. Merino, Physics of Plasmas, vol. 17, 073501, 2010]. In the following, main achievements are summarized briefly.

A first task was to reach a better understanding of the competition among the different forces that shaped the plasma expansion, parallel and perpendicular to the magnetic field lines [1]. For electrons, electric and magnetic forces are confining ones, while pressure gradients and centrifugal forces are expanding ones. We highlighted that uniform and non-uniform plasma jets at the entrance behave in a different way. Uniform jets (a simpler and popular case, but less realistic) bear only a Hall current and a magnetic force at the plasma/vacuum edge. For isothermal electrons, the influence of pressure does not decay downstream and the electric field does not go to zero. It seems plausible that electrons cool downstream but the involved mechanism needs to be established, and the consequences on the final stage of the expansion must be analyzed. This last aspect can be studied with an adiabatic model; some preliminary work has been done.

The second task has been to clarify the thrust transmission process in a magnetic nozzle.
The main role of a magnetic nozzle is to produce an increment of thrust from an emitted plasma beam. This requires (1) the conversion of internal energy into axial directed energy of the plasma and (2) a way to obtain thrust from it. In a solid nozzle the second feature takes place through the gas pressure on the divergent walls. In a magnetic nozzle, it takes place through the magnetic force exerted on the thruster coils by the magnetic field induced by the azimuthal plasma currents. A positive thrust gain requires these plasma currents to be diamagnetic. Some previous studies on magnetic nozzles work with cold (i.e. hypersonic) plasmas. Clearly there is no internal energy to convert and therefore no thrust gain in these scenarios; indeed, there is a thrust loss because of the development of some paramagnetic currents. In order to demonstrate our claims we have extended the principal case of a sonic plasma (i.e. Mach number M=1) at the nozzle throat to supersonic cases (i.e. M>1) and have shown how the thrust gain decreases and the nozzle loses its function [2].

In some experiments with plasma sources, electron populations with two different temperatures have been detected. This leads to a steepening of the plasma profile, in an intermediate location of the expansion. The 2D model has been extended to take into account this case and the profile steepening has been reproduced [3]. The related paper got a first prize in a AIAA-sponsored student competition.

When the two electron temperatures differ by a factor larger than 10, approximately, the steepening becomes a non-neutral double layer. A very detailed study of this surface discontinuity has been culminated [4]. It had been claimed that the presence of this DL could be an innovative way of propulsion, materialized in the Helicon Double layer Thruster. Together with other authors we dispute that claim, showing that the DL does not produce any thrust gain. All gain comes from the ambipolar electric field in the magnetic nozzle. Recent experimental work by Longmier and coworkers support the ambipolar acceleration.

The last achievement on the 2D model has been to include electron inertia in the formulation [5]. An inspired manipulation of the electron equations has shown that the mathematical structure of the model remains surprisingly unaltered. Ion equations constitute a set of

hyperbolic differential equations whereas electron equations reduce mostly to algebraic (i.e. conservation) relations. Electron-inertia makes the electron streamtubes to detach outwardly from the magnetic streamtubes; interestingly, the shape of the electron streamtubes can be determined without solving the whole plasma flow. In principle, electron-inertia effects are rather small, but the conservation, in each electron streamtube, of the angular velocity of the electron fluid means that the electron azimuthal velocity increases downstream and the effect can become relevant away from the nozzle throat. Simulations to evaluate this are pending. One important result of the model, independent of electron inertia, is the non fulfillment of current ambipolarity in the 2D expansion.

A hybrid formulation of the magnetic nozzle problem, with a PIC model for heavy species and a fluid formulation for electrons, is being developed [6]. This would complement and tackle with aspects that are out of the possibilities of the fluid model. Subjects that we aim to study are: plasma resistivity, finite ion gyroradius effects, subsonic plasma flows, and the plasma-vacuum interface.

The rest of the tasks were devoted to assess plasma detachment mechanisms. Three detachment mechanisms had been proposed so far in the literature, based on: plasma resistivity (Moses and coworkers, 1992), electron-inertia (Hooper, 1993), and magnetic stretching (Arefiev-Breizman, 2004). Detailed models were developed only for the two last ones. The three mechanisms have been disputed by us as either incorrect or non-applicable to a magnetic nozzle [7,2].

We showed first that electron-inertia and resistivity are two similar forms of electron diffusion in a plasma beam and both tend to drift the electron streamtubes outwards of the magnetic streamtubes [2,5]. Therefore, they do not seem useful for an inwards detachment of the beam. This conclusion disagrees radically with the detachment scenario of Hooper, who claims that electron-inertia leads to inwards detachment of the beam. In order to investigate this disagreement and confirm our conclusions, we included electron-inertia in our model (as explained before), thus being able to reproduce the conditions assumed by Hooper. What we have found out is that Hooper, when manipulating the electron momentum equation, forgot to include one term (misled by his notation probably). This error was fatal, since he then missed a scalar equation, and substituted it by the current ambipolarity condition [5], ending then with a nonphysical model.

Magnetic stretching takes place when the plasma currents are paramagnetic and the induced magnetic field reinforces the applied one. In the case of a propulsive magnetic nozzle, the plasma current is diamagnetic and the induced field increases the divergence of the resulting nozzle. Therefore the detachment mechanism is not through magnetic-stretching (against prevailing theory) but because of plasma demagnetization, favoured doubly by the divergence of the applied field and the induced field [8]. Solutions illustrating this have been obtained. Nonetheless, because of the elliptic character of the induced field computation, certain mathematical issues remain in the far plume. Further work should simulate the downstream transition from a magnetized plume to an unmagnetized one.

Finally, another subject to be worked out is a more consistent matching between the subsonic plasma flow inside the source and the supersonic flow in the nozzle. This seems more relevant for the case of a high-density plasma, when induced field effects are already important at the source exit. A model of the source with induced field effects has just been finished [9].

Conclusions

Significant achievements have been made on the understanding of the 2D plasma expansion and detachment on a magnetic nozzle. An advanced fluid model and code on the subject have been built up. Key clarifications of main processes have been unveiled, sometimes at the cost of

disputing previous theories. The subject will benefit greatly from continuing the research along the following lines:

1. Analysis of the effect of an adiabatic model for electrons. The issue is whether the vanishing of pressure can modify qualitatively the far beam behaviour.
2. Extension of the study to more general conditions on the ion flow at the entrance, such as ion swirl and hot ions, of interest for some plasma sources
3. Completion of the study of plasma detachment via demagnetization. The aim is to confirm present results, to solve the issue of formation of magnetic singularities, and to match with nonzero-beta plasma from the source.
4. Extension of plasma model beyond turning point of the magnetic nozzle. It is needed to analyze the far beam. It requires a more sophisticated integration technique.
5. Plasma detachment via non-neutral separation. We proposed this mechanism but its analysis cannot be performed without completing the previous task.
6. Development of the hybrid code, which, beyond supporting the fluid code, will allow taking into consideration new aspects and effects, such as plasma resistivity, ion gyroradius effects, the matching with the internal source, and probably the transition to an unmagnetized plume.

Publications based on this project

1. 'Simulation of plasma flows in divergent magnetic nozzles', M. Merino and E. Ahedo, to appear in IEEE Transactions Plasma Science, 2011.
2. 'On plasma detachment in propulsive magnetic nozzles', E. Ahedo and M. Merino, Physics of Plasmas 18, 053504 (2011).
3. '2D plasma flow in a magnetic nozzle with a bi-modal electron energy distribution function', M. Merino, First prize at the 7th AIAA-Pegasus Student Conference, Torino, Italy, 2011.
4. 'Double-layer formation and propulsive assessment for a three-species plasma expanding in a magnetic nozzle', E. Ahedo, Physics of Plasmas 18, 033509 (2011)
5. 'On electron inertia and current ambipolarity in magnetic nozzle models', E. Ahedo and M. Merino, IEPC 2011-050.
6. 'A hybrid code of the plasma plume in a magnetic nozzle', J. Navarro and E. Ahedo, IEPC 2011-048.
7. **'**Preliminary assessment of detachment in a plasma thruster magnetic nozzle', E. Ahedo and M. Merino, AIAA paper 2010-6613.
8. 'Plasma detachment mechanisms in a magnetic nozzle', M. Merino and E. Ahedo, AIAA-2011-5999.
9. 'Magnetic confinement of a high-density cylindrical plasma', E. Ahedo, submitted to Phys. Plasmas.

Simulation of plasma flows in divergent magnetic nozzles

Mario Merino and Eduardo Ahedo
Universidad Politécnica de Madrid, Spain

***Abstract* – Images from the simulation code DIMAGNO illustrate the roles of pressure, electric, and magnetic forces in the two-dimensional plasma expansion in a magnetic nozzle and the generation of thrust.**

Magnetic nozzles, created by a longitudinal magnetic field, are being proposed as plasma acceleration devices in advanced propulsion systems. There is a clear analogy between the subsonic-to-supersonic flows of plasmas in a magnetic nozzle and of neutral gases in a solid nozzle. However, plasma dynamics in a magnetic nozzle are more complex, because of the existence of electric currents, different acceleration mechanisms, and downstream detachment. These plasma features can be analyzed with the code DIMAGNO, which implements a 2D, steady-state model of the plasma expansion in a divergent magnetic nozzle [1]. Typically, the plasma is collisionless, fully-ionized, current-free, low-beta, and supersonic. The strength of the guide magnetic field assures that electrons are strongly-magnetized whereas ions are partially-magnetized. The use of the method of characteristic surfaces (i.e. ion streamlines and Mach lines) for integrating the hyperbolic equations makes the code fast, accurate, and efficient.

Figure 1 shows a 2D map of plasma density and several pairs of electron and ion stream-tubes with the same cross-section at the nozzle throat. There, the plasma jet is sonic, with radially nonuniform density, and no ion rotation, which are typical characteristics of, at least, a helicon-source plasma. The electron and magnetic streamtubes coincide but, due to weak magnetization, ion streamtubes are less divergent, except at the plasma-vacuum edge, where quasineutrality causes the ion and electron tubes at the edge to match. This matching results from an increased electric field perpendicular to ***B***, which also fosters plasma rarefaction at the edge. The relative focusing of the plasma jet compensates partially the nozzle divergence. The separation of ion and electron streamtubes breaks the longitudinal current-density ambipolarity (here imposed at the throat) while quasineutrality and the global current–free condition are still satisfied.

Plasma confinement and (supersonic) acceleration

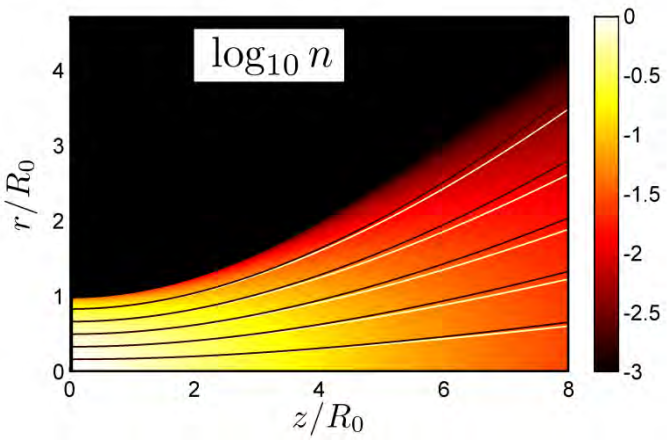

Fig.1. Logarithmic map of the normalized plasma density and pairs of electron (dark) and ion (light) streamtubes.

are governed by the ion and electron momentum equations,

$$m_i n \vec{u}_i \cdot \nabla \vec{u}_i - \vec{j}_i \times \vec{B} = en\vec{E} = -T_e \nabla n + \vec{j}_e \times \vec{B} \,,$$

where symbols are conventional. In general, $j_i << j_e \approx j_{\theta e}$ and ions are driven almost exclusively by the ambipolar electric force. The electron equation states the balance among the pressure, electric, and magnetic forces. Figure 2(a) depicts the relative weight of the three radial forces, the expanding pressure being compensated by both electric and magnetic confinement. The radial electric force, negligible at the nozzle throat, develops downstream and compels the ions to diverge. Figure 2(b) illustrates the more complex axial balance. The axial pressure force accelerates near the axis and decelerates near the edge. Thus, near the beam center, $f_{z,p} \approx f_{z,e}$, whereas near the edge, $f_{z,m} \approx -f_{z,p}$. This behavior, unrecoverable by a 1D model, is caused by the strong 2D density rarefaction.

The purpose of a propulsive magnetic nozzle (PMN) is to increment the thrust imparted by the plasma jet. In a solid nozzle this is achieved by the gas pressure on the walls. In a PMN, thrust comes from the reaction force to $f_{z,m} = -j_{\theta e} B_r$ on the thruster magnetic circuit. Figure 2(c) plots this force (and its integral along a z = const. section, $F_{z,m}$) showing that it is concentrated near the edge on the near plume. The thrust gain due to the PMN is the integral of $F_{z,m}$. A positive gain

Manuscript received -----
M. Merino and E. Ahedo are with the Universidad Politécnica de Madrid, Spain.
Work was supported by Gobierno de España, ESP-2007-62694.
Publisher Identifier S XXXX-XXXXXXX-X

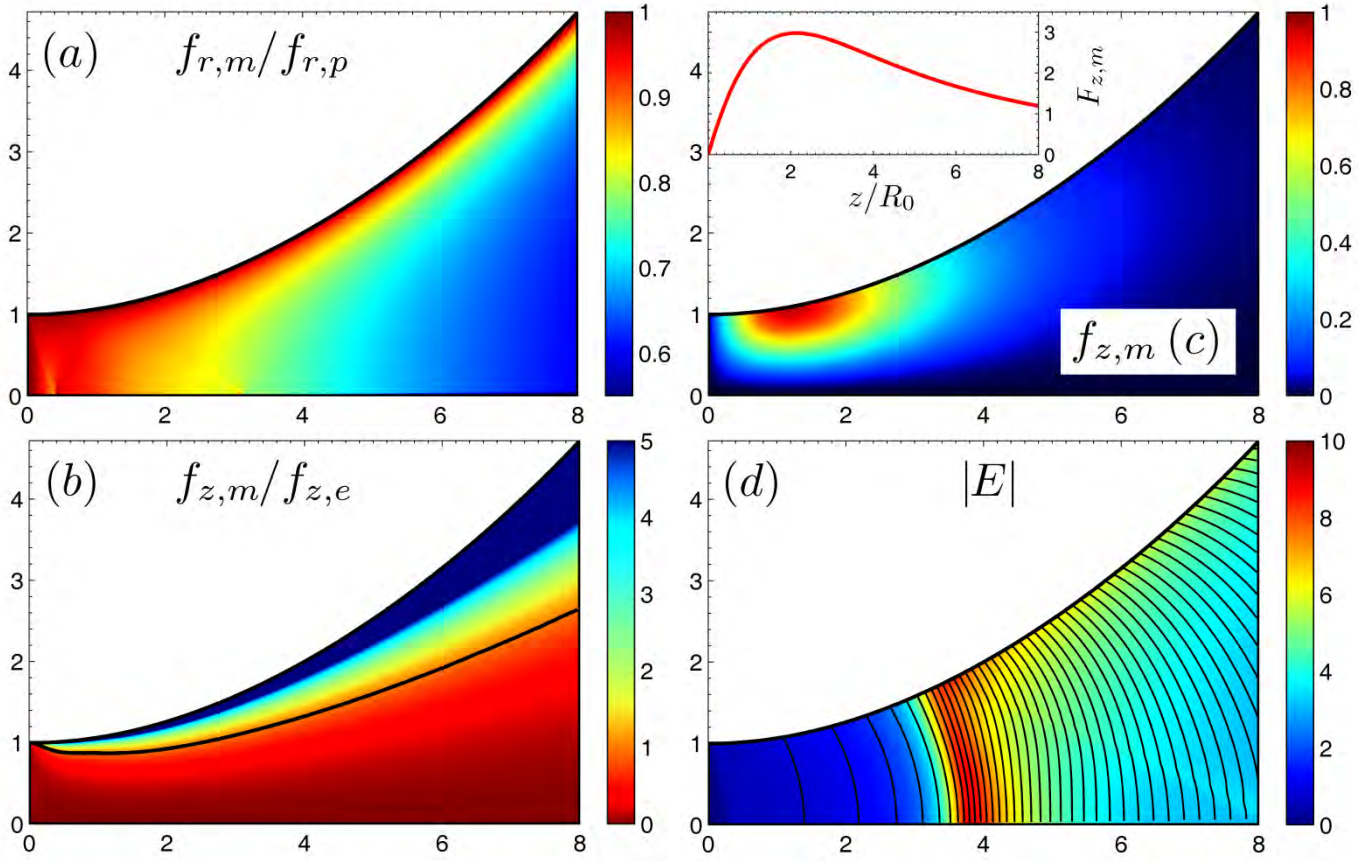

Fig.2. (a) Magnetic-to-pressure radial force ratio. (b) Magnetic-to-electric radial force ratio; the black line separates regions of positive and negative pressure axial force. (c) Magnetic axial force per unit-volume, $f_{z,m}$, and its integral, $F_{z,m}$, on a z = const disk. (d) Ambipolar electric field and equipotential lines for plasmas with a 0.2 fraction of 9-times hotter electrons at the nozzle throat. Axes are the same than in Fig. 1.

requires the Hall current, $j_{\theta e}$, to be diamagnetic, which, fortunately, is the one naturally occurring in PMN, and also the condition supporting a radially-confining and axially-accelerating magnetic force. Furthermore, a diamagnetic Hall current induces a magnetic field that opposes the applied field and increases the divergence of the resulting nozzle and plasma jet, a scenario contrary to the magnetic-stretching detachment theory (see [2] and references therein).

Figure 2(d) illustrates that DIMAGNO can also simulate the expansion of plasmas with a small extra population of hot electrons. These plasmas would explain the formation of current-free double layers in helicon-source plasma beams (see [3] and references therein). In Fig. 2(d), the red curved region of maximum electric field is the steepened layer, with an electric potential fall of the order of the energy of hot electrons. That layer acts as a formidable barrier for 'cold' electrons, so that the initially-small population of hot electrons dominates completely the plasma flow downstream of the layer.

In conclusion, the code DIMAGNO produces images that provide much understanding of the multifaceted plasma behavior in a magnetic nozzle.

REFERENCES

[1] E. Ahedo and M. Merino, 'Two-dimensional supersonic plasma acceleration in a magnetic nozzle', Phys. Plasmas 17, 073501 (2010).

[2] E. Ahedo and M. Merino, 'On plasma detachment in propulsive magnetic nozzles', Phys. Plasmas 18, to appear in May 2011.

[3] E. Ahedo 'Double-layer formation and propulsive assessment for a three-species plasma expanding in a magnetic nozzle' Phys. Plasmas 18, 033510 (2011)

Manuscript received -----

M. Merino and E. Ahedo are with the Universidad Politécnica de Madrid, Spain.

Work was supported by Gobierno de España, ESP-2007-62694.
Publisher Identifier S XXXX-XXXXXXX-X

On plasma detachment in propulsive magnetic nozzles

Eduardo Ahedo[a] and Mario Merino
E.T.S. Ingenieros Aeronáuticos, Universidad Politécnica de Madrid, Madrid 28040, Spain

(Received 1 February 2011; accepted 6 April 2011; published online 27 May 2011)

Three detachment mechanisms proposed in the literature (via resistivity, via electron inertia, and via induced magnetic field) are analyzed with an axisymmetric model of the expansion of a small-beta, weakly collisional, near-sonic plasma in a diverging magnetic nozzle. The model assumes cold, partially magnetized ions and hot, isothermal, fully magnetized electrons. Different conditions of the plasma beam at the nozzle throat are considered. A central feature is that a positive thrust gain in the nozzle of a plasma thruster is intimately related to the azimuthal current in the plasma being diamagnetic. Then, and contrary to existing expectations, the three aforementioned detachment mechanisms are divergent, that is, the plasma beam diverges outwards of the guide nozzle, further hindering its axial expansion and the thrust efficiency. The rate of divergent detachment is quantified for the small-parameter range of the three mechanisms. Alternative mechanisms for a convergent detachment of the plasma beam are suggested. © *2011 American Institute of Physics*. [doi:10.1063/1.3589268]

I. INTRODUCTION

A diverging magnetic nozzle, created by a longitudinal magnetic field, is being proposed as an acceleration mechanism for a magnetized plasma in advanced propulsion devices, such as the helicon thruster,[1–4] the Applied-Field MagnetoPlasmaDynamic Thruster (AFMPDT),[5] the Diverging Cusped Field Thruster (DCFT),[6] and the VAriable Specific Impulse Magneto Rocket (VASIMR).[7] In particular, the magnetic nozzle constitutes the acceleration stage of the helicon thruster, located downstream of the chamber where the plasma is created and heated. The plasma flow, channeled by the diverging magnetic lines, expands supersonically in a similar way to a hot gas in a solid nozzle.[8] Beyond this basic analogy, conventional gas dynamics in a solid nozzle are much simpler than plasma dynamics in a magnetic nozzle.

In order to understand these ones, we developed a macroscopic, two-dimensional (2D) model of the stationary expansion of a plasma with fully magnetized, hot electrons and partially magnetized, cold ions, in the diverging magnetic nozzle created by solenoids.[9] Plasma conditions at the nozzle throat include sonic and supersonic flows, and radially non-uniform or uniform profiles of the beam density. The model consists of a closed set of conservation and differential equations which are integrated efficiently with the method of characteristic surfaces. The model includes several relevant design/operation parameters, which allowed our analysis to go beyond the simulation of some particular cases, into investigating the influence of an ample region of the parametric space in the plasma response. The model was designed specifically to analyze plasma acceleration in an helicon thruster, due to the conversion of electron thermal energy into ion directed energy. It could be partially suitable for the AFMPDT and the DCFT, but the detailed physics of these devices are not understood enough yet. The model is not apt for studying plasma acceleration in the VASIMR nozzle, caused by conversion of ion gyrokinetic energy into nozzle parallel energy.

Since the nozzle magnetic lines close on themselves, once the plasma beam has been accelerated and before the turning point of the magnetic nozzle, the plasma jet needs to detach from the magnetic lines; otherwise, part of the plasma would turn back towards the thruster walls and the thrust gain will drop. Experiments seem to suggest that most of the plasma detaches, but more measurements are needed and detachment mechanisms is poorly known. In this context and in order to optimize the design of magnetic nozzles for plasma thrusters, one crucial subject is to understand how the plasma detaches from the magnetic nozzle. Three detachment mechanisms of the plasma *from the guide magnetic field* have been proposed in the literature: resistive detachment by Moses *et al.*,[10] electron-inertia detachment by Hooper,[11] and magnetic self-field detachment by Arefiev and Breizman[12] and Breizman *et al.*[13] In the two first cases, either resistive or electron-inertia forces detach the plasma jet from the guide field nozzle. In the third case, the induced magnetic field modifies the original nozzle of the guide field; the plasma, by remaining attached to the resulting magnetic nozzle, detaches effectively from the guide field. The three detachment studies either obtain or assume that the detachment is *convergent*, i.e., the plasma beam diverges less than the guide field nozzle, thus facilitating the axial plasma expansion.

This paper analyzes these three detachment mechanisms, both qualitatively and quantitatively (in the small-parameter range), computing perturbed quantities from the 2D solution for a collisionless, zero-beta plasma with massless electrons. Several observations related to the frame of our study are worth to comment. First, as the title announces, the detachment assessment is going to be centered in the case of a *propulsive magnetic nozzle* (PMN), of which nozzel's main role is to enhance the thrust by acceleration of a near-sonic

[a]Electronic mail: eduardo.ahedo@upm.es.

plasma and conversion of its internal energy into directed kinetic energy. The PMN is not the case treated by Hooper and Arefiev and Breizman, who consider a plasma that is already hypersonic at the nozzle entrance; in fact, Arefiev and Breizman report a decrease of the axial flux of plasma momentum along the nozzle, i.e., a thrust loss. Second, although detachment is expected to manifest mainly after the plasma has been accelerated, both processes are not independent and well separated in the nozzle; thus, it is preferable to analyze them within a unique model.

The rest of the paper is organized as follows. Section II reviews succinctly the PMN model and the relation between plasma currents and the thrust increment. Section III analyzes resistive and electron-inertia detachment. Section IV is devoted to magnetic detachment. Conclusions and ideas for further research are presented in Sec. V. First results on this subject were presented in a recent conference.[14]

II. THRUST GAIN AND PLASMA CURRENTS

The plasma/nozzle model and the nomenclature used hereafter are exactly the same ones of Ref. 9, so we will omit their description as far as comprehension of the present work is not affected. A current-free, fully ionized plasma jet of radius R, is injected sonically at the throat (located at $z=0$) of a nozzle created by a guide magnetic field of strength B. The plasma at the throat satisfies

$$\lambda_{d0} \ll \ell_{e0} \ll R, \qquad \Omega_{i0}R/u_{i0} = O(1), \tag{1}$$

$$m_e/m_i \ll 1, \quad R/\lambda_{ei0} \ll 1, \quad \beta_0 \equiv \mu_0 n_0 T_e/B_0^2 \ll 1, \tag{2}$$

where subscript 0 refers always to values at $(z,r)=(0,0)$, R is the radius of the plasma jet at $z=0$, n is the plasma density, u_i is the macroscopic ion longitudinal velocity, λ_d is the Debye length, ℓ_e is the electron gyroradius, λ_{ei} is the electron-ion collision mean-free-path, $\Omega_i = eB/m_i$ is the ion gyrofrequency, and the rest of symbols are conventional. Table I of Ref. 9, detailing parameters of two helicon thruster experiments,[2,3] shows that conditions (1) and (2) are appropriate for studying the plasma discharge in those thrusters. Then, we can consider that the plasma is collisionless and quasineutral, electrons are massless and fully magnetized, ions are mildly magnetized, and the induced magnetic field B^* is negligible. Electron streamtubes are the magnetic streamtubes, but ion streamtubes do not coincide with electron streamtubes, except at the jet axis and edge $r=R_V(z)$ (see Fig. 6 of Ref. 9).

Reference 9 is centered on the zero asymptotic limit of the parameters of Eq. (2). Then, the plasma expansion model consists of Eqs. (20)–(22) and (24)–(27), which determine the ion and electron velocities, $\mathbf{u}_i$ and $\mathbf{u}_e$, plasma density n, and electric potential ϕ. The upstream boundary conditions for these equations are Eqs. (29)–(35) of Ref. 9. Downstream, the integration cannot proceed beyond the turning point of the magnetic tube containing the plasma jet. This forces us to limit our study to a finite axial section downstream of the nozzle.

An exam of the equations shows that the plasma/nozzle model is characterized by the divergence rate of the magnetic topology (parameter R_L/R for a single loop in Ref. 9); $\hat{\Omega}_{i0} = \Omega_{i0}R/c_s$, measuring the magnetic strength (on ions); $M_0 = u_{i0}/c_s$, the ion Mach number at the throat, with $c_s = \sqrt{T_e/m_i}$ the plasma sound speed; and σ, measuring the non-uniformity of $n(z=0,r)$ in Eq. (33) of Ref. 9. At least for an helicon thruster, the plasma at the nozzle throat is expected to be highly non-uniform ($\sigma \approx 1$), quasi-sonic ($M_0 \simeq 1$), and ions to be weakly magnetized ($\hat{\Omega}_{i0} \leq 1$).[15,16] These entrance conditions are very different from the ones considered by Arefiev and Breizman[12] and Breizman *et al.*[13]: a plasma which is radially uniform ($\sigma = 0$), cold ($M_0 \to \infty$), and strongly magnetized($\hat{\Omega}_{i0} \to \infty$). Leaving aside the relevance of the Arefiev-Breizman model for a propulsive nozzle, these two disparate parametric ranges provide a good opportunity to understand how thrust gain and detachment depend on the upstream plasma conditions. We will approach Arefiev-Breizman conditions by taking $\hat{\Omega}_{i0}$ and M_0 large but finite; for instance, for $M_0 = 3$, the plasma is almost hypersonic, since the influence of the plasma pressure on the nozzle expansion is reduced to about a 10%.

According to Eqs. (40)–(42) of Ref. 9, the accumulated thrust gain at a cross-section $S_z : z = \text{const}$ is measured by the dimensionless function

$$\kappa_{noz}(z) = \Delta F(z)/F_0, \tag{3}$$

where $F = F(0)$ is the momentum axial flux of the plasma at $z=0$ and

$$\Delta F(z) = \int_{\mathcal{V}(z)} d\mathcal{V}\ (-j_\theta)B_r + \int_{A_V(z)} dA\ (-J_\theta)B_r \tag{4}$$

is the gain in momentum axial flux, with $\mathcal{V}(z)$ and $A_V(z)$ the volume and area of the region bounded by the nozzle throat, the section S_z, and the plasma/vacuum edge V. Thus, the increase of momentum flux of the plasma beam along the nozzle is due to the axial magnetic force exerted by the thruster magnetic circuit on the volumetric and superficial azimuthal currents, j_θ and J_θ respectively, induced on the plasma. Since the supersonic fluid information travels only downstream, $\kappa_{noz}(z)$ represents the thrust gain for a nozzle of length z.

Without loss of generality, the convention $B_r, B_z > 0$ is adopted in the model. Then, Eq. (4) states that a positive thrust gain requires the azimuthal electric current be negative, which, as we will see below, corresponds to a diamagnetic current. The superficial current J_θ, due to pressure gradients at the plasma edge, is negative always. The current density $j_\theta = j_{\theta i} + j_{\theta e}$ has ion and electron contributions (called, respectively, *swirl* and *Hall* currents[17]), which, respectively, are positive and negative.[9] Therefore, the Hall current accelerates the plasma and the swirl current decelerates it.

Sketches of the two physical arrangements of plasma currents are shown in Figs. 1(a) and 1(b). They show the azimuthal currents in the magnetic circuit and in the plasma plume (either internal or at the edge). These two sets of currents create, respectively, the applied magnetic field, $\mathbf{B}$, and the plasma-induced magnetic field, $\mathbf{B}^*$. The Ampere's law for the longitudinal (main) component of the induced field is

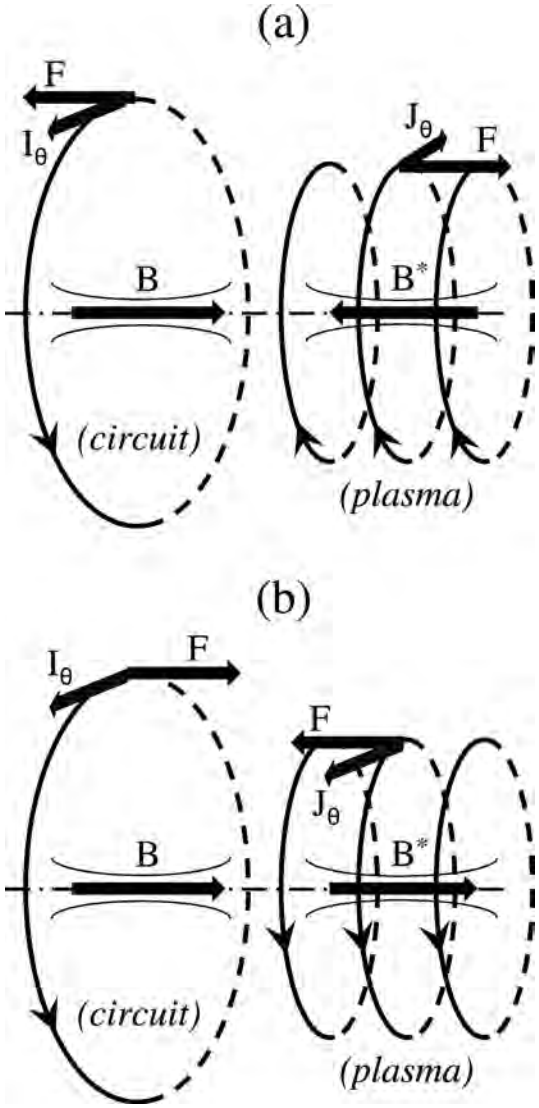

FIG. 1. Sketches of the azimuthal currents in the external circuit and the plasma beam, the magnetic fields they create, and the mutual force between them. (a) Diamagnetic case, corresponding to plasma acceleration and positive thrust gain in the nozzle, the suitable configuration for a plasma thruster. (b) Paramagnetic case, corresponding to plasma deceleration and negative thrust gain.

$$\nabla \times \tilde{\mathbf{B}}^* = \mu_0 j_\theta \mathbf{1}_\theta. \tag{5}$$

Two sets of parallel currents repel or attract each other, with the mediation of the magnetic fields they create, depending on whether they run in the opposite or the same direction, respectively.[18] The case of mutual repulsion, shown in Fig. 1(a), is the suitable one for a PMN: the plasma current is pushed downstream and the circuit current (tied to the thruster) is pushed back, thus yielding a positive thrust gain. The case of the mutual attraction, sketched in Fig. 1(b), leads to plasma deceleration and $\kappa_{noz} < 0$.

The thrust gain for cases with $M_0 = 1.05$ and $M_0 = 3$ is plotted in Fig. 2(a). For the simplest case of an initially uniform plasma with unmagnetized ions, κ_{noz} behaves similarly to the case of a conventional gas in a solid nozzle: κ_{noz}

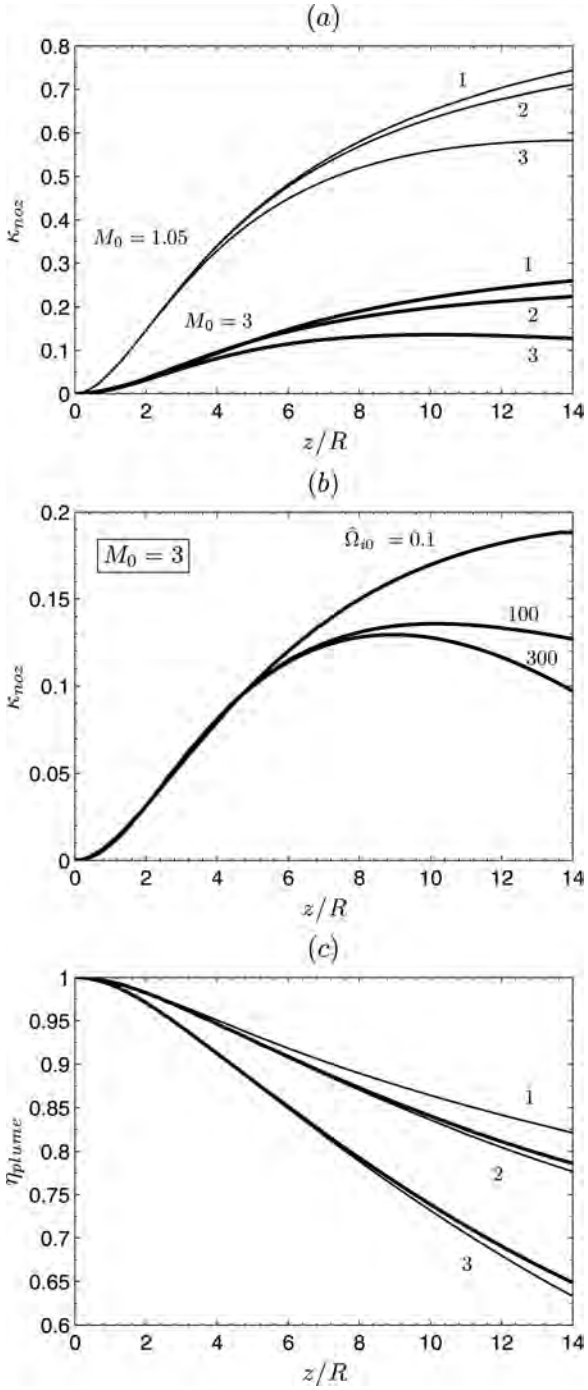

FIG. 2. (a) Comparison of the thrust gain for $M_0 = 1.05$ (thin lines) and $M_0 = 3$ (thick lines). Numbers (1)–(3) indicate $\hat{\Omega}_{i0} = 0.1$, $\sigma = 0.99$; $\hat{\Omega}_{i0} = 100$, $\sigma = 0.99$; and $\hat{\Omega}_{i0} = 100$, $\sigma = 0$, respectively. (b) Influence of the magnetic field strength on the thrust gain for $M_0 = 3$. (c) Plume efficiency versus the nozzle length for $M_0 = 1.05$. Lines and numbers are as in plot (a). In all figures, simulations are for the large divergence-rate nozzle of Ref. 9.

depends on the ratio on the electron-to-ion momentum flux ratio, which is highest for $M_0 = 1$ and is zero for a hypersonic plasma. Figure 2(a) shows that κ_{noz} is about 3 times lower for $M_0 = 3$ than for $M_0 \approx 1$, and $\kappa_{noz} \to 0$ is expected for a cold plasma. With respect to the other two parameters, κ_{noz} increases when either σ increases (which augments the positive Hall current) or $\hat{\Omega}_{i0}$ decreases (which reduces the

negative swirl current). Both effects are observed in Fig. 2(a) too.

Since the swirl current is found negligible in the plasma source[15] and develops almost exclusively along the nozzle (because of the separation of magnetic and ion streamtubes), its negative effect on thrust increases as the plasma moves downstream. As a consequence, $\kappa_{noz}(z)$ can reach a maximum at a certain distance from the throat. This is clearly observed in Fig. 2(b): for $M_0 = 3$ and $\hat{\Omega}_{i0} = 300$, the thrust gain is maximum for $z/R \approx 9$, and the swirl current is larger than the Hall current downstream of that location.

In the limit case of $\hat{\Omega}_{i0} \gg 1$ and $M_0 \gg 1$, the Hall current is negligible [see Eqs. (24) and (25) of Ref. 9] and the paramagnetic, decelerating swirl current leads to $\kappa_{noz}(z) < 0$. Indeed, Arefiev and Breizman define a "nozzle efficiency" (based on thrust) that is similar to $1 + \kappa_{noz}$, which is plotted in Fig. 6 of Ref. 13; losses up to $-\kappa_{noz} \sim 38\%$ are shown. The sketch of Fig. 4 of Ref. 12 corresponds to the one in Fig. 1(b) here. The "nozzle efficiency" of Arefiev and Breizman must not be mistaken with the plume efficiency of Ref. 9, $\eta_{plume}(z) = P_{zi}/P_i$, where P_{zi} and P_i are the axial and total fluxes of ion energy at section S_z, defined in Eqs. (44) and (47) of Ref. 9. The plume efficiency is a genuine 2D effect that measures the penalty in thrust efficiency caused by the beam radial expansion. Figure 2(c) shows that η_{plume} is weakly influenced by M_0. As the thrust gain, the plume efficiency is higher for a non-uniform jet with unmagnetized ions, since this presents the lowest (effective) divergence.[9]

III. DIFFUSIVE DETACHMENT

Each one of the three detachment mechanisms proposed in the literature is due to one of the small parameters of Eq. (2). In this section and Sec. IV, these mechanisms are studied in the small-parameter limit, assuming that the plasma response is the sum of the zeroth-order (attached) solution plus a first-order solution. This one isolates each detachment phenomenon, determines its character, and quantifies it (up to first order).

Diffusive detachment considers that the plasma detaches from the magnetic lines by either resistive[10] or inertial[11] forces on electrons. The key equation for diffusive detachment is the one for electron azimuthal momentum which, including resistivity and inertia, becomes

$$eu_{\perp e}B = (m_e/r)\tilde{\mathbf{u}}_\mathbf{e} \cdot \nabla(ru_{\theta e}) + m_e \nu_{ei} u_{\theta e}, \tag{6}$$

with $\nu_{ei} \equiv c_s/\lambda_{ei}$, the Coulomb collision frequency. The massless and collisionless, zeroth-order solution reduces Eq. (6) to $u_{\perp e} = 0$. The first-order solution of $u_{\perp e}$ is obtained by implementing the zeroth-order solution on the right-hand side of Eq. (6). Using Eq. (25) of Ref. 9, the inertial contribution to Eq. (6) becomes $\tilde{\mathbf{u}}_\mathbf{e} \cdot \nabla(ru_{\theta e}) = 2u_{\theta e}u_{re}$, with $u_{re} = u_{\parallel e} \sin\alpha$ and α, the local angle of $\mathbf{B}$ with respect to the plasma axis. Thus, the perpendicular velocity satisfies the algebraic relation

$$u_{\perp e} = \bar{\chi} u_{\theta e}, \tag{7}$$

where the *inverse Hall parameter*, $\bar{\chi} = \bar{\chi}_{res} + \bar{\chi}_{ine}$, has contributions from resistivity and electron inertia,

$$\bar{\chi}_{res} = \nu_{ei}/\Omega_e, \qquad \bar{\chi}_{ine} = 2u_{re}/r\Omega_e, \tag{8}$$

and

$$\Omega_e = \Omega_i m_e/m_i.$$

Two conclusions are straightforward from Eqs. (7) and (8). First, electron-inertia effects have a resistive character with an effective collision frequency $2u_{re}/r \geq 0$; thus, the ratio $2u_{re}/(r\nu_{ei})$ determines which one is the main diffusive phenomenon. Second, the ratio $u_{\perp e}/u_{\theta e}$ is positive always. Since a PMN has $u_{\theta e} \geq 0$ (with convention $B_z > 0$), one has $u_{\perp e} \geq 0$, and diffusion (either resistive or inertial) makes the plasma beam to detach *divergently*. This result disagrees with Hooper,[11] who claimed that electron inertia leads to convergent detachment. Hooper's model is limited to a hypersonic, uniform plasma beam at the nozzle throat and assumes that current ambipolarity is fulfilled everywhere. Reference 9 demonstrates that current ambipolarity is not satisfied, so the disagreement on the character of the diffusive detachment is very likely motivated on that assumption.

The rate of diffusive detachment is measured by the ratio

$$\delta = u_{\perp e}/u_{\parallel e} = \bar{\chi} u_{\theta e}/u_{\parallel e} = \delta_{res} + \delta_{ine}, \tag{9}$$

with

$$\delta_{res} = \frac{\nu_{ei} u_{\theta e}}{\Omega_e u_{\parallel e}}, \quad \delta_{ine} = \frac{2u_{\theta e} \sin\alpha}{r\Omega_e}, \tag{10}$$

as the detachment rates for resistivity and electron-inertia. Figure 3 illustrates the behavior of resistive detachment for a typical PMN case. The normalization parameters for the inverse Hall parameter and the detachment rate are

$$\delta_{res,0}\hat{\Omega}_{i0} \equiv \bar{\chi}_{res,0} = \hat{\nu}_{ei0}/\hat{\Omega}_{e0},$$

with $\hat{\Omega}_{e0} = \hat{\Omega}_{i0} m_e/m_i$; typical values of $\bar{\chi}_{res,0}$ (as for the plasmas of Table I of Ref. 9) are in the range $10^{-4} - 10^{-3}$. Except near the plasma edge, where rarefaction is enhanced, one has $\bar{\chi}_{res} \propto n/B \propto 1/M$ and $\delta_{res} \propto R_V/M^2$, which explains that $\delta_{res}\delta_{res,0} \ll 1$ everywhere. Therefore, resistive detachment is expected to be negligible in practical PMNs. Moses *et al.* [10] suggest that anomalous resistivity or electron cooling could increase the effective collision frequency. Some observations are pertinent. First, this will further increase divergent detachment. Second, as far as we know, there is not experimental evidence of anomalous diffusion in magnetic nozzles. And third, although some electron cooling is known to exist, it is unlikely that ν_{ei} increases by even one order of magnitude.

Figure 4 illustrates inertia-based detachment for the same zeroth-order conditions than Fig. 3. Now, the normalization parameters are

$$\delta_{ine,0}\hat{\Omega}_{i0} \equiv \bar{\chi}_{ine,0} = 2/\hat{\Omega}_{e0}$$

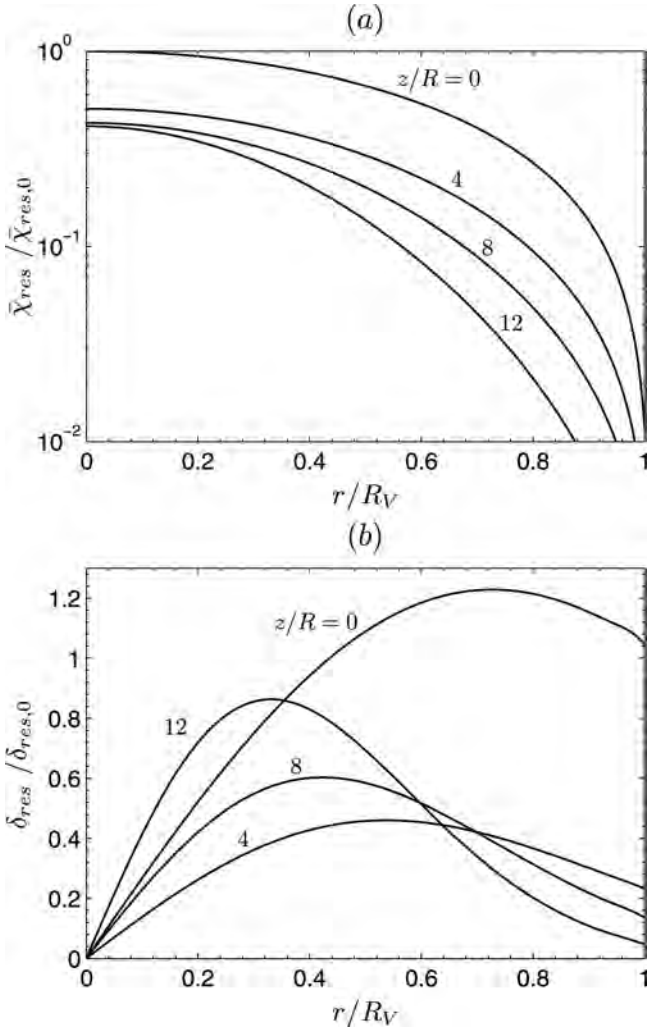

FIG. 3. Resistive detachment for $M_0 = 1.05$, $\sigma = 0.99$, and $\hat{\Omega}_{i0} = 0.1$. (a) Inverse Hall parameter and (b) divergent detachment slope.

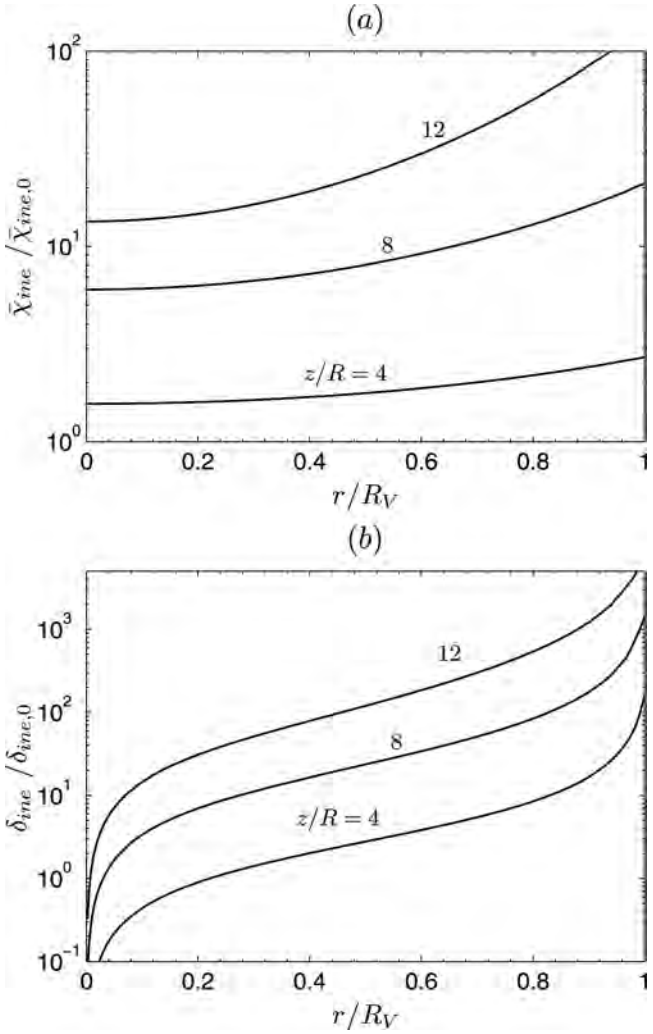

FIG. 4. Electron-inertia detachment for $M_0 = 1.05$, $\sigma = 0.99$, and $\hat{\Omega}_{i0} = 0.1$. (a) Inverse Hall parameter and (b) divergent detachment slope.

with $\bar{\chi}_{ine,0} \sim 10^{-5} - 10^{-4}$, typically. Except near the plasma edge, it is $\bar{\chi}_{ine} \propto MR_V \sin\alpha$ and $\delta_{ine} \propto R_V^2 \sin\alpha$. Contrary to resistivity, inertial detachment increases considerably as the plasma moves downstream and u_{re} develops. Additionally δ_{ine} increases at $r/R_V \sim 1$ because of the sharp increase of $u_{\theta e}$ near the plasma-vacuum edge.[9] For the envisaged range of parameters for a PMN, electron-inertia effects yield a larger divergent detachment than resistivity. Although $\delta_{ine,0} \ll 1$, the large values of $\delta_{ine}/\delta_{ine,0}$ suggest that inertial detachment can become a zeroth-order effect downstream, unless that non-linear effects in Eq. (6) prevent it, as we discuss below.

Diffusive detachment is based on the electron response exclusively; in particular, on the development of a Hall current that balances (partially or totally) the pressure gradient. Therefore, this detachment is divergent even for a supersonic plasma at the nozzle throat. Furthermore, we can interpret the outwards diffusion in the nozzle as the continuation of the one that takes place inside a cylindrical plasma source[15,16]: the radially outwards flux of a plasma constrained by an axial magnetic field and a cylindrical vessel is made possible by (1) plasma resistivity in the bulk plasma region and (2) electron-inertia in a thin inertial layer, separating the bulk region and the Debye sheath. The continuation of the inertial and Debye layers into the nozzle would occupy the regions here named plasma edge and vacuum (although their study is out of the present model capabilities). In our model, the plasma injected at the nozzle throat corresponds only to the bulk region; the large increment of $u_{\theta e}(0, r)$ near the beam edge, Eq. (34) of Ref. 9, announces the presence of the inertial layer. The key point here is that, within the inertial layer of the cylindrical source model, the first term of the right-hand-side of Eq. (6) dominates over the second one. This non-linear behavior of the inertia term invalidates Eq. (7) and limits the growth of $u_{\theta e}$ to $O(\sqrt{T_e/m_e})$. The same non-linear bounding mechanism is present in the 2D expansion here, so we expect it to limit the divergent growth of inertial detachment far downstream.

IV. MAGNETIC DETACHMENT

The Ampere's law (5) states that the azimuthal plasma current induces a longitudinal magnetic field $\mathbf{B}^*$ that added to the guide field modifies the magnetic nozzle. For small-

β_0, the induced field can be obtained by solving Eq. (5) or its integral Biot-Savart form with the zeroth order solution for j_θ. We will center the discussion in a plasma with $M \simeq 1$, $\sigma = 0$, and $\hat{\Omega}_{i0} < 1$, when the azimuthal plasma current is reduced to the Hall current developing around the plasma/vacuum edge, $J_\theta = -(p_e/B)_{r=R_V}$. This current distribution is a continuous sequence of simple loops that induces the magnetic streamfunction[9,18]

$$\psi^*(z,r) = \frac{\mu_0}{4\pi}\int_0^{z_F} dz_1 \frac{p_e}{B_z}\sqrt{(r+R_V)^2+(z-z_1)^2} \times [(2-m)\mathbf{K}(m) - 2\mathbf{E}(m)] \tag{11}$$

where $\mathbf{K}$ and $\mathbf{E}$ are complete elliptic integrals,

$$m = \frac{4R_V r}{(r+R_V)^2+(z-z_1)^2},$$

p_e/B_z is evaluated at $(z,r) = (z_1, R_V(z_1))$, and z_F is the length of the nozzle. The longitudinal components of the induced magnetic field satisfy $(B_z^*, B_r^*) = r^{-1}(\partial\psi^*/\partial r, -\partial\psi^*/\partial z)$, which yields

$$\hat{B}_z^*(\hat{z},\hat{r}) = -\frac{\beta_0}{4\pi}\int_0^{z_F} d\hat{z}_1 \frac{\hat{p}_e}{\hat{B}_z}\sqrt{\frac{m}{\hat{r}\hat{R}_V}} \times \left[\mathbf{K}(m) - \frac{\hat{r}^2 - \hat{R}_V^2 + (\hat{z}-\hat{z}_1)^2}{(\hat{r}-\hat{R}_V)^2+(\hat{z}-\hat{z}_1)^2}\mathbf{E}(m)\right], \tag{12}$$

$$\hat{B}_r^*(\hat{z},\hat{r}) = \frac{\beta_0}{4\pi}\frac{\hat{z}}{\hat{r}}\int_0^{z_F} d\hat{z}_1 \frac{\hat{p}_e}{\hat{B}_z}\sqrt{\frac{m}{\hat{r}\hat{R}_V}} \times \left[\mathbf{K}(m) - \frac{\hat{R}_V^2 + \hat{r}^2 + (\hat{z}-\hat{z}_1)^2}{(\hat{r}-\hat{R}_V)^2+(\hat{z}-\hat{z}_1)^2}\mathbf{E}(m)\right], \tag{13}$$

where the hats over the variables indicate that they have been non-dimensionalized with B_0, n_0T_e, and R. These equations show that $B_z^*B_z < 0$ and $B_r^*B_z > 0$, so that $B_z + B_z^* < B_z$ and $B_r + B_r^* > B_r$. For $\nu_{ei} \to 0$ and $m_e/m_i \to 0$, the plasma remains attached to the total magnetic nozzle, $\mathbf{B} + \mathbf{B}^*$, and therefore detaches *divergently* from the guide field.

The divergent character of the magnetic detachment is inherent to the diamagnetic character of the azimuthal plasma current in a PMN with a positive thrust gain, as the sketch of Fig. 1(a) illustrates: the counterstreaming circuit and plasma currents induce magnetic fields that oppose one to the other and reduce the total magnetic field. This increases the radial divergence of magnetic field lines. This simple argument would justify that magnetic detachment is also divergent for the more general case of $\sigma \neq 0$, when the volumetric $j_{\theta e}$ develops inside the plasma beam.

Figure 5(a) illustrates the divergent detachment of the magnetic nozzle caused by the induced field and how it increases downstream. The magnetic detachment rate is

$$\delta_{ind} = B_\perp^*/B = (B_r^*\cos\alpha - B_z^*\sin\alpha)/B, \tag{14}$$

which is, of course, proportional to β_0. This detachment rate is plotted in Fig. 5(b) and can be compared to the diffusive detachment rates of Figs. 3(b) and 4(b). Figure 5(c) shows how the relative strength of the induced field, $|B^*/\beta_0 B|$ increases downstream, facilitating plasma demagnetization.

The elliptic character of the Ampere's law (5) is evident in Eqs. (12) and (13): the induced field at a certain location (z,r) is determined from the plasma currents in the *whole* finite nozzle $0 \le z \le z_F$. Nonetheless, a plasma current loop at (z_1, r_1) influences mostly the region around it; besides, J_θ decreases downstream. Figure 5(d) plots the contributions of the set of plasma currents to $B_z^*(z,0)$ at different axial locations; dB_z^* means the whole integrand of Eq. (12). The curves of this figure indicate that the extension of the nozzle beyond $z_F/R = 14$ will not modify the induced field for $z < z_F/2$ roughly.

The inclusion of the elliptic law (5) within our hyperbolic nozzle model would invalidate our numerical integration scheme. This does not rule out that an iterative procedure on the induced field and the plasma currents, superimposed on the hyperbolic equations for a given magnetic field, might be successful. However, a robust numerical scheme for that procedure has not been developed yet, partially because of difficulties related to the discontinuity introduced by the plasma edge and to the effect of the induced field upstream of the nozzle throat, which modifies the throat conditions. This last problem has been discussed by Ahedo recently: he analyzed, as function of β_0, the cancelation of the axial guide field inside a cylindrical source by the diamagnetic plasma current, taking into consideration resistivity and electron inertia.[19]

Contrary to the case of diffusive detachment, which is always divergent, magnetic detachment is divergent as long as the diamagnetic Hall current dominates over the paramagnetic swirl current. Magnetic detachment of convergent character would take place for a cold plasma at the nozzle throat, when the Hall current is negligible but the swirl current still develops. Then, we are in the case of Fig. 1(b), when the plasma current induces a magnetic field that reinforces the guide field, leading to nozzle stretching. This conclusion agrees with the results obtained by Arefiev and Breizman[12] and Breizman *et al.*[13]

Simulations on magnetic detachment have also been performed by Winglee *et al.*[2] These authors adopt a multifluid approach with time-dependent Maxwell equations to simulate the expansion of a uniform, sonic plasma. In spite of the significant differences with the Arefiev-Breizman framework, they propose a similar detachment scenario. Seemingly their simulations show both plasma acceleration and magnetic stretching. The information they provide have not permitted us to identify the source of the disagreement with the basic (although stationary) physical principles sketched in Fig. 1.

V. FINAL DISCUSSION

The analysis of the expansion of a sonic plasma flow injected in a divergent magnetic nozzle has determined that the three detachment mechanisms proposed in the literature increase the radial divergence of the plasma plume, further hindering the efficient beam expansion to $z \to \infty$. The key physical principles for this behavior are: first, a positive

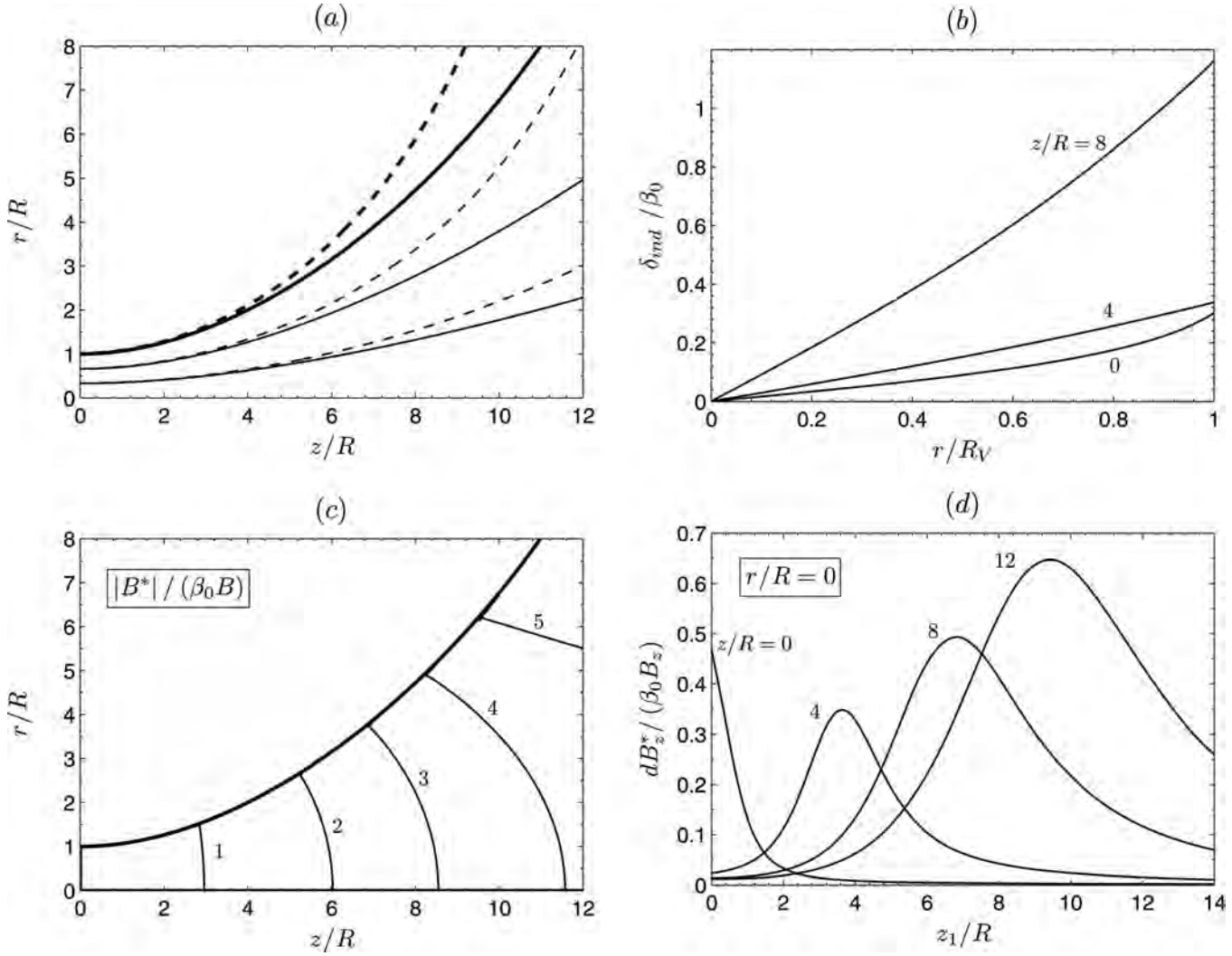

FIG. 5. Magnetic detachment for an initially uniform jet ($\sigma = 0$) and $M_0 = 1.05$, $\hat{\Omega}_{i0} = 0.1$. (a) Magnetic streamtubes for applied field (solid) total field for $\beta_0 = 0.1$ (dashed). Thick lines correspond to the plasma-vacuum edge. (b) Divergent detachment slope. (c) Map of induced-to-applied magnetic field ratio, $|B^*|/\beta_0 B$. (d) Differential induced field of the differential plasma current at $(\hat{z}_1, R_V(z_1))$ on different locations $(\hat{z}, 0)$ of the beam axis.

thrust gain in a PMN is intrinsically linked to the development of a diamagnetic electric current in the plasma, and second, this current always induces outward diffusion (either resistive or inertia-based) and a magnetic field that opposes the guide field and thus increases the divergence of the magnetic nozzle.

Plasma detachment was studied both qualitatively and quantitatively in terms of, on the one hand, the nozzle strength and the plasma conditions at the nozzle throat (Mach number and non-uniformity of the density profile), and on the other hand, the parameters defining the different detachment mechanisms (resistivity, electron-ion relative mass, and upstream beta parameter). The quantitative analysis was limited to the small-parameter range, but the basic physical principles explaining the plasma response support that the three detachment mechanisms will continue to be divergent in a PMN when non-linear effects account. Within our model frame, convergent detachment is limited to the induced-field mechanism and the case of a cold plasma at the nozzle throat, with no interest for propulsion applications.

The clear physical foundation of the divergent plasma response also supports that certain assumptions of our model are not contaminating the conclusions. In particular, divergent detachment of a sonic plasma beam will continue to occur under more general thermodynamic models for electrons. To this respect, a diamagnetic Hall current and a positive thrust gain have been confirmed when, instead of isothermal electrons, we implemented (1) electron cooling through a polytropic state law[20] and (2) a two-temperature electron population[21] (a case observed in some studies related to helicon thrusters[1,22–24]). As we already commented in the Introduction, the problem that still remains out of the bounds of our model is the propulsive and detachment behavior of the magnetic nozzle in the VASIMR.

Therefore, this work concludes that electron diffusion and magnetic stretching are not candidates for convergent separation of a hot plasma beam from a propulsive magnetic nozzle. Nonetheless, the analysis suggests two other basic processes as candidates for that separation, but they require extensions of the model and are left for further research. The first candidate for convergent detachment is simply *plasma*

demagnetization, which here means electron demagnetization. This is measured by the ratio ℓ_e/L_∇, with ℓ_e and L_∇ as the local electron gyroradius and plasma gradient length, respectively. Far from the throat, we find $O(R) \leq L_\nabla \leq O(R_V)$, with $L_\nabla = O(R)$ near the plasma edge, the region where detachment would initiate. The demagnetization parameter increases rather quickly, as

$$\ell_e/L_\nabla \propto B^{-1} \propto R_V^2. \tag{15}$$

Thus, if the nozzle divergence rate is not very large, demagnetization will take place upstream of the turning point of nozzle and beam. Furthermore, in a PMN with $\beta_0 \neq 0$, the induced magnetic field favors demagnetization: indeed, B and R_V in Eq. (15) must be understood as those corresponding to the resulting magnetic nozzle. A plasma/nozzle model (either fluid or particle-based) for this scenario is not simple to build, since it must tackle with both the magnetized and the unmagnetized regions of the plasma plume.

The second candidate for convergent detachment can be termed *electrostatic separation*. To this respect, convergent ion detachment from the magnetic and electron streamtubes was already demonstrated in Ref. 9 – see Figs. 6(a) and 6(b). The ion-electron separation is enhanced when ion magnetization is decreased, which is also the optimal case for κ_{noz} and η_{plume} in a PMN. Physically, electrons follow the increasingly divergent magnetic lines, whereas ions, weakly magnetized, supersonic, and massive, are not inclined to diverge radially. This sets up a strong electric field, perpendicular to **B**, and, associated to it, a strong rarefaction of the plasma density near the plasma edge, as Fig. 4(d) of Ref. 9 shows. In the vicinity and downstream of the nozzle turning point plasma rarefaction and electric field are going to increase sharply, and space-charge effects can matter even. Thus, even if electrons would continue to be magnetized, only a small fraction of the ion beam would turn back. The confirmation and evaluation of this detachment scenario requires a more general integration scheme, capable of extending the integration along characteristic surfaces beyond the nozzle turning point.

ACKNOWLEDGMENTS

This work has been sponsored by the Air Force Office of Scientific Research, Air Force Material Command, USAF, under grant number FA8655-10-1-3085. The U.S Government is authorized to reproduce and distribute reprints for Governmental purpose notwithstanding any copyright notation thereon. Additional support came from the Gobierno de España (Project AYA-2010-16699). The authors thank Professor Martínez-Sánchez for his smart comments, Dr. Mitat Birkan for his support, and Ismael Martínez for helping in the computations.

[1]C. Charles and R. Boswell, Appl. Phys. Lett. **82**, 1356 (2003).
[2]R. Winglee, T. Ziemba, L. Giersch, J. Prager, J. Carscadden, and B. R. Roberson, Phys. Plasmas **14**, 063501 (2007).
[3]O. Batishchev, IEEE Trans. Plasma Sci. **37**, 1563 (2009).
[4]D. Pavarin, F. Ferri, M. Manente, D. Curreli, Y. Guclu, D. Melazzi, D. Rondini, S. Suman, J. Carlsson, C. Bramanti, E. Ahedo, V. Lancellotti, K. Katsonis, and G. Markelov, in *Proceedings of the 31st International Electric Propulsion Conference, Ann Arbor, MI* (Electric Rocket Propulsion Society, Fairview Park, OH, 2009), paper 205.
[5]G. Krülle,M. Auweter-Kurtz, and A. Sasoh, J. Propul. Power **14**, 754 (1998).
[6]D. Courtney and M. Martínez-Sánchez, in *Proceedings of the 30th International Electric Propulsion Conference, Florence, Italy* (Electric Rocket Propulsion Society, Fairview Park, OH, 2007), paper 39.
[7]A. Arefiev and B. Breizman, Phys. Plasmas **11**, 2942 (2004).
[8]S. A. Andersen, V. O. Jensen, P. Nielsen, and N. D'Angelo, Phys. Fluids **12**, 557 (1969).
[9]E. Ahedo and M. Merino, Phys. Plasmas **17**, 073501 (2010).
[10]R. W. Moses, R. Gerwin, and K. Schoenberg, in *Proceedings of the Ninth Symposium on Space Nuclear Power Systems, Albuquerque, New Mexico, 1992*, AIP Conf. Proceedings No. 246, (American Institute of Physics, Woodbury NY, 1992), pp. 1293–1303.
[11]E. B. Hooper, J. Propul. Power **9**, 757 (1993).
[12]A. Arefiev and B. Breizman, Phys. Plasmas **12**, 043504 (2005).
[13]B. N. Breizman, M. R. Tushentsov, and A. V. Arefiev, Phys. Plasmas **15**, 057103 (2008).
[14]E. Ahedo and M. Merino, in *Proceedings of the 46th Joint Propulsion Conference, Nashville, TN* (American Institute of Aeronautics and Astronautics, Washington, DC, 2010), paper 6613.
[15]E. Ahedo, Phys. Plasmas **16**, 113503 (2009).
[16]E. Ahedo, in *Proceedings of the 31st International Electric Propulsion Conference, Ann Arbor, MI* (Electric Rocket Propulsion Society, Fairview Park, OH, 2009), paper 193.
[17]A. Sasoh, Phys. Plasmas **1**, 464 (1994).
[18]J. Jackson, *Classical Electrodynamics* (Wiley, New York, 1999).
[19]E. Ahedo, "Beta-induced effects in a plasma confined by a cylindrical vessel and an axial magnetic field," Phys. Plasmas (submitted).
[20]M. Merino, "Toberas magnéticas para motores espaciales de plasma," Engineer Degree thesis (Universidad Politécnica de Madrid, Madrid, Spain, 2010).
[21]M. Merino and E. Ahedo, in *Proceedings of the Space Propulsion 2010, San Sebastián, Spain* (European Space Agency, Noordwijk, The Netherlands, 2010), paper 1841391.
[22]E. Ahedo and M. Martínez-Sánchez, Phys. Rev. Lett. **103**, 135002 (2009).
[23]A. Sefkow and S. Cohen, Phys. Plasmas **16**, 053501 (2009).
[24]E. Ahedo, Phys. Plasmas **18**, 033510 (2011).

2D plasma flow in a magnetic nozzle with a bi-modal Electron Energy Distribution Function

M. Merino-Martínez*

Universidad Politécnica de Madrid, Spain

A two-dimensional plasma beam model is used to investigate the influence of a bi-modal Electron Energy Distribution Function, based on hot and cold electron populations, on the expansion of a current-free plasma through a divergent magnetic nozzle. Main results include the 2D plasma property profiles along the nozzle, for the complete quasineutral expansion regime; an analysis of quasineutral profile steepening and double layer formation in terms of the electron population parameters; the 2D structure of these flow features; and a study of their influence in the thrust, specific impulse, and plume efficiency provided by the nozzle.

I. Introduction

Magnetic nozzles constitute a promising accelerating device for electric space propulsion applications, and currently are one of the central elements in the development of advanced plasma thrusters, such as the *VAriable Specific Impulse Magnetoplasma Rocket* (VASIMR),[1] the *Applied-Field Magneto-Plasma-Dynamic Thruster* (AF-MPDT),[2,3] the *Helicon Thruster* (HT)[4,5,6] and the *Diverging Cusped field thruster* (DCFT).[7] They also present attractive benefits for a number of material processing and manufacturing applications.[8]

These nozzles consist in a convergent-divergent magnetic field, capable of guiding the plasma produced in the thruster chamber and accelerating it into vacuum. The plasma flow in a magnetic nozzle shows certain similarities with that of a heated neutral gas in a solid, *de Laval* nozzle,[9] as the plasma displays a sonic transition at the section of maximum magnetic field, B, and expands supersonically thereafter. Nevertheless, the key role of the electromagnetic interactions in a magnetic nozzle, the variety of acceleration mechanisms, and the involved plasma physics, give rise to new phenomena and complex flow characteristics, not present in the expansion of a neutral gas. Some of these phenomena can be benefited from for space propulsion applications, and can produce attractive gains in terms of the device performances.

The basic woking principle of these devices is based on the large mass difference between ions and electrons: while the former are heavier and fundamentally unaffected by moderated magnetic fields, the latter, much lighter, are completely magnetized, meaning that their trajectories are attached to the field and follow its geometry. Because of this, an appropriate magnetic field is able to radially confine the electron thermal expansion. As electrons describe the converging-diverging trajectory, an ambipolar electric field ensues in the plasma, which forces the (cold) ions to expand likewise. In this way, plasma internal (thermal) energy is converted to directed kinetic energy through the electric field.

The main advantages of magnetic nozzles over other accelerating devices are the ability to vary the produced thrust and specific impulse during operation, by altering the geometry and intensity of the applied magnetic field (the central idea behind the VASIMR, after which it is named), and the reduction/avoidance of plasma-wall contact due to the so-called magnetic screening effect, preventing serious temperature, heat transfer, efficiency decrease, and life reduction issues. Another key aspect is that, in order to neutralize the current-free beam, no external electrode is needed in principle, whose short life sets the limits of the durability of most space electric thrusters. Nevertheless, there are still some challenging aspects of magnetic nozzles which are not yet fully understood, such as the mechanisms of plasma detachment from the closed magnetic field lines far downstream, once the jet has been accelerated.

This article presents selected results from the MSc final project of the author, which has been carried out in the Polytechnic University of Madrid as part of the 'Helicon Plasma-Hydrazine combined micro'

*MSc Aerospace Engineer, mario.merino@upm.es

(HPH.com)[10] project of the 7th Framework Programme of the European Community[a]. The project HPH.com aims to produce a 50 W, dual-mode (hydrazine and plasma) thruster. In the plasma mode, it consists of a cylindrical helicon source where the plasma is produced and heated, and then, it expands and accelerates into the vacuum through a magnetic nozzle. Expected thruster performances are: 1.5 mN of thrust and a specific impulse $I_{sp} > 1200$ s.

The core aim of the MSc project is the formulation of a coherent physical model and simulation of the two-dimensional plasma expansion in a magnetic nozzle. A simulation code, baptized *DiMagNo* 2D,—acronym from 'Divergent Magnetic Nozzle,'—has been developed from zero in the project. This software implements and integrates the model numerically employing the Method of Characteristics (MoC), which makes it remarkably agile and precise, and the first of its type devoted to the simulation of magnetic nozzle flows.

Making use of the aforementioned model and code, this article presents the results of the investigation of the plasma expansion, flow phenomena and propulsive performances of a low-β, totally-ionized, collisionless plasma consisting of cold ions and hot electrons. It is shown that, under the right conditions, the inclusion of a small population of hotter electrons in the plasma, which results in a *bi-modal electron energy distribution function* (EEDF), causes the formation of certain plasma flow features known as quasineutral steepening layers (QSL) or current-free (CF) double layers (DL). This bi-modal EEDF, for the sake of simplicity, has been modeled as the superposition of two Maxwellian electron populations with distinct temperatures. The electric potential fall across these layers accelerates ions to high velocities in a short distance, which makes them an interesting phenomenon for space propulsion applications. The first set of results of the MSc Project, pertaining the plasma response and performances for a Maxwellian EEDF (a single electron species), has been recently presented.[11,12]

The rest of the paper is organized as follows: after briefly introducing the key ideas behind QSL and CF-DL formation, the role of non-Maxwellian EEDF, and commenting on some relevant experimental results in subsection A below, section II describes the full 2D model of the three-species plasma and the integration scheme, and characterizes the two-dimensional structure of the flow and its layer features in the nozzle. Next, section III highlights the main results regarding the device performances and plume efficiency, and the influence of the special EEDF on them. Finally, section IV summarizes the main conclusions of this work.

A. Plasma flow layer features and Non-Maxwellian EEDF

Essentially, a *quasineutral steepening layer* (QSL) is an electric potential fall of the order of the electron temperature, localized in a thin region of the flow, in which the plasma remains macroscopically quasineutral. When the thickness of this layer is of the order of some Debye lengths ($< 100\lambda_D$), plasma quasineutrality at the layer is not fulfilled, and one speaks of a double layer. A double layer consists of a positive and a negative Debye sheath, and connects two quasineutral regions of plasma. If no net electric current traverses the layer, it is called current-free (CF-DL). Because of its thinness in propulsive plasmas, the double layer is observed as a jump in the profiles of the electric potential and the plasma density.

Some of the most interesting phenomena appearing in magnetic nozzle flows, including QSL and CF-DL, are related to non-standard EEDF, such as when two coexisting electron populations of diverse temperature, one cold (c) and one hot (h), produce a bi-modal EEDF. This type of EEDF may be established during certain ionization and heating processes, such as those of helicon sources, where there is experimental evidence of the formation of energetic electron beams.[13]

The experiments of Hairapetian-Stenzel[14] prove the relation between the presence of hot electrons in an expanding collisionless plasma and a steepening of the electric potential profile, giving rise to a QSL, which under the right parameters becomes a CF-DL. The CF-DL is formed only in a limited range of temperature and density ratios of the two electron species.[15,16] Calling τ the hot-to-cold temperature ratio and α_0 the hot-to-total density ratio far upstream, a CF-DL forms for approximately $\tau > 10$ and a relatively low value of α_0.

Steepened but fully quasineutral QSL are formed for parametric values close to those leading to a double layer formation, which is also evidenced by their experiments. To this respect, it should be taken into account that distinction between a 'quasineutral region' and a 'non-neutral layer' has full sense only in the formal zero Debye length limit, i.e. $\lambda_D \ll L_c$, with L_c the other characteristic length of the problem.

[a]See http://www.hphcom.eu/

Charles and Boswell[4] have recently reported the formation of electric potential steepenings near the exit of a helicon source tube to a larger diffusion chamber, in the form of a CF-DL. Later, they detected ion beams with a large supersonic velocity (corresponding to a Mach number $M \simeq 2$),[17] which agrees with a potential jump in the double layer, about 3–4 times larger than the plasma temperature in the source. Due to all this evidence, the 'CF-DL helicon thruster' has been suggested as an innovative and attractive propulsion device.

When considering the energy equation of an ion in a collisionless plasma, $m_i u_i^2/2 + e\phi = \text{const}$, it is seen that whether the potential fall is more or less steepened, forming or not a double layer, is marginal for ion acceleration: as long as the plasma remains collisionless in the acceleration region, the ion beam kinetic energy is determined by the total fall of the electric potential. This fall depends on the hot electron temperature.[14] Nevertheless, it is desirable to accelerate ions in the shortest distance possible, since longer magnetic nozzles require stronger magnetic fields—and heavier field generators. Hence, ensuring that most of the potential fall will occur in a CF-DL or a QSL taking place in the near field of the nozzle is of interest for propulsive applications.

II. 2D Model formulation and numerical integration

The theoretical study of the plasma expansion in a magnetic nozzle requires establishing an appropriate model that captures all the physics of interest of the problem. The advantage of a two-dimensional model over a 1D one is the ability to recover the radial characteristics of the flow field, which among other benefits, allows to evaluate the plume efficiency of the nozzle—i.e., the divergence (or radial) losses of the jet. This section starts by formulating and describing the principal aspects of our 2D model. Unless indicated otherwise, the nomenclature used is conventional.

Consider a fully-ionized, collisionless, low-β plasma (defined as $\beta = 2\mu_0 p/B^2$, parameter that measures the relative importance of thermal pressure to magnetic pressure). Assume that the plasma is constituted of three species: cold (c) and hot (h) electron populations, and singly-charged cold ions (i). Further assume that this plasma is injected at ion-sonic velocity at the throat of an axisymmetric, diverging magnetic field, which will conform our magnetic nozzle. Under the hypothesis that the scale hierarchies

$$\lambda_D \ll \ell_e \ll R \ll \lambda_{col};\ m_e \ll m_i \tag{1}$$

are fulfilled—with ℓ_e the electron gyroradius, R the nozzle characteristic radius, and λ_{col} the shortest mean-free path of all collisional processes,—the evolution of the plasma can be adequately described with the following macroscopic, steady-state equations:

$$\nabla \cdot n_j \boldsymbol{u}_j = 0,\ (j = i, c, h)\,, \tag{2}$$

$$m_i n_i \boldsymbol{u}_i \cdot \nabla \boldsymbol{u}_i = -e n_i \nabla\phi + e n_i \boldsymbol{u}_i \wedge \boldsymbol{B}, \tag{3}$$

$$0 = -\nabla p_j + e n_j \nabla\phi - e n_j u_{\theta j} B \mathbf{1}_\perp = 0,\ (j = c, h)\,, \tag{4}$$

where $\mathbf{1}_\perp$ belongs to the orthonormal base $\{\boldsymbol{b} = \boldsymbol{B}/B, \mathbf{1}_\perp = \mathbf{1}_\theta \wedge \boldsymbol{b}, \mathbf{1}_\theta\}$, defined from the local magnetic field. Notice that, under these hypotheses, electron inertia and ion pressure have been neglected. From the length scale hierarchy of Eq. 1, it follows that electrons are completely magnetized—i.e., electron streamtubes (each species) coincide with magnetic streamtubes,—although ions can have any magnetization degree. As a consequence of the quasineutrality condition, implicitly expressed by $\lambda_D \ll R$, the last electron streamtube is also the last ion streamtube. Continuity equations (Eq. 2) show that a streamfunction ψ_j that verifies $\nabla\psi_j = n_j r \mathbf{1}_\theta \wedge \boldsymbol{u}_i$ exists for each species in the plasma ($j = i, c, h$). Similarly, there exists a magnetic streamfunction ψ_m satisfying $\nabla\psi_m = r\mathbf{1}_\theta \wedge \boldsymbol{B}$. As electron streamtubes are magnetic streamtubes, $\psi_j = \psi_j(\psi_m)$, for $j = c, h$.

Projecting Eq. 4 along $\boldsymbol{b}$ and modeling the electrons as two separate isothermal species provides

$$T_j \ln(n_j/n_{jS}) - e\phi = H_j(\psi_m)\,,\ (j = c, h) \tag{5}$$

where the subindex S denotes the throat section, $z = 0$, and n_{jS} is the particle density of species j at the origin. The function $H_j(\psi_m)$ is constant if the plasma is initially uniform. The same equation projected along $\mathbf{1}_\perp$ yields

$$e u_{\theta j}/r = -dH_e/d\psi_m, \tag{6}$$

which allows to calculate $u_{\theta j}$. From this expression it follows that, if $u_{\theta j}$ is initially zero in our non-collisional plasma, *it remains so throughout the expansion*. The ion momentum equation (Eq. 3) along $\mathbf{1}_\theta$ can be integrated to obtain

$$r m_i u_{\theta i} + e\psi = D_i\left(\psi_i\right), \tag{7}$$

which states the conservation of ion axial angular momentum. These relations conform a set of algebraic equations that provide n_c, n_h, and $u_{\theta j}$ $(j = i, c, h)$ as functions of ϕ, initial conditions, and the local value of the magnetic field.

Since ion flow is supersonic in the diverging nozzle, to obtain the variables u_{zi}, u_{ri} and ϕ, the method of characteristics (MoC) is employed to reduce the remaining partial differential equations—ion continuity equation, and ion momentum in the z and r directions—into ordinary differential equations along characteristic lines. The MoC exploits the physical properties of the problem, namely, that perturbations propagate along these curves. Due to this, the method is one of the fastest and most accurate for the solution of hyperbolic problems.[18]

The resulting equations along the Mach lines (denoted as the C_+, C_- curve families) and the ion streamlines (C_o) are:

$$u_{ri}\left.\frac{du_{zi}}{dz}\right|_{C_\pm} - u_{zi}\left.\frac{du_{ri}}{dz}\right|_{C_\pm} \mp \frac{e\sqrt{M^2-1}}{m_i}\left.\frac{d\phi}{dz}\right|_{C_\pm} = \\ = \left(u_{ri} - \lambda_\pm u_{zi}\right) f + \lambda_\pm g - h \tag{8}$$

$$\left.\frac{d}{dz}\right|_{C_o}\left(\frac{1}{2}m_i u_i^2 + e\phi\right) = 0 \tag{9}$$

where $\lambda_\pm = \left(u_{zi}u_{ri}/c_s^2 \pm \sqrt{M^2-1}\right)/\left(u_{zi}^2/c_s^2 - 1\right)$ and $\lambda_o = u_{ri}/u_{zi}$ are the local slopes of the characteristic curves, and

$$f = \sum_{j=c,h}\left(\frac{e n_j u_{\theta j}}{n T_j}\right)\left(u_{ri}B_z - u_{zi}B_r\right) - \frac{u_r}{r};$$

$$g = -u_{\theta i}\frac{eB_r}{m_i};\quad h = u_{\theta i}\frac{eB_z}{m_i} + \frac{u_{\theta i}^2}{r},$$

where c_s is the local ion sound velocity, $c_s = \sqrt{\gamma T/m_i}$, with γ the (effective) specific heat ratio defined as

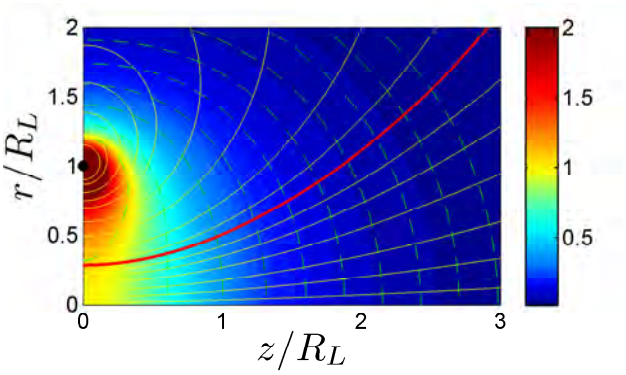

Figure 1: Meridian plane of the magnetic field created by a current loop placed at $r = R_L$. Yellow lines are field lines. The line chosen as nozzle outer line has been highlighted in red. Green, dashed lines represent B-constant lines. The background color shows the magnetic field intensity relative to B_S, its value at the origin.

$$\gamma = \frac{n}{p}\frac{dp}{dn} = \frac{n^2}{\left(n_h T_h + n_c T_c\right)\left(n_h/T_h + n_c/T_c\right)}, \tag{10}$$

and T the average electron temperature,

$$T = \left(n_h T_h + n_c T_c\right)/n. \tag{11}$$

Notice that Eq. 9 expresses the conservation of ion mechanical energy along streamlines, and that generally $H_i\left(\psi_i\right)$ can vary across streamlines, if initial conditions are not uniform.

Electron continuity equations then provide

$$\frac{n_j u_{\parallel j}}{B} = G_j\left(\psi_j\right),\ (j = c, h), \tag{12}$$

which, with a proper boundary condition, yield $u_{\parallel j}$, the component of the electron fluid velocity in the meridian plane (parallel to the magnetic field).

Although the model is applicable to any divergent magnetic nozzle, for the sake of illustration in the following the magnetic circuit is here reduced to a single current loop placed at $(z, r) = (0, R_L)$, with an intensity I_L flowing along 1_θ. For such a current loop, the magnetic streamfunction is:[19]

$$\psi_m\left(z, r\right) = \frac{2B_S R_L^2 r}{\pi}\cdot\frac{\left(2-k^2\right)\mathbf{K}\left(k^2\right) - 2\mathbf{E}\left(k^2\right)}{k^2\sqrt{\left(R_L + r\right)^2 + z^2}}, \tag{13}$$

where $k^2 = 4R_L r[(R_L + r)^2 + z^2]^{-1}$, $B_S = B_z(0,0) = \mu_0 I_L/(2R_L)$, and $\mathbf{K}(m)$ and $\mathbf{E}(m)$ are the complete elliptic integrals of the first and second kind.[20] The dimensionless number R_L/R_S, where R_S is the plasma radius at the throat, controls the divergence rate of the nozzle. The condition $\beta \ll 1$ implies that the magnetic field induced by the plasma internal currents can be neglected with respect to the applied field (at least, in the near-region of the nozzle). Hence, our nozzle's magnetic field geometry coincides with that of the guide field. Fig. 1 presents this magnetic field.

The mathematical expressions of the model can be made non-dimensional using n_S (total electron density at the origin), T_c, e, m_i, and R_S. Dimensionless variables will be distinguished with a hat, i.e., $\hat{u}_{zi} = u_{zi}/\sqrt{T_c/m_i}$ for the ion velocity, $\hat{\phi} = e\phi/T_c$ for the potential, and so on.

The model depends on the following non-dimensional parameters: $\tau = T_h/T_c$, the already introduced temperature ratio between the two electron species, and $\alpha_S = n_{hS}/n_S$, the hot-to-total density ratio at the origin. These two parameters are the object of our analysis. The problem also depends on R_L/R_S, which describes the divergence rate of the nozzle, and $\hat{\Omega}_{iS}$, the non-dimensional ion gyrofrequency at the origin, which evaluates the degree of ion magnetization. The values $\hat{R}_L = 3.5$ and $\hat{\Omega}_{iS} = 0.1$ were chosen as representative values of current thruster designs based on magnetic nozzles.[5,21] Also, nozzle performances improve for slowlier diverging fields and low ion magnetization, although plasma flow is almost uninfluenced by variations of the latter of these parameters in the range 0.01–10.[12]

The dependency of $\hat{n}$, $\hat{T}$, $\hat{c}_s$ and γ on $\hat{\phi}$ is illustrated in Fig. 2, which portraits the anomalous thermodynamics of the plasma, caused by the bi-modal EEDF. The most outstanding feature is the unusual behavior of the specific heat ratio, γ, whose value $\gamma < 1$ means that the average electron temperature T increases as the plasma travels downstream. This is due to the fact that cold electrons are effectively confined by the electric potential fall that occurs as the plasma expands, while hotter, more energetic electrons are able to travel further downstream. As it will be seen, this effect is responsible of the formation of special layer features in the flow.

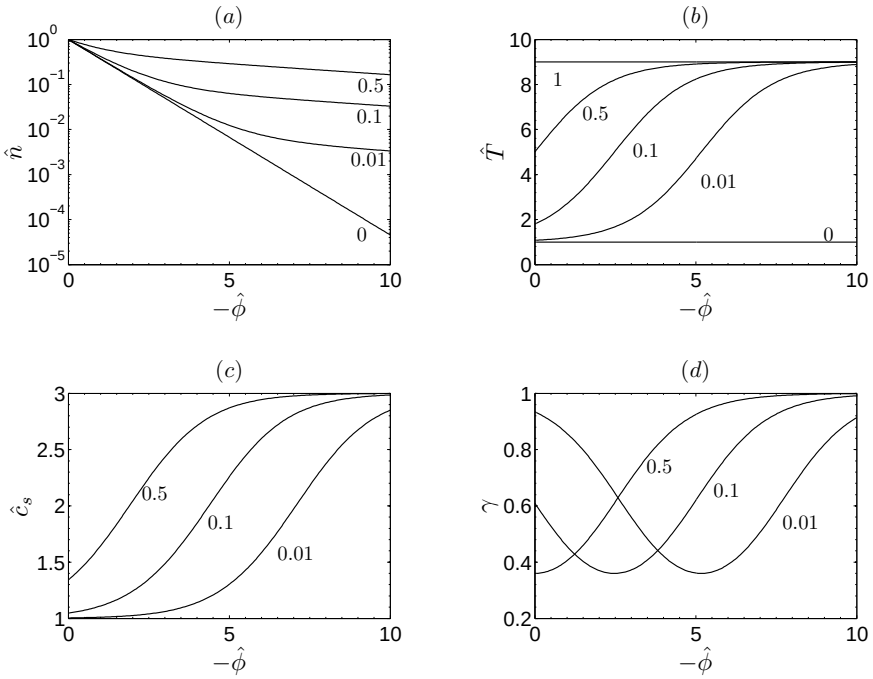

Figure 2: Dependence of the main variables with ϕ for $\tau = 9$. Numbers by the lines indicate the value of α_S of each line.

In regard to the initial conditions at the throat, for this analysis we will choose a uniform plasma with no electrical currents, entering the nozzle at a velocity slightly higher than the sonic velocity, to make the problem completely hyperbolic in order to apply the MoC (a ion Mach number $M_S = 1.05$ was chosen, after checking that the solution was insensitive to small variations of M_S when $M_S - 1 \ll 1$).

Previous work by Ahedo and Martínez-Sánchez[15,16] using a 1D model point out the existence of different

parametric regions where a CF-DL forms in the convergent side, throat or divergent side of the nozzle. Fig. 3 presents the region of the τ, α_S plane where a CF-DL forms in the divergent nozzle, which is delimited by a curve. In the following, we will perform our 2D analysis by studying the plasma response as we increase α_S and approach $\alpha_{S,1}$ for different values of τ.

Fig. 4 covers a number of cases with $\tau = 9$. In these graphs, the different variables have been referred to T_S,

$$T_S = (1 - \alpha_S)\, T_c + \alpha_S T_h, \tag{14}$$

which allows to compare the behavior of each plasma in equal terms with respect to their internal energy at the throat. This shows an interesting increase in the total potential fall for the three-species plasma, when compared against a single electron species plasma, between sections S and the chosen exit section at $\hat{z} = 6$, E (which has an exit radius of $\hat{R}_E = 3.15$, and hence the nozzle's area ratio is roughly $\varepsilon \simeq 10$).

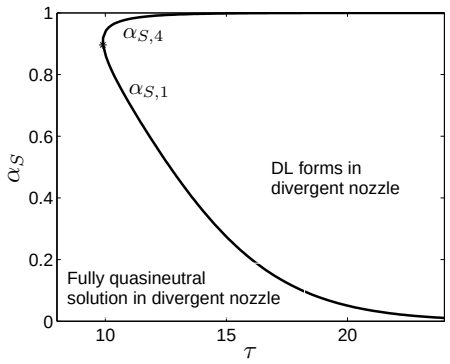

Figure 3: Parametric regions of the plane τ, α_S, portraying a quasineutral expansion region and a zone where CF-DL form. The curve given by the functions $\alpha_S(\tau) = \alpha_{S,1}$ and $\alpha_{S,4}$ separate both regions. (Adapted here from the 1D model analysis of Ahedo and Martínez-Sánchez[16]).

As it can be seen, a mild QSL forms at different positions in the nozzle, and it moves toward the throat as α_S increases. The Mach number decreases and reaches a minimum around this spot. This outstanding behavior is a result of the specific heat ratio being lower than 1, as seen in fig. 2, which makes the average plasma temperature and the sonic velocity c_s to increase, while the ion Mach number decreases. This is an effect of the anomalous thermodynamics, and causes a large electric potential fall to concentrate in this region, giving rise to the QSL. The 2D expansion points out that the minimum Mach number is reached first on the plasma edge than on the axis. Actual ion velocity is always monotonic, and increases substantially with respect to the reference case, due to the increased electric potential fall produced by the presence of hot electrons. This velocity presents large differences between its value on the outer and inner lines, specially around the QSL. This difference decreases after this steepening, to start increasing slowly afterward again. The fact that $u_i/\sqrt{T_S/m_i}$ is larger in the simulation with $\alpha_S = 0.2$ (blue) than in the one with $\alpha_S = 0.1$ (red) in spite of the nearly equal final potential $\hat{\phi}$ is due to the role of the specific heat ratio function: from the equation of ion energy, Eq. 9: $u_i^2/(T_S/m_i) = 1 - 2e\phi/(T_S\gamma)$.

Fig. 4 (c) shows that downstream of the QSL, the potential at the exterior line falls at a higher rate than at the center line. This difference of potential translates into a radial electric field that accelerates ions, adding to the radial losses. The QSL has a maximum E_z electric field on the axis, fig. 4 (d), at roughly $\alpha_S = 55\%$ when measured relative to T_c, and at low α_S relative to T_S. However, this larger maximum of the electric field for low α_S takes place always further downstream as α_S is decreased, revealing the necessity to operate with ever larger magnetic nozzles—and therefore ever stronger magnetic fields—to take advantage of this flow phenomenon. Therefore, for propulsion applications, where the objective is to deliver maximal thrust at minimum weight, it may be interesting to position the QSL closer to the nozzle throat, so ions are earlier accelerated by this structure.

Analogously, Fig. 5 presents the results for $\tau = 18$. In this case, as we are approaching the limit line $\alpha_{S,1}(\tau)$, the Mach number at the steepening point decreases rapidly to 1, again due to the anomalous behavior of γ. The simulation with $\alpha_S = 0.09$ presents a very sharp minimum of M on both the outer and center streamlines, which for $\alpha_{S,1}$ would actually become an angulous point, revealing the onset of a CF-DL discontinuity, and at the same time the flow would become (sub)sonic. On this line and beyond, the existence of a secondary sonic transition turns the system of equations parabolic at that position, and the integration with the MoC is stopped. At any rate, the cases of propulsive interest are those where the hot-to-total electron density ratio is small, say $\alpha_S < 0.1$, and we will focus our analysis on them. Ion velocity differences between both streamlines in the neighborhood of the QSL become much larger for $\tau = 18$ than for $\tau = 9$. Interestingly, the potential along these streamlines does not diverge as much as for $\tau = 9$ after the steepening. The maximum electric field on the axis is very acute, and would become infinite when the CF-DL discontinuity develops, at $\alpha_{S,1}$.

As it can be seen in Figs. 4 and 5, the evolution of the plasma along the axis line and the outer streamline

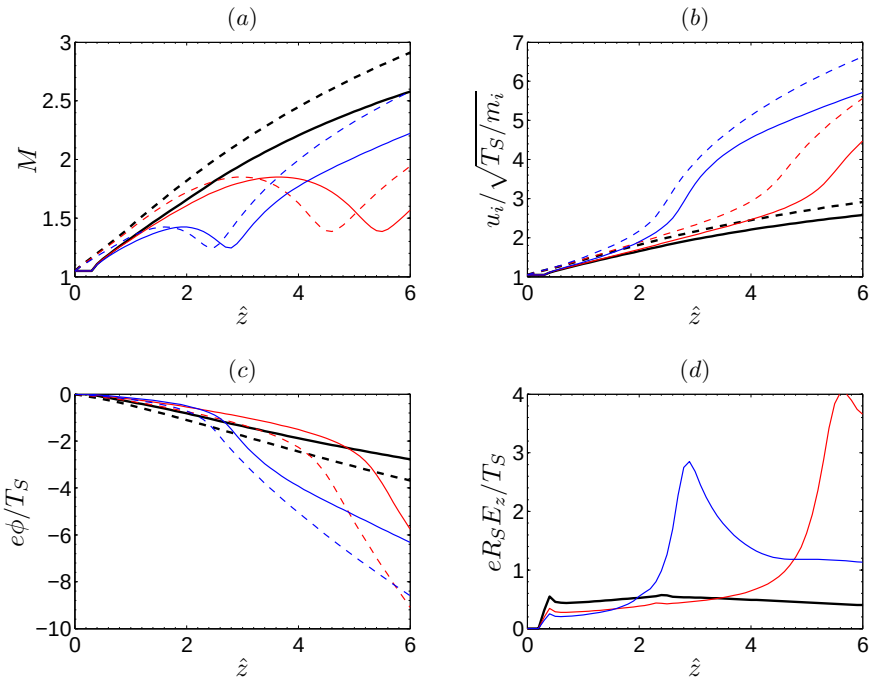

Figure 4: 2D plasma expansion profiles with $\tau = 9$. Various simulations with different α_S have been plotted: thick lines represent the reference two-species plasma ($\alpha_S = 0$ or $\alpha_S = 1$, which coincide since results are referred to T_S). Red lines show $\alpha_S = 0.1$, and blue lines $\alpha_S = 0.2$. Values at the center line are in solid lines. Dashed lines refer to the exterior streamline. End section, $\hat{z}_E = 6$, has $\hat{R}_E \simeq 3.15$.

is similar for each variable, but the position of the QSL on the outer one occurs slightly before than on the center one. This reveals the 2D structure of this flow feature, which can be better appreciated in Fig. 6. While potential isolines possess a near-parabolic shape, with a curvature that increases further downstream (note however that in the $\tau = 18$ case this shape becomes slightly more complicated downstream of the QSL), the geometry of the region of maximum electric field, $eR_S E/T_S$, does not exactly coincide with these lines, and presents a slightly different shape. This is due to the fact that ϕ-isolines are less spaced at the outer streamline than at the axis, because of their increasing curvature. This shows that radial differences exist that affect the way ions are accelerated, and additionally indicates that it is preferable to have the QSL close to the throat, as it becomes more planar and most ion acceleration across it would be in the z-direction, reducing radial losses.

III. Propulsive performances of the three-species plasma

After characterizing the plasma expansion in the quasineutral parametric region with the 2D model, we now turn our attention to the influence of the hot electron tail on the propulsive parameters of the nozzle. Although our plasma model can estimate the propulsive gains and the radial losses, it cannot provide information on the global efficiencies of the device. This would require matching with (a) the upstream process of plasma ionization and heating, and (b) the modeling of the magnetic detachment far downstream, which is out of the scope of the present work.

The main parameters of interest that describe the potential of the system as an accelerating device are the produced thrust F_E, the specific impulse $I_{sp} = F_E/\dot{m}_i$ (here in velocity units), and the plume efficiency η_{plume}. Since I_{sp} is the effective plasma velocity at the nozzle exhaust, its increment with respect to ion velocity at the entrance is approximately proportional to the square root of the total potential fall between stations S and E: $I_{sp} \propto \sqrt{2e\left(\phi_S - \phi_E\right)/m_i}$. A first measure of the energy spent on the plasma in the thruster chamber is the average electron temperature at the origin, T_S. Therefore, for propulsion applications it is of great interest to analyze the potential fall obtained for different τ, α_S, relative to this

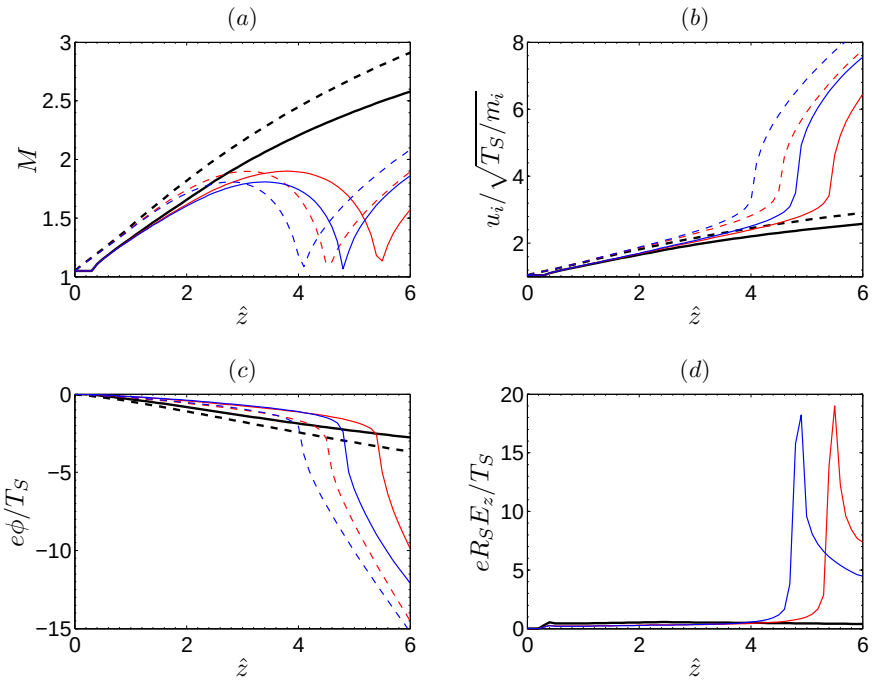

Figure 5: 2D plasma expansion profiles with $\tau = 18$. Similarly to the previous figure, thick lines are for the reference, two-species plasma ($\alpha_S = 0$ or $\alpha_S = 1$). Red lines show $\alpha_S = 0.07$, and blue lines $\alpha_S = 0.09$, very close to the limit line $\alpha_{S,1}(\tau)$ of CFDL formation. Values at the center line are in solid lines. Dashed lines refer to the exterior streamline. Again end section is located at $\hat{z}_E = 6$, with $R_E \simeq 3.15$.

temperature. This fall was shown in Figs. 4 and 5. As it can be seen, a small fraction of hot electrons ($\alpha_S \simeq 0.1$) can more than triple the normalized potential fall along the nozzle. This outstanding result claims that three-species plasmas can bring important benefits, in terms of higher propulsive performances. A minor decrease in potential fall is registered for α_S too small. This is due to the QSL taking place after section E, which would otherwise increase this fall as for higher α_S.

The plasma total momentum flux along the nozzle at $z = \text{const}$ sections, $F(z)$, can be separated into its ion/momentum and electron/pressure contributions, i.e.,

$$F(z) = F_i(z) + F_e(z), \tag{15}$$

with

$$F_i = \int_{A(z)} m_i n u_i^2 dA,\ F_e = \int_{A(z)} (n_c T_c + n_h T_h) dA. \tag{16}$$

As the magnetic nozzle transforms internal plasma energy into kinetic energy, ion/momentum thrust increases while electron/pressure thrust decreases. Fig. 7 depicts this thrust development, comparing a two-species plasma with diverse three-species ones. As it can be seen, the hot electron tail causes a large increase in ion/momentum thrust at the location of the QSL, becoming more than two times larger in certain cases. The total plasma momentum also increases with respect to the reference, two-species plasma, although this increase is not concentrated at any particular position. The differences between the profiles of the total momentum for different values of α_S are smaller than for the ion momentum. This is due to the electron/pressure contribution to the total momentum, which registers a large fall at the QSL position, compensating for the increase in ion/momentum thrust.

The ratio of thrust between stations S and E is defined as F_E/F_S, which coincides with the ratio of the specific impulse to $F_S/\dot{m}_i$ — i.e., the specific impulse that would be obtained if no nozzle existed. These two factors are independent of the plasma internal energy at the throat, but depend largely on the electron population parameters τ, α_S.

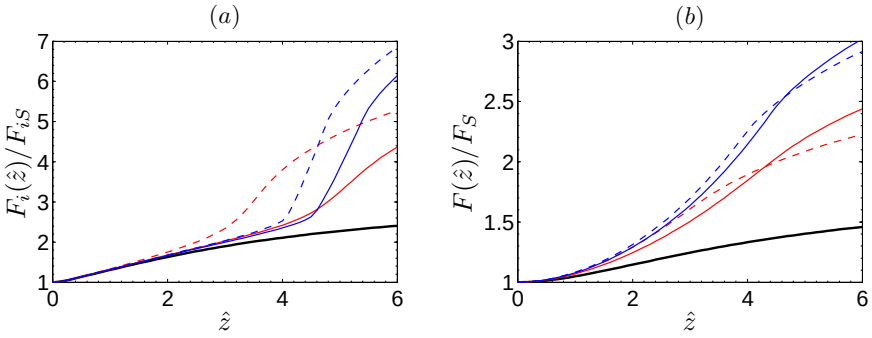

Figure 7: Ion and total plasma momentum evolution along the nozzle at $z = \text{const}$ sections. Thick black lines are the reference two-species plasma. Red lines denote $\tau = 9$ (with $\alpha_S = 0.1$ for the solid line, and $\alpha_S = 0.2$ for the dashed line). Blue lines indicate $\tau = 18$ (with $\alpha_S = 0.07$ for the solid line, and $\alpha_S = 0.09$ for the dashed line).

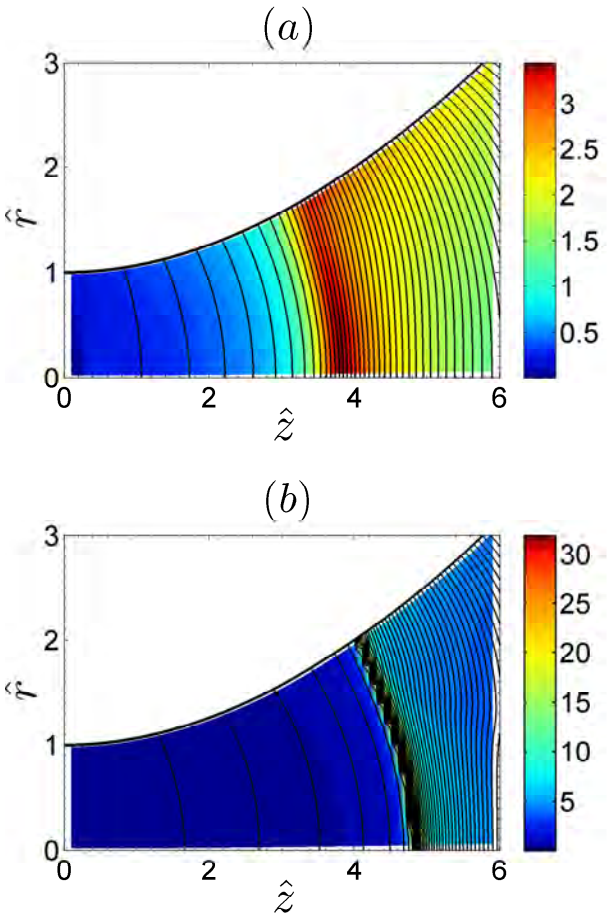

Figure 6: Electric field intensity inside the nozzle, eR_SE/T_S (background color), and plasma potential isolines. Figure (a) shows a mild QSL, for $\tau = 9$ and $\alpha_S = 0.2$. Figure (b) presents a much more intense QSL, for $\tau = 18$ and $\alpha_S = 0.09$.

The nozzle (or plume) efficiency η_{plume} reflects the amount of kinetic energy that is wasted in radial losses, and it is one of the factors contributing to thrust efficiency of the whole thruster. Defined at each $z = \text{const}$ section, its expression is:

$$\eta_{plume}(z) = \frac{P_{zi}(z)}{P_i(z)} \simeq \frac{F_i^2(z)}{2\dot{m}_i P_i(z)} \tag{17}$$

with the axial and total ion kinetic powers defined as

$$P_{zi}(z) = \int_{A(z)} \frac{1}{2} m_i n u_{zi}^3 dA,$$
$$P_i(z) = \int_{A(z)} \frac{1}{2} m_i n u_i^2 u_{zi} dA. \tag{18}$$

Simulation results presented in Fig. 8 point out that no relevant change in plume efficiency occurs. However, a slight decrease in η_{plume} with respect to the two-species plasma case is found locally around the QSL, which is afterward recovered. In some cases ($\tau = 18$, for instance), η_{plume} reaches a minimum, after which it increases again in a small region. This apparently surprising result can be explained if we consider the 2D structure of the plasma expansion: as we saw in Fig. 6, the QSL takes place along a slightly curved line, and not at $z = \text{const}$. When ions cross this line, they experience a large acceleration, and due to its curved shape, ions near the outer border are accelerated first, and acquire a strong radial component. This affects the overall efficiency at that $z = \text{const}$ section, lowering it. Some distance downstream, centerline ions cross the QSL, gaining a large axial velocity, which compensates for this decrease, and (temporarily) rises the value of η_{plume} again.

To separate the influence of the 2D geometry of the problem at hand, we shall also define the plume

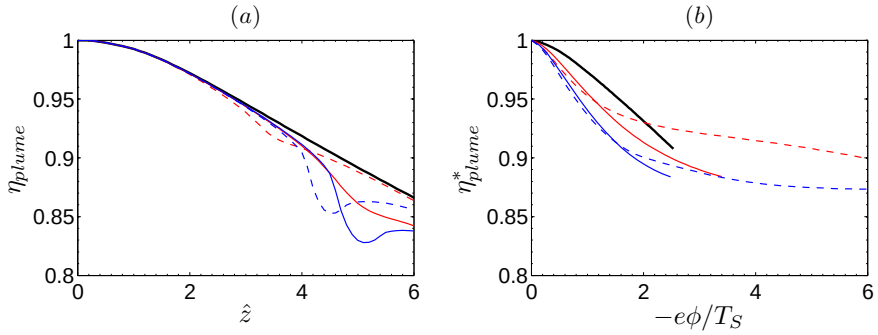

Figure 8: Plume efficiency obtained with the magnetic nozzle for different plasmas. Figure (a) presents this value on z-constant surfaces. Figure (b) displays the value of η_{plume} on ϕ-constant surfaces, denoted by η^*_{plume}. Thick black lines show the reference, two-species plasma case. Red lines correspond to $\tau = 9$ (solid: $\alpha_S = 0.1$, dashed: $\alpha_S = 0.2$), and blue lines to $\tau = 18$ (solid: $\alpha_S = 0.07$, dashed: $\alpha_S = 0.09$).

efficiency at ϕ-constant surfaces, η^*_{plume}:

$$\eta^*_{plume}(\phi) = \frac{P^*_{zi}(\phi)}{P^*_i(\phi)}, \tag{19}$$

where

$$P^*_{zi}(\phi) = \int_{A(\phi)} \frac{1}{2} m_i n u_{zi}^2 \boldsymbol{u}_i \cdot \boldsymbol{n} dA,$$
$$P^*_i(\phi) = \int_{A(\phi)} \frac{1}{2} m_i n u_i^2 \boldsymbol{u}_i \cdot \boldsymbol{n} dA. \tag{20}$$

The graph of Fig. 8 (b) presents the value of η^*_{plume} at constant-$(e\phi/T_S)$ surfaces. As it can be seen, now the efficiency decreases monotonically. Notice that, since each simulation reaches a different final value of the potential, ϕ_E, each line ends at a different abscissa. From this figure, some conclusions can be drawn about the actual behavior of the plume efficiency in terms of τ and α_S. First of all, the presence of a hot electron tail causes a minor negative effect on the efficiency, slightly increasing radial losses. This effect seems to be more pronounced for higher τ. With respect to the influence of α_S, η^*_{plume} is maximal for $\alpha_S = 0$ (two-species plasma). As α_S increases from 0, this efficiency starts to decrease and soon reaches a minimum. For higher values of α_S, the efficiency slowly increases again, since lines for $\alpha_S = 1$ and $\alpha_S = 0$ coincide.

IV. Conclusions

This paper has analyzed the influence of a bi-modal electron energy distribution function (modeled as two coexisting hot and cold electron populations) on the plasma expansion through a divergent magnetic nozzle. A 2D model has been used to characterize the three-species plasma flow, and discuss the appearance of quasineutral steepening layers in the plasma magnitudes. These special flow features can coalesce into non-neutral current-free double layers, depending on the value of the electron species parameters that define the EEDF: the electron temperature ratio τ, density ratio at the throat α_S. Results reveal that a small hot electron tail can induce vast benefits on the propulsive performances of the magnetic nozzle. The relative thrust and specific impulse can more than double if the temperature and density ratios are adequate. Although the plume efficiency, η_{plume}, suffers a minor decrease, it is nevertheless outweighed by the largely increased total potential fall that the three-species plasma cause. Simulations reveal the curved shape of the ϕ-constant lines, and that the maximal E field line does not coincide with them.

Additionally, all the analyses lead us to conclude that the gains are due to the increased potential fall caused by the anomalous thermodynamics—characterized by an effective specific heat ratio γ lower than 1, meaning that the plasma temperature rises as it expands. The magnitude of this fall depends strongly on the temperature ratio τ. Whether this fall occurs in a quasineutral steepening layer or a double layer is irrelevant for the plasma response, as long as it takes place in the near plasma field. Actually, the difference

between both is a matter of scale only. The double layer formation has no role in the propulsion gain, it is only another consequence of these thermodynamics.

During this project a fast and accurate software called DiMagNo 2D has been developed for the investigation of magnetic nozzles, which employs the method of characteristics to calculate the flow field in the diverging nozzle. Due to its modularity, it allows to study magnetized plasma flows under many different conditions. Our current research is focused on the problem of plasma detachment from the magnetic nozzle, for which the DiMagNo code has proven to be a valuable tool.

Acknowledgments

The author would like to express his gratitude to E. Ahedo for our long, mind-opening discussions, and his invaluable support and dedication as the supervisor of this MSc project.

This work was financed by Gobierno de España (Plan Nacional de I+D, Project ESP2007-62694) and the European Community (7th Framework Programme, Grant 218862, project HPH.com).

References

[1]Arefiev, A. and Breizman, B., "Theoretical components of the VASIMR plasma propulsion concept," *Physics of Plasmas*, Vol. 11, No. 5, 2004, pp. 2942–2949.

[2]Sasoh, A. and Arakawa, Y., "Electromagnetic effects in an applied-field magnetoplasmadynamic thruster," *Journal of Propulsion and Power*, Vol. 8, No. 1, 1992, pp. 98–102.

[3]Krülle, G., Auweter-Kurtz, M., and Sasoh, A., "Technology and application aspects of applied field magnetoplasmadynamic propulsion," *J. Propulsion and Power*, Vol. 14, 1998, pp. 754–763.

[4]Charles, C. and Boswell, R., "Current-free double-layer formation in a high-density helicon discharge," *Applied Physics Letters*, Vol. 82, No. 9, 2003, pp. 1356–1358.

[5]Batishchev, O., "Minihelicon Plasma Thruster," *IEEE Transaction on Plasma Science*, Vol. 37, 2009, pp. 1563–1571.

[6]Ziemba, T., Carscadden, J., Slough, J., Prager, J., and Winglee, R., "High Power Helicon Thruster," *41th Joint Propulsion Conference, Tucson, AR*, AIAA 2005-4119, American Institute of Aeronautics and Astronautics, Washington DC, 2005.

[7]Courtney, D. and Martinez-Sanchez, M., "Diverging Cusped-Field Hall Thruster," *30th International Electric Propulsion Conference, Florence, Italy*, IEPC-2007-39, Electric Rocket Propulsion Society, Fairview Park, OH, 2007.

[8]Schoenberg, K., Gerwin, R., Moses, R., Scheuer, J., and Wagner, H., "Magnetohydrodynamic flow physics of magnetically nozzled plasma accelerators with applications to advanced manufacturing," *Physics of Plasmas*, Vol. 5, 1998, pp. 2090–2104.

[9]Andersen, S. A., Jensen, V. O., Nielsen, P., and D'Angelo, N., "Continuous Supersonic Plasma Wind Tunnel," *Phys. Fluids*, Vol. 12, 1969, pp. 557–560.

[10]Ferri, D. P. F., Manente, M., Curreli, D., Guclu, Y., Melazzi, D., Rondini, D., Suman, S., Carlsson, J., Bramanti, C., Ahedo, E., Lancellotti, V., K.Katsonis, and Markelov, G., "Design of 50W Helicon Plasma Thruster," *31th International Electric Propulsion Conference, Ann Arbor, Michigan, USA*, IEPC 2009-205, Electric Rocket Propulsion Society, Fairview Park, OH, 2009.

[11]Ahedo, E. and Merino, M., "Two-dimensional plasma acceleration in a divergent magnetic nozzle," *44th Joint Propulsion Conference, Hartford, CT*, AIAA 2009-5361, American Institute of Aeronautics and Astronautics, Washington DC, 2008.

[12]Ahedo, E. and Merino, M., "Two-dimensional supersonic plasma acceleration in a magnetic nozzle," *Physics of Plasmas*, Vol. 17, 2010, pp. 073501.

[13]Chen, R. T. S. and Hershkowitz, N., "Multiple Electron Beams Generated by a Helicon Plasma Discharge," *Physical Review Letters*, Vol. 80, 1998, pp. 4677–4680.

[14]Hairapetian, G. and Stenzel, R. L., "Particle dynamics and current-free double layers in an expanding, collisionless, two-electron-population plasma," *Physics of Fluids B*, Vol. 3, No. 4, 1991, pp. 899–914.

[15]Ahedo, E. and Martinez-Sanchez, M., "The Role Of Current-Free Double-Layers In Plasma Propulsion," *44th Joint Propulsion Conference, Hartford, CT*, AIAA 2008-5005, American Institute of Aeronautics and Astronautics, Washington DC, 2008.

[16]Ahedo, E. and Martinez-Sanchez, M., "Theory of a stationary current-free double-layer in a collisionless plasma," *Physical Review Letters*, Vol. 103, 2009, pp. 135002.

[17]Charles, C. and Boswell, R., "Laboratory evidence of a supersonic ion beam generated by a current-free 'helicon' double-layer," *Physics of Plasmas*, Vol. 11, 2004, pp. 1706–1714.

[18]Zucrow, M. and Hoffman, J., *Gas dynamics* , Wiley, New York, 1976.

[19]Jackson, J., *Classical Electrodynamics*, Wiley, New York, 1999.

[20]Abramowitz, M. and Stegun, I., *Handbook of Mathematical Functions*, Dover, New York, 1965.

[21]Winglee, R., Ziemba, T., Giersch, L., Prager, J., Carscadden, J., and Roberson, B. R., "Simulation and laboratory validation of magnetic nozzle effects for the high power helicon thruster," *Physics of Plasmas*, Vol. 14, 2007, pp. 063501.

Double-layer formation and propulsive assessment for a three-species plasma expanding in a magnetic nozzle

Eduardo Ahedo[a)]
ETS Ingenieros Aeronáuticos, Universidad Politécnica de Madrid, Madrid 28040, Spain

(Received 22 October 2010; accepted 23 February 2011; published online 29 March 2011)

The quasi one-dimensional expansion of a collisionless plasma with a hot-electron tail in a gentle convergent-divergent nozzle is studied. A parametric investigation of the plasma response is carried out in terms of the relative density and temperature of the hot-electron population. The formation of a steepened layer is shown to be due to the anomalous thermodynamic behavior of the plasma, which creates a local minimum of the Mach number. The change from a quasineutral to a non-neutral steepened layer occurs when this minimum goes below one and several sonic points appear. The non-neutral double layer does not introduce further changes in the plasma response. All gain in plasma momentum and thrust is related to the supersonic expansion in the divergent nozzle, with zero contribution of the double layer. A comparative analysis of thrust efficiency of plasmas with and without hot electrons does not find any gain in the presence of hot electrons; instead, a small penalty in the expansion efficiency seems to exist. The study is limited to Maxwellian electron populations and finite nozzles. © *2011 American Institute of Physics*.
[doi:10.1063/1.3567159]

I. INTRODUCTION

Space plasma thrusters based on helicon sources are a subject of current research.[1–4] In its simplest design, a helicon thruster consists of a discharge chamber and a magnetic nozzle. The chamber is a cylindrical helicon source where the plasma is produced and heated. Then, the magnetic nozzle transforms the plasma internal energy into a supersonic ion beam, with the aid of the ambipolar electric field.[5–7] The helicon thruster is an electrothermal thruster and no external cathode is needed to neutralize the ejected current-free plasma.

Charles and Boswell reported the formation of a current-free double layer (CFDL) near the interphase of a helicon source and a larger diffusion chamber[1] and related the presence of a supersonic ion beam to the jump in electric potential across the CFDL.[8] These experiments aroused a large expectation because it was suggested that 'the CFDL in an expanding plasma could be the basis of an enhanced type of space plasma thruster',[1] referred to later as the Helicon Double Layer Thruster (HDLT).[9]

A double layer (DL) consists of a positive and a negative Debye sheath, connecting two quasineutral regions of the plasma. Because of its thinness, the double layer is observed as a jump in the profiles of the electric potential and the plasma density; theoretical models invoke the zero Debye length limit and treat the DL as a discontinuity in the quasineutral plasma. The CFDL is a particular case of DL known from studies on the expansion of laser-produced plasma coronas[10–12] and material processing with electronegative plasmas.[13–16] In *all* these studies, the CFDL is formed within a plasma that contains two negative species *with disparate temperatures*, and for a limited range of the density ratio of these species. It makes basically no difference whether these species are either electrons and (cold) negative ions or cold and hot electrons. An excellent experiment on the formation and properties of a CFDL is due to Hairapetian and Stenzel,[17] who studied the expansion of a collisionless plasma with a controlled population of hot electrons, about 20 times hotter than the main electron population. They demonstrated (i) the direct relation between the presence of hot electrons and the formation of a steepened potential profile, and (ii) the scaling of the supersonic ion beam energy with the hot-electron temperature.

In addition to the Charles–Boswell experiment, the presence of a CFDL has been claimed in other helicon sources.[18–20] Also, a hot-electron tail has been reported in several helicon-based plasmas.[19,21–24] However, important issues related to both the CFDL properties and its relevance as a propulsion mechanism remain unanswered. First, the CFDL does not form in all helicon source experiments and the same seems to be true with respect to the hot-electron tail. Thus, the operational conditions that assure the presence of the hot-electron tail and the CFDL and the connection between these two phenomena must be clarified.

Second, it is uncertain whether the Charles–Boswell DL is identical to the Hairapetian–Stenzel one. In the last case, all the plasma is produced upstream and then expanded into vacuum (which is also the desirable scenario for a space plasma thruster). In the Charles–Boswell experiment, there is a significant plasma production downstream the DL, which leads to an extra population there of trapped low-energy ions and additional cold electrons that are likely to have some effect on the DL formation.

Third, the CFDL is a weak type of double layer, in the sense that the degree of non-neutrality (measured as the ratio of the electric charge density to the dominant plasma density) is small (~0.4% in the Hairapetian–Stenzel experi-

[a)]Electronic mail: eduardo.ahedo@upm.es.

ment). This makes the DL extend tens or hundreds of Debye lengths. As a consequence, in real experiments where the Debye length is finite, the distinction between a non-neutral layer and a mere quasineutral steepened layer (QSL) is unclear.

Fourth, a supersonic ion beam does not prove the presence of a CFDL, since a quasineutral plasma also becomes supersonic when expanding along a convergent-divergent magnetic nozzle, as Andersen *et al.* demonstrated experimentally.[6] Furthermore, a double layer is known to conserve the plasma momentum[25–27] so no thrust enhancement is expected from it.[28] This raises the question of whether a CFDL has any propulsive role or, more generally stated, whether the presence of a hot-electron tail yields any propulsive gain to the plasma thruster.

In a recent letter,[29] Ahedo and Martínez-Sánchez analyzed the formation of a CFDL in a collisionless fully-ionized plasma with a hot-electron tail (which we call a *three-species* plasma) flowing in a convergent-divergent nozzle. The DL was shown to be a limit case of a QSL. The DL characteristics were different depending on whether it formed at the nozzle divergent side, convergent side, or throat. The connection of each type with previous CFDL studies on other applications was established. The CFDL formed in the divergent nozzle agrees well with the Hairapetian–Stenzel DL and is the most interesting case for plasma thrusters.

This paper extends the study initiated in that letter with several goals. The first one is to interpret the formation of a QSL and a CFDL in terms of the peculiar thermodynamics of a three-species plasma, and to show that the CFDL forms when the quasineutral solution presents several sonic points, and only one can be crossed regularly. This result contrasts sharply with recent studies by Fruchtman[28] and Chen.[30] Fruchtman claims that a CFDL is formed in a *simple* (i.e., two-species) plasma when there are abrupt changes of the nozzle shape or localized ionization. Chen claims that 'the "double layers" of Charles *et al.* are actually single layers and are predictable from classical sheath theory'.

The second goal of our study is to discuss (within a unique model) the respective roles of the DL and the magnetic nozzle on enhancing the momentum flux of a three-species plasma. The plasma downstream velocity and momentum flux measure, respectively, the specific impulse and thrust of the propulsive device ejecting the plasma. The third goal is to discuss whether the presence of a DL or, more generally, a hot-electron tail brings any propulsive gain over a simple plasma.

The paper layout is as follows. Section II presents the one-dimensional (1D) model of Ref. 29 and discusses the anomalous thermodynamics of the fluid representing the three-species plasma. Section III discusses the different regimes, with and without DL, in terms of plasma properties. Section IV analyzes, first, the spatial variation of the ion and electron momenta in DL and nozzle, and second, discusses the thrust efficiency of three-species and simple plasmas for similar thruster operation conditions. Conclusions are in Sec. V. An Appendix, based on Ref. 29, explains how the DL solutions are obtained.

II. MODEL FORMULATION

As in Ref. 29, we consider a collisionless, fully-ionized, three-species plasma, constituted of singly-charged ions (i) and cold (c) and hot (h) electron populations satisfying the Boltzmann relation. This plasma is accelerated through a convergent-divergent magnetic nozzle, whose cross-section area, $A(z)$, varies gently. Furthermore, we expect dA/dz to increase in the divergent side of a magnetic nozzle, which assures supersonicity.

An asymptotic two-scale analysis is carried out, based on the length hierarchy

$$\lambda_D \ll \ell_e \ll L \ll \lambda_{col},$$

with $L \sim dz/d\ln A$ the nozzle divergence length, ℓ_e the electron gyroradius, and λ_{col} the shortest mean-free path of possible collisional processes.

This simplified and partial model of the plasma discharge is thought suitable enough for providing a correct response to the goals enumerated above. A full and consistent model of the plasma thruster discharge should include: (1) the plasma ionization and heating processes, taking place at the upstream region of the nozzle, (2) a better kinetic model for electrons, (3) the two-dimensional aspects of the plasma expansion, and (4) the nozzle/plasma detachment, at the downstream end of the nozzle. The upstream plasma region for the case of a helicon thruster was treated by Fruchtman *et al.*[31] and Ahedo.[32] The loss of the Maxwellian character of collisionless electrons due to the combination of electrostatic barriers and inverse magnetic mirror effects has been treated, for a simple plasma, by Arefiev and Breizman, who also suggested the electron adiabatic cooling caused by the expansion of the plasma plume boundary.[33] A two-dimensional (2D) model of the supersonic expansion of a collisionless plasma in a divergent magnetic nozzle was developed by Ahedo and Merino.[7] An important result, which supports the present study, is that a quasi-1D model, although ignoring radial gradients and electric currents, approximates well the radially-averaged behavior of the 2D response of main plasma variables. Nozzle/plasma detachment[34–36] in a plasma thruster seems a major theoretical problem, in need of deep revision.[37]

The plasma equations of the quasi-1D model are

$$d(Ag_i)/dz = 0, \quad g_i = n_i u_i, \tag{1}$$

$$d(Am_i u_i g_i)/dz = -en_i A d\phi/dz, \tag{2}$$

$$0 = en_j d\phi/dz - T_j dn_j/dz \quad (j = c,h), \tag{3}$$

$$\epsilon_0 d^2\phi/dz^2 = e(n_c + n_h - n_i), \tag{4}$$

where symbols are conventional. The two electron populations are assumed isothermal (or their temperature varying in a larger scale than the acceleration scale) and ions are considered cold with respect to the temperature T_c of cold electrons.

Carrying out the first-integrals of Eqs. (1)–(3) and using subindex 0 for far-upstream conditions and S for the nozzle throat, one has

$$An_iu_i = \text{const} = G, \quad G = A_S g_S, \tag{5}$$

$$m_i u_i^2/2 + e\phi = 0, \tag{6}$$

$$n_j = n_{j0}\exp(e\phi/T_j) \quad (j = c,h). \tag{7}$$

The small Debye length limit allows us to consider the plasma quasineutral everywhere, with

$$n_i = n_c + n_h \equiv n \tag{8}$$

substituting to Eq. (4), except where a thin non-neutral layer forms; this will be treated as a discontinuity on the quasineutral scale.

The three-species plasma and the solution of the model are characterized by the temperature and upstream-density ratios between the two electron populations,

$$\tau = T_h/T_c, \quad \alpha_0 = n_{h0}/n_0, \tag{9}$$

with $n_0 = n_{c0} + n_{h0}$. Cases with $\alpha_0 = 0$ and 1 (which are equivalent) will be called *simple* plasmas, while cases with $0 < \alpha_0 < 1$ will be called *three-species* plasmas. The practical range of interest is α_0 small, but the whole range of α_0 is considered for the sake of completeness. Parameters n_0 and T_c are used to define dimensionless variables, which, except for the dimensionless electric potential, $\psi = -e\phi/T_c$, are distinguished by an overbar, that is, $\overline{n_i} = n_i/n_0$, $\overline{u_i} = u_i/\sqrt{T_c/m_i}$, etc.

The quasineutral plasma satisfying Eq. (8) may be viewed as a single fluid of velocity, u_i, and pressure and (effective) temperature defined by

$$p = T_h n_h + T_c n_c, \quad T = p/n = (1-\alpha)T_c + \alpha T_h, \tag{10}$$

with

$$\alpha(z) = n_h/(n_c + n_h) \tag{11}$$

the local density fraction of hot electrons. The equation of motion of that fluid is

$$2\frac{d\ln u_i}{dz} = \frac{d\ln(-\phi)}{dz} = \frac{2}{M^2-1}\frac{d\ln A}{dz}, \tag{12}$$

where $M = u_i/c_s$ is the Mach number based on the local sound speed c_s, which is defined by

$$\frac{1}{m_i c_s^2} = \frac{dn}{dp} = \frac{1-\alpha}{T_c} + \frac{\alpha}{T_h}. \tag{13}$$

Notice that in this fluid picture, the electrostatic energy $e\phi$ plays the role of the specific enthalpy in conventional gas dynamics.[10]

Figure 1 shows, for α_0 and τ given, the dependence of plasma magnitudes on the electric potential ψ. The main feature for a three-species plasma is that n_c decreases much faster than n_h with ψ, so that hot-electron properties dominate for ψ large enough; this is illustrated by the change of slope of $n(\psi)$ in Fig. 1(a). As a consequence, the (average) electron temperature T shifts from $\sim T_c$ to $\sim T_h$, Fig. 1(b). It turns out that the local sound speed changes faster with ψ (from $\sim\sqrt{T_c/m_i}$ to $\sim\sqrt{T_h/m_i}$) than the plasma velocity u_i, leading to local extrema of the Mach number observed in Fig. 1(c). The presence of a local minimum of M below 1

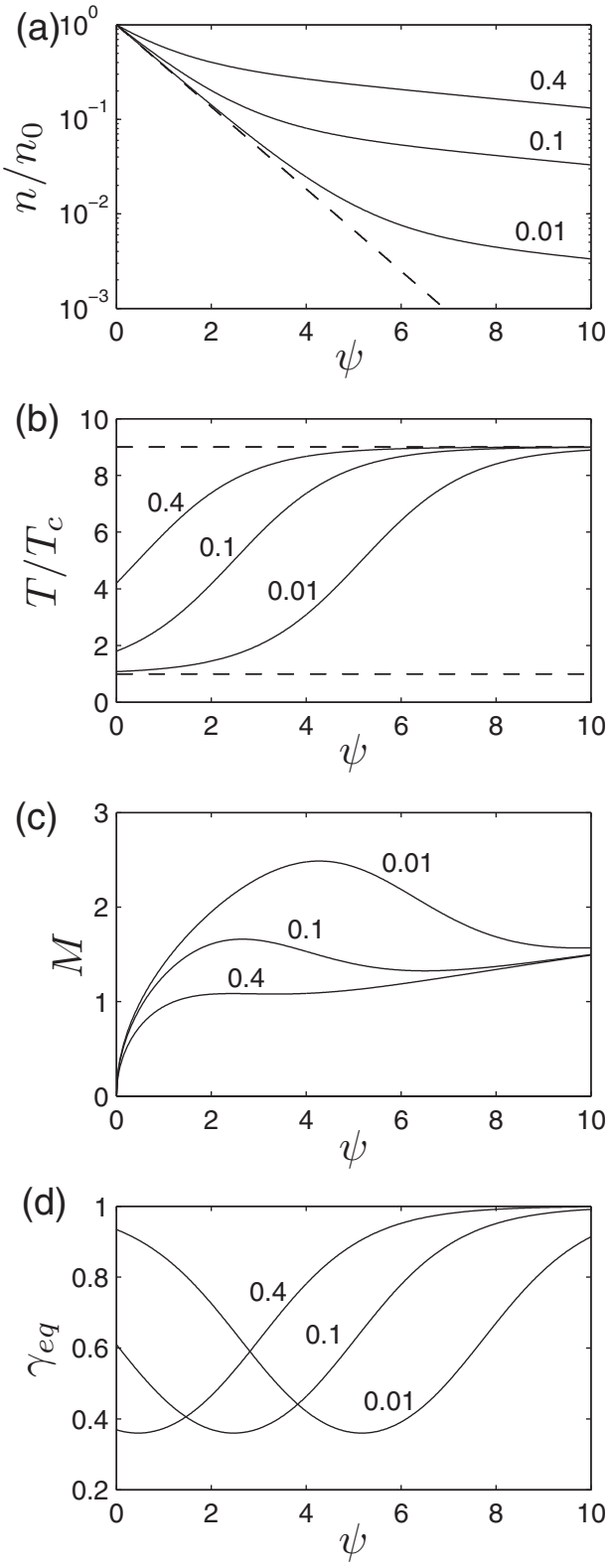

FIG. 1. Thermodynamic properties of a three-species plasma for $\tau = 9$, and $\alpha_0 = 0.01$, 0.1, and 0.4. The dashed line in (a) is for $\alpha_0 = 0$.

and, therefore, of various sonic points will be the cause of the formation of non-neutral layers within the expansion. Another illustration of the *anomalous thermodynamics* of the three-species plasma is the behavior of the 'equivalent specific heat ratio'[10]

$$\gamma_{eq} = d\ln p/d\ln n = m_i c_s^2/T \leq 1. \tag{14}$$

Figure 1(d) shows that $\gamma_{eq}(\psi)$ is close to 1 when one of the two electron species dominate, but presents an intermediate minimum, which tends to zero when $\tau \gg 1$. Since $\gamma_{eq}=1+d\ln T/d\ln n$, to have $\gamma_{eq}<1$ means that the plasma temperature *increases* as its density *decreases*.

Observe that the current-free condition is not a strict assumption in our model. Only the ion current appears explicitly in the equations and is part of the solution. Indeed, the present model is valid for current-carrying plasmas, as long as the driven electron current is much less than the electron thermal current, so that most electrons are effectively confined.

III. PLASMA EXPANSION REGIMES

In dimensionless form, Eqs. (6) and (7) yield

$$\overline{u_i}(\psi) = \sqrt{2\psi}, \quad \overline{n_c}(\psi) = (1-\alpha_0)\mathrm{e}^{-\psi}, \quad \overline{n_h}(\psi) = \alpha_0 \mathrm{e}^{-\psi/\tau}, \tag{15}$$

and the plasma flux for a quasineutral expansion is

$$\overline{g}(\psi) = (\overline{n_c} + \overline{n_h})\overline{u_i}. \tag{16}$$

The substitution of Eq. (16) into Eq. (5) yields an implicit equation for the potential profile $\psi[A(z)]$, in terms of the area variation,

$$\overline{g}(\psi)/\overline{g_S} = A_S/A(z). \tag{17}$$

The right-hand side of Eq. (17) presents a maximum at the nozzle throat. For the solution to be regular across the throat and assuming that $d\psi/dz|_S \neq 0$, $\overline{g}(\psi)$ must be maximum there. Then, Eq. (12) states that the flow is sonic at the throat, $M_S=1$.

For the plasma expansion to be fully quasineutral, $\overline{g}(\psi)$ must have only a single maximum. The local extrema of $\overline{g}(\psi)$ are the solutions of

$$0 = d\overline{g}/d\psi. \tag{18}$$

There are one or three extrema depending on the values of α_0 and τ.[29] There is a single maximum for any α_0, if τ is below the threshold value $\tau^* = 5+\sqrt{24} = 9.90$. For $\tau > \tau^*$, there are two maxima (located at $\psi \sim 1/2$ and $\psi \sim \tau/2$) when α_0 is between two limit curves, $\alpha_{0,1}(\tau)$ and $\alpha_{0,2}(\tau)$, that correspond to fulfill

$$d\overline{g}/d\psi = 0, \quad d^2\overline{g}/d\psi^2 = 0, \tag{19}$$

simultaneously, and are plotted in Fig. 2.

In order to separate the spatial gradients caused by the plasma characteristics from those due exclusively to the nozzle shape, $A(z)$, the dimensionless spatial-like variable

$$\zeta = \mathrm{sign}(z)\sqrt{A/A_S - 1} \tag{20}$$

is used. For instance, the local electric field is measured by

$$\frac{d\psi}{dz} = \frac{d\zeta}{dz}\frac{d\psi}{d\zeta}, \tag{21}$$

and the first and second factors on the right-hand side account, respectively, for the contributions of the nozzle shape and the plasma itself. The influence on the electric field of a known nozzle shape is obvious, and certainly an abrupt change of $\zeta(z)$ leads to a QSL (but not to a DL). Our attention here is devoted to profile steepening coming from $d\psi/d\zeta \gg 1$ and caused by a three-species fully-ionized plasma.

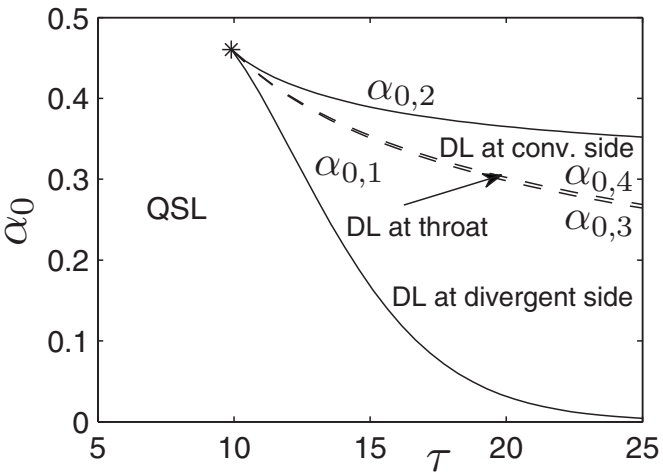

FIG. 2. Parametric regimes in plane (α_0, τ) for the formation of either a QSL or a DL.

In the parametric region where the expansion is fully quasineutral, Eqs. (16) and (18) determine $\psi_S(\tau,\alpha_0)$ and $\overline{g_S}(\tau,\alpha_0)$, thus completing the solution. Figure 3 plots spatial profiles (along ζ) of main plasma magnitudes for different α_0 and $\tau=9$. For the simple plasma with $\alpha_0=0$, one has $\psi_S=1/2$ and $\overline{g_S}=\mathrm{e}^{-1/2}$; for $\alpha_0=1$, it is $\psi_S=\tau/2$ and $\overline{g_S}=(\tau/\mathrm{e})^{1/2}$. As α_0 increases from zero, Figs. 3(a) and 3(b), plotting the electric potential and field, show the formation of a quasineutral steepened layer (QSL) for $\psi(\zeta)$. The profile steepening is observed in all magnitudes that depend on ψ, such as $\overline{n_c}$, $\overline{n_h}$, $\overline{u_i}$, $\overline{T}$, and $\overline{c_s}$. The formation of the QSL takes place mainly at α_0 small (which is the expected practical range) and the maximum steepening is reached around $\alpha_0 \sim 0.3$. For $\alpha_0 > 0.5$, roughly, the QSL has disappeared and the expansion is almost insensitive to α_0. Notice that small fractions of hot electrons produce large effects: the maximum electric field for $\alpha_0 \sim 6\%$ is similar to the one for $\alpha_0 > 0.5$. As α_0 increases, the location of the QSL moves upstream, but it remains in the divergent side for the main range, $\alpha_0 < 0.5$. For α_0 small, the QSL is observed only if the nozzle expansion area is large enough.

Figure 3(c) measures the relative density of hot electrons. The QSL acts as an effective barrier for cold electrons; instead, $\overline{n_h}$ remains almost constant upstream of the QSL and dominates the electron population downstream of it. Consistent with the behavior of $\overline{n_h}$, the local sound speed c_s increases across the QSL from $\sim\sqrt{T_c/m_i}$ to $\sim\sqrt{T_h/m_i}$. This abrupt increase explains the minimum of the Mach number M in the QSL region, observed in Fig. 3(d).

The transition from a plasma expansion with an intermediate QSL to an expansion with a non-neutral DL corresponds to the case when the ambipolar electric field in the QSL becomes infinite, $d\psi/d\zeta = +\infty$. This is the condition that leads to Eq. (19) defining the parametric curves $\alpha_{0,1}(\tau)$ and

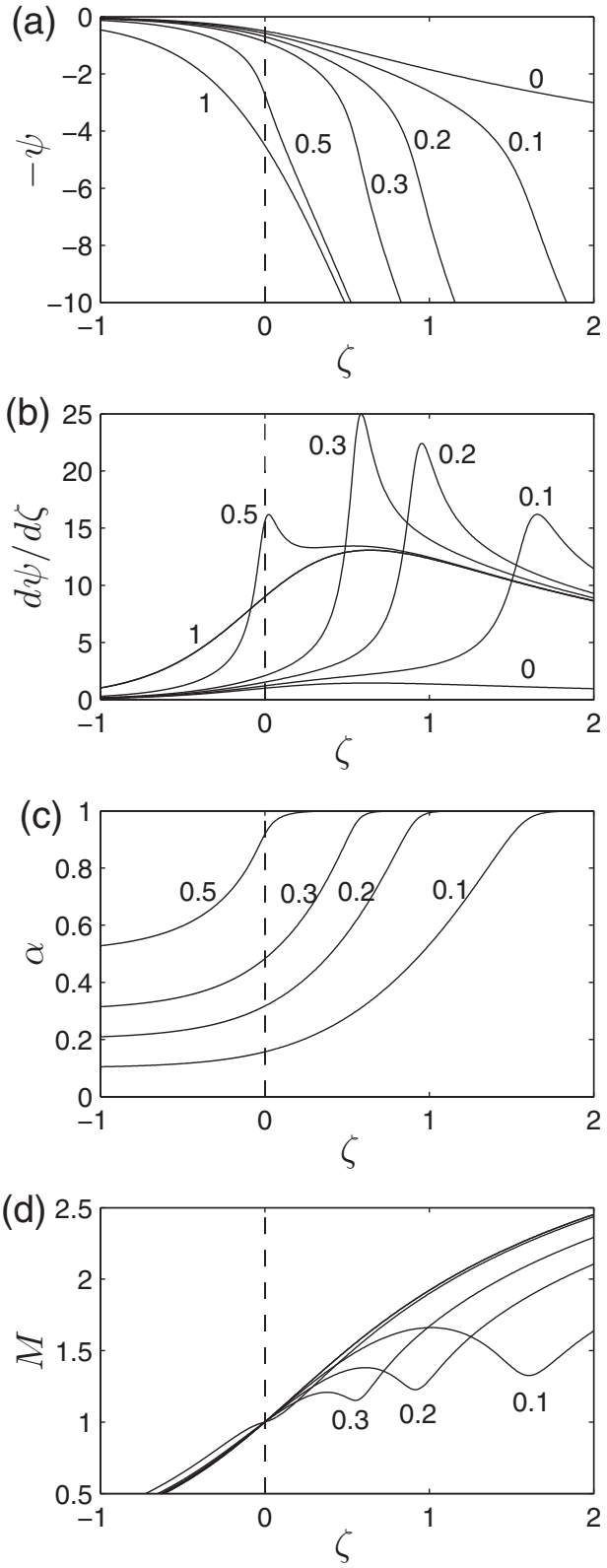

FIG. 3. Spatial variation of (a) plasma potential ($-\psi = e\phi/T_c$), (b) electric field, (c) relative density of hot electrons ($\alpha = n_h/n$), and (d) ion Mach number for $\tau = 9$, and $\alpha_0 = 0$, 0.10, 0.2, 0.3, 0.5, and 1. The spatial-like variable ζ depends on nozzle area expansion. The nozzle throat is at $\zeta = 0$.

$\alpha_{0,2}(\tau)$. From Eq. (12), the flow becomes sonic where $d\psi/d\zeta = +\infty$. Therefore, the formation of a DL is linked to the plasma encountering a second sonic point that cannot be crossed in a regular way.

TABLE I. Double layer conditions in the different regimes.

	DL entrance A	DL exit B	DL location
$\alpha_{0,1} < \alpha_0 < \alpha_{0,3}$	Supersonic	Supersonic	In divergent side
$\alpha_0 = \alpha_{0,3}$	Sonic	Supersonic	A reaches the throat
$\alpha_{0,3} < \alpha_0 < \alpha_{0,4}$	Sonic	Supersonic	In nozzle throat
$\alpha_0 = \alpha_{0,4}$	Sonic	Sonic	B reaches the throat
$\alpha_{0,4} < \alpha_0 < \alpha_{0,2}$	Sonic	Subsonic	In convergent side

An intermediate double layer forms for $\tau > \tau^*$ and $\alpha_{0,1}(\tau) < \alpha_0 < \alpha_{0,2}(\tau)$.[29] Indeed, three parametric subregions are distinguished depending on the DL type, the subregions limited by curves $\alpha_{0,3}(\tau)$ and $\alpha_{0,4}(\tau)$ of Fig. 2. Appendix A details the derivation of the solutions for the different double layers. Table I summarizes the DL conditions in the five parametric regions. Points A and B represent the entrance and exit boundaries of the DL.

Figure 4 shows the plasma profiles for $\tau = 18$ and different values of α_0, covering cases in all parametric regions. Notice, as α_0 varies, the continuous transition from solutions with a QSL to those with a DL. The continuous transition of the solutions with the temperature ratio τ is illustrated by the comparison of Figs. 3 and 4. The location of the DL moves upstream when either α_0 or τ are increased. Figures 4(c) and 4(d) show the profiles of the Mach number when the DL is located in the divergent and convergent sides, respectively. As in Fig. 3(d), for the DL in the divergent side there is a pronounced minimum of M, reaching values near 1, around the DL; notice that there is no conservation of the Mach number across the DL.

IV. PERFORMANCE AND PROPULSIVE ANALYSIS

A consequence of the isothermal model used for electrons is that for $A \to \infty$, one has $\psi \to \infty$ and $u_i \to \infty$. Of course, there are different phenomena (2D expansion effects, closure of magnetic lines, loss of magnetization, detachment, Coulomb collisions, etc.) that would invalidate the 1D model before $A \to \infty$, but the fact that u_i does not reach a finite limit value downstream constrains our propulsive analysis to *finite nozzles*, i.e., to magnetic nozzles with a finite expansion ratio, $\sigma = A_F/A_S$, with subscript F naming the final section of our nozzle. This limitation should not be very severe for our pursued comparison of plasmas with and without a hot-electron tail. Anyway, the finite nozzle case is the relevant one: for a nozzle that intersects a wall (as in plasma-based material processing[38]); presumably, for a nozzle tested inside a vacuum chamber; or when it covers the region where most of the thrust is imparted.

A. Enhancement of plasma momentum

Figure 5(a) plots, for $\tau = 18$, the variation with α_0 of the dimensionless electric potential, $e\phi/T_c$, at the distinguished locations S, A, and B. The broken line S, representing ψ_S, separates the subsonic and supersonic regions of the quasineutral expansion. For τ large but smaller than τ^*, there is a sharp but continuous change of $-\phi_S$ from $\sim T_c/2e$ to

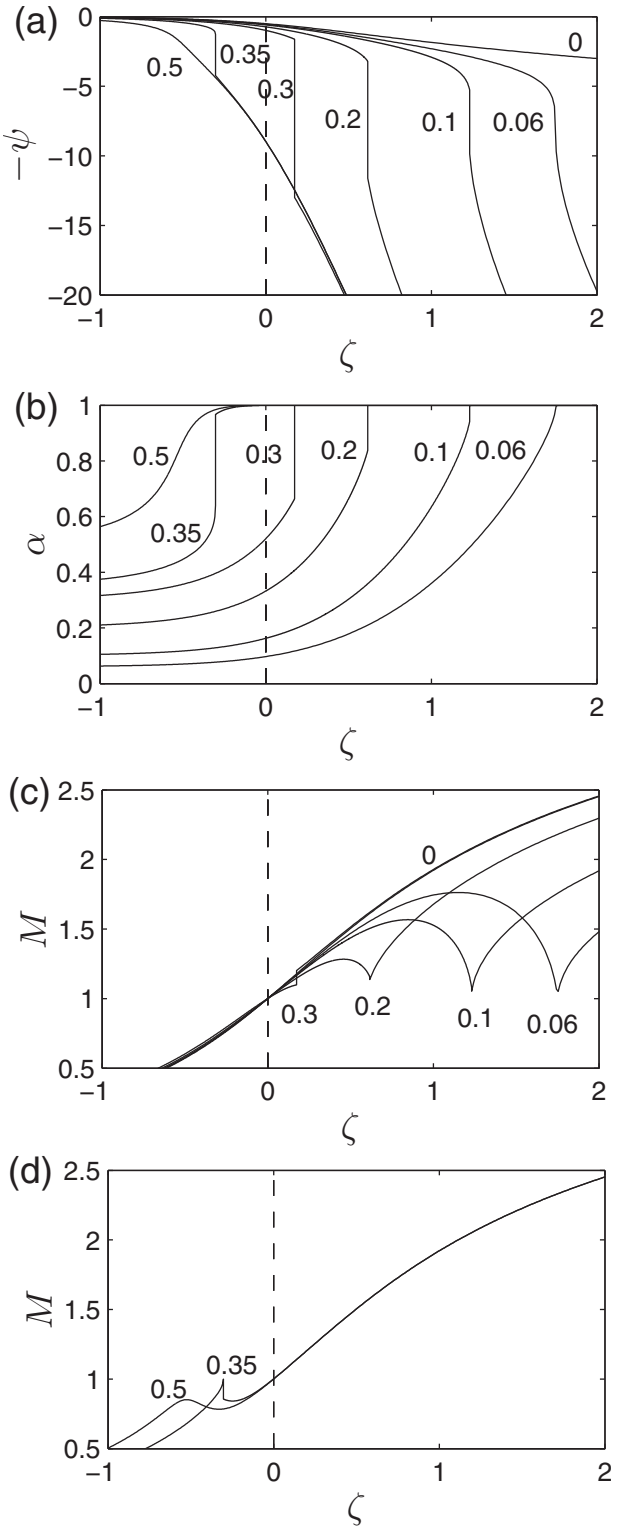

FIG. 4. Spatial variation of (a) plasma potential, (b) relative density of hot electrons, and [(c)–(d)] ion Mach number for $\tau=18$, and $\alpha_0=0$, 0.06, 0.10, 0.20, 0.30, 0.35, and 0.50. A double layer is formed for $\alpha_0=0.10$, 0.20, and 0.30 at the divergent side and for 0.35 at the convergent side.

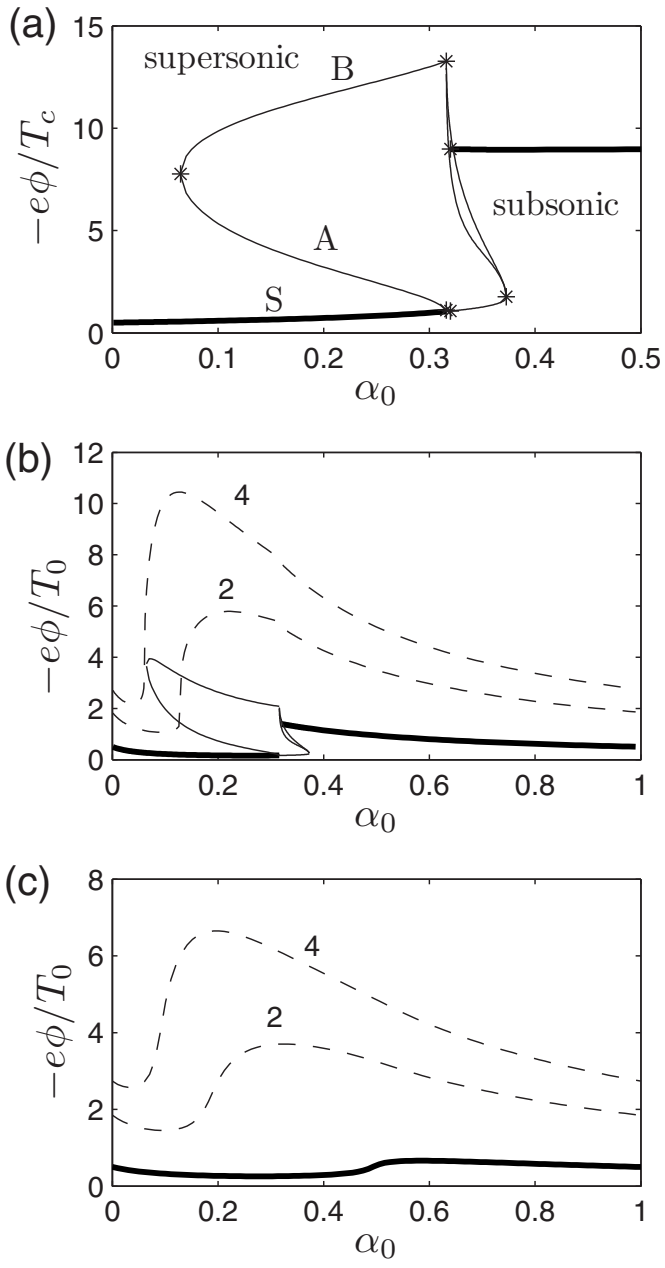

FIG. 5. Plasma potential at distinguished locations for $\tau=18$ in (a) and (b); and $\tau=9$ in (c), normalized with T_c in (a), and with T_0 in (b) and (c). Thick solid lines are for the nozzle throat S, thin solid lines for the DL boundaries A and B, and dashed lines for $A/A_S=2$ and 4. Asterisks in (a) mark the limits of each parametric regime. The horizontal scale of (b) and (c) differs from that of (a).

$\sim T_h/2e$, around $\alpha_0\sim 0.45$. For $\tau>\tau^*$, this change happens in the thin region $\alpha_{0,3}<\alpha_0<\alpha_{0,4}$ when the DL discontinuity is at the throat (although ψ_S is not strictly defined within that region). The potential jump across the double layer is maximum in that region too. In region $\alpha_{0,3}<\alpha_0<\alpha_{0,2}$, we can observe, first, the small rippling of the DL exit values, and second, that point A is a singular sonic point (the regular subsonic/supersonic transition of the plasma being located at the throat S, except for the undefined case of region $\alpha_{0,3}<\alpha_0<\alpha_{0,4}$).

The upstream (average) electron temperature, $T_0=(1-\alpha_0)T_c+\alpha_0 T_h$, is a better normalization parameter than T_c for measuring the relative variation of the electric potential along the nozzle. Figure 5(b) plots, for $\tau=18$, the renormalized potential at points S, A, and B, showing (i) that cases $\alpha_0=0$ and 1 are identical, (ii) the nonmonotonic behavior of $e|\phi_S|/T_0$, and (iii) its abrupt increment when the DL location

crosses the nozzle throat (at $\alpha_0 \simeq \alpha_{0,3}$). Figure 5(c) demonstrates that, for the case of $\tau=9$, with only a QSL, the behavior of $e|\phi_S|/T_0$ is similar to the previous case, with the sharp increment taking place at $\alpha_0 \sim 0.45$, when the QSL crosses the nozzle throat.

Figures 5(b) and 5(c) show how the ion energy per ion, $-e\phi$, increases with the ratio A/A_S in the divergent nozzle (i.e., as the plasma moves downstream). Only a fraction of the ion energy is gained at the steepened layer. For A/A_S given, observe the large increment of $|\phi|$ at a certain α_0. For nozzles with a finite expansion ratio, $\sigma=A_F/A_S$, that potential increment indicates that there is a minimum value of α_0 (i.e., a minimum upstream-density ratio of hot electrons) for the QSL to form within the finite nozzle; that value decreases when σ and τ increase.

The plasma total momentum flux along the nozzle, $F(z)$, sum of the ion and electron contributions, is

$$F(z) = F_i(z) + F_e(z) = m_i n u_i^2 A + pA. \tag{22}$$

In our 1D model, $F(z)$ is identified as the function yielding the increment of thrust along the nozzle. For a finite nozzle, thrust and specific impulse are defined as F_F and $I_{sp}=F_F/\dot{m}$. To compare performances, we consider next plasma beams with the same mass flow $\dot{m}=m_i A_S g_S$ and upstream (average) temperature T_0. Then, reference values for plasma momentum and density, based on $\dot{m}$ and T_0 (instead of n_0 and T_c), are

$$F_* = \dot{m}c_0, \quad n_* = \dot{m}/(A_S m_i c_0), \tag{23}$$

with $c_0=\sqrt{T_0/m_i}$ [not to be mistaken with the local sound speed c_{s0}, Eq. (13)]. By fixing $\dot{m}$: first, we cancel the obvious effect of the beam size, so that thrust and specific impulse behave in the same way; and second, the upstream plasma density n_0 becomes an output parameter, controlled by the choking of the plasma flow at the throat.

Figures 6(a)–6(c) show parameters characterizing the plasma expansion in the convergent nozzle as a function of α_0 for two values of τ. Figure 6(a) plots the ratio n_0/n_*: it is equal to $e^{1/2}$ for a simple plasma, but it can be considerably larger for a three-species plasma, which means a higher choking for the same $\dot{m}$. For $\tau > \tau^*$, the maximum value of n_0/n_* takes place when the DL reaches the throat from the divergent side. Figure 6(b) plots the normalized plasma momentum flux at the nozzle throat, F_S/F_*, which behaves similar to n_0/n_*. Finally, Fig. 6(c) depicts the relative contribution of ion momentum to F_S. As expected, it is $F_{iS}=F_{eS}=F_S/2$ for a simple plasma. The same result is found for a three-species plasma when the DL is in the convergent side, implying that at the throat the plasma is already a 2-species one. On the contrary, F_{iS}/F_S can be considerably smaller than 1/2 when the DL or QSL are located in the divergent nozzle (i.e., for small values of α_0). Observe that: the behavior of F_{iS}/F_S follows that of n_*/n_0; and $F_{iS}/F_{eS}=m_i c_{sS}^2/T_S$ so that $F_{iS}/F_{eS}<1$ reflects the fact that the 'equivalent specific heat ratio', Eq. (14), is smaller than 1.

Figures 7(a) and 7(b) plot the spatial variation of the plasma momentum flux in the divergent nozzle, illustrating the two main actions of that nozzle region: (a) the conversion of electron momentum into ion momentum and (b) the increase of plasma momentum. The most relevant features are, first, the abrupt increase of ion momentum across a QSL or a DL, and, second, the *zero change* of plasma momentum across a DL. This last property, well-known in double layer theory,[25–28] is immediate from the plasma momentum equation

$$\frac{dF}{dz} = \frac{\epsilon_0}{2}\frac{d}{dz}\left(\frac{d\phi}{dz}\right)^2 + p\frac{dA}{dz}, \tag{24}$$

which is obtained from Eqs. (2)–(4). The first term in the right-hand side yields the variation of F within the double layer, which *cancels out* at the two DL sides, i.e., $F_A=F_B$.

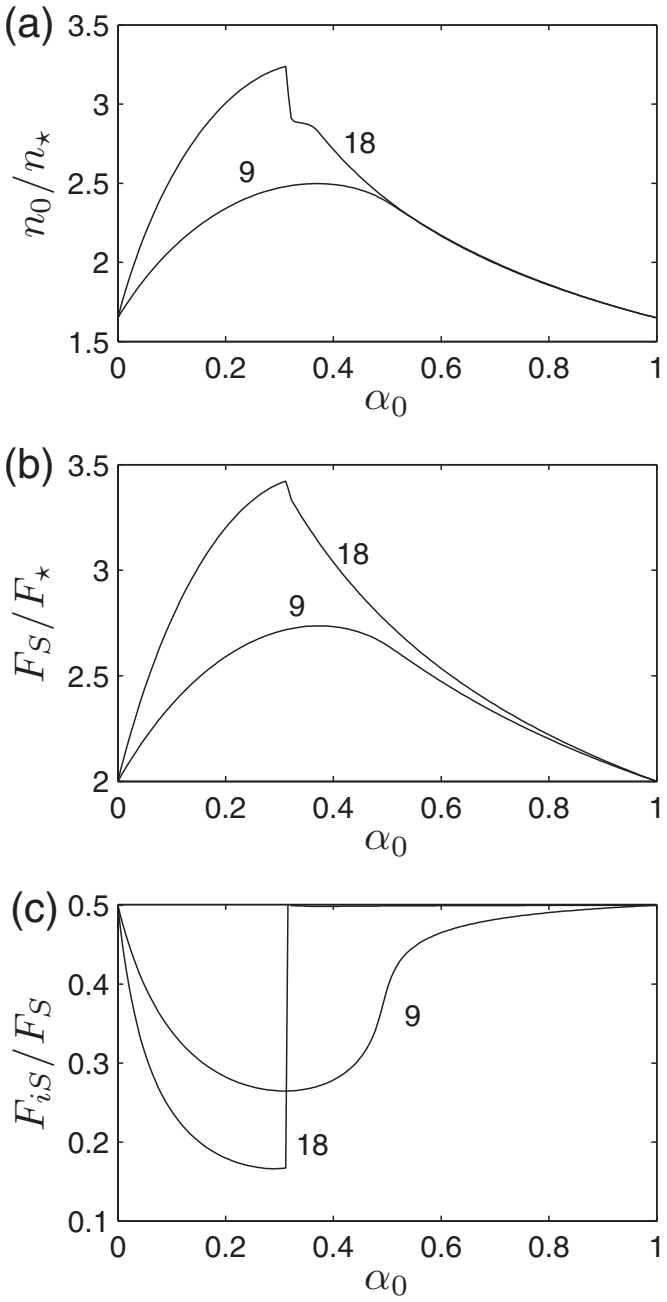

FIG. 6. Plasma response in the convergent side of the nozzle vs α_0, for $\tau=9$ and 18. (a) Upstream plasma density (for a given mass flow), (b) plasma momentum flux at the throat, and (c) relative contribution of ions to the plasma momentum flux at the throat.

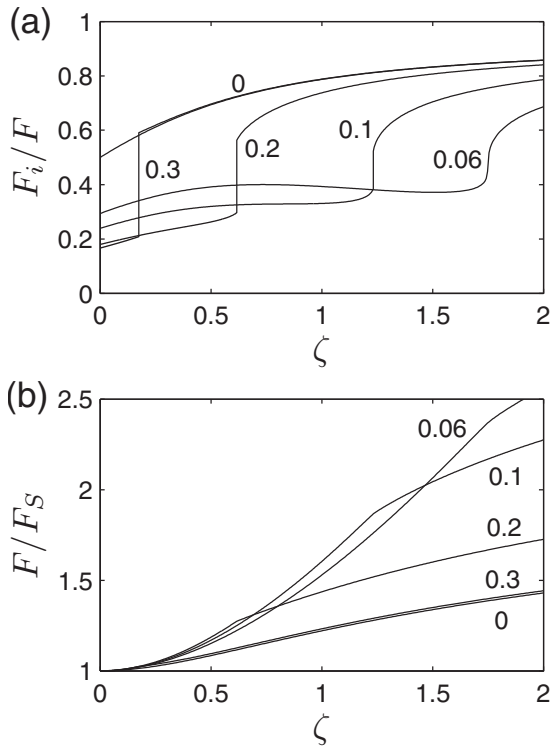

FIG. 7. Variation of plasma momentum flux in the divergent nozzle for $\tau=18$ and $\alpha_0=0$, 0.06, 0.1, 0.2, and 0.3: (a) relative contribution of ion momentum flux; (b) increase of plasma momentum flux relative to the value at the throat.

Therefore, a DL just converts electron momentum into ion momentum and does not constitute by itself a mechanism for imparting thrust. On the contrary, the supersonic plasma expansion in the divergent nozzle *does* increment the thrust, as Fig. 7(b) illustrates. Nonetheless, the physical thrust mechanisms are different in solid and magnetic nozzles. In classical gas dynamics flowing inside solid nozzles, the thrust comes from the pressure on the diverging walls. In a magnetic nozzle the pressure gradient at the plasma/vacuum edge generates a diamagnetic azimuthal current, and the Lorentz force associated to that current on the nozzle magnetic circuit produces the thrust.[7]

Once the DL has been disregarded as a thrust mechanism, the point that remains to be discussed is whether a three-species plasma still presents any propulsive gain over a simple plasma. Figure 8(a) plots the specific impulse relative to the upstream sound velocity for different three-species plasmas and two finite nozzles. Notice that I_{sp}/c_0 is equivalent to F_F/F_* and is sometimes called the thrust coefficient.[39] The increase of the thrust coefficient that corresponds to the divergent side of the nozzle, i.e., F_F/F_S, can be inferred from Figs. 8(a) and 6(b). The thrust coefficient I_{sp}/c_0 increases with the expansion ratio, as expected. More interestingly, (i) it reaches a marked maximum with α_0 corresponding always to the steepened layer located in the divergent nozzle, and (ii) it does not increase with τ when the steepened layer is on the convergent nozzle.

In order to compare three-species plasmas with simple plasmas, Fig. 8(b) plots the ratio of I_{sp} versus $I_{sp,0}$, the specific impulse of the simple plasma *with the same* T_0. The ratio $I_{sp}/I_{sp,0}$ is closely related to $(e|\phi_F|/T_0)^{1/2}$, plotted in Figs. 5(b) and 5(c). Figure 8(b) emphasizes the fact that the performances of a three-species plasma differ from those of a simple plasma only when the steepened layer is on the divergent nozzle. Since the equivalent specific ratio γ_{eq} is a function of α_0 [Fig. 1(d)], the dependence of I_{sp} on α_0 of Fig. 8(b) bears a resemblance to the dependence of the specific impulse I_{sp} on the specific heat ratio, γ, in isentropic gas dynamics,[39] where $\partial I_{sp}/\partial\gamma<0$, although the effect of γ_{eq} is stronger here.

B. Thrust efficiency

Figure 8(b) seems to suggest that three-species plasmas present a large gain in specific impulse (up to a factor of ~ 2 in the figure) with respect to simple plasmas. However, a comparison based on the same T_0 is not valid to assess the propulsive quality of different collisionless plasmas, since they can require very different power deposition, P_d, to reach the same T_0. Here lies an important difference between chemical and electric thrusters. In a chemical thruster, the specific power, $P_d/\dot{m}$, is an intrinsic property of the propellant, the upstream temperature is set locally and satisfies $T_0 \propto P_d/\dot{m}$; thus, comparisons based on the same $P_d/\dot{m}$ or the same T_0 are similar. In electric thrusters, the available power P_d comes from an external source (through electrodes or antennas) and, more importantly, for near-collisionless plasmas, the temperature of the *confined* electrons is not determined locally but comes out from an energy balance (at kinetic level) on the whole expansion region;[33] this relates in a very different way T_0 to $P_d/\dot{m}$.

Therefore, a correct assessment of the propulsive quality of a plasma/thruster system must consider plasmas with the same $\dot{m}$, same P_d, and same nozzle. Then, the appropriate propulsive parameter is the thrust efficiency,

$$\eta = F_F^2/2\dot{m}P_d = I_{sp}^2\dot{m}/2P_d. \tag{25}$$

The power deposited in the plasma can be split into useful power, P_{use}, and power losses. In our limited 1D model for a finite nozzle and a current-free plasma, the useful power is the downstream plasma (ion plus electron) power,

$$P_{use} = \left(\frac{u_{iF}^2}{2} + 2a\frac{T_F}{m_i}\right)\dot{m},$$
$$a = \frac{1+(\tau^{3/2}-1)\alpha}{[1+(\tau-1)\alpha][1+(\tau^{1/2}-1)\alpha]}. \tag{26}$$

Here, the expression of parameter a must be seen as a simple estimate only; it is based on the assumption of a similar behavior of the high-energy tails of cold and hot electrons in a three-species plasma, and it is $a=1$ for a simple plasma. For a nozzle with a large expansion ratio, the electron contribution to P_{use} is small and the uncertainties on the expression of a should not matter much.

The contributions to power losses are ionization and radiation, wall deposition, plume divergence, and detachment. Their analysis is outside of the possibilities of our model so that the comparison here must be limited to plasmas with the

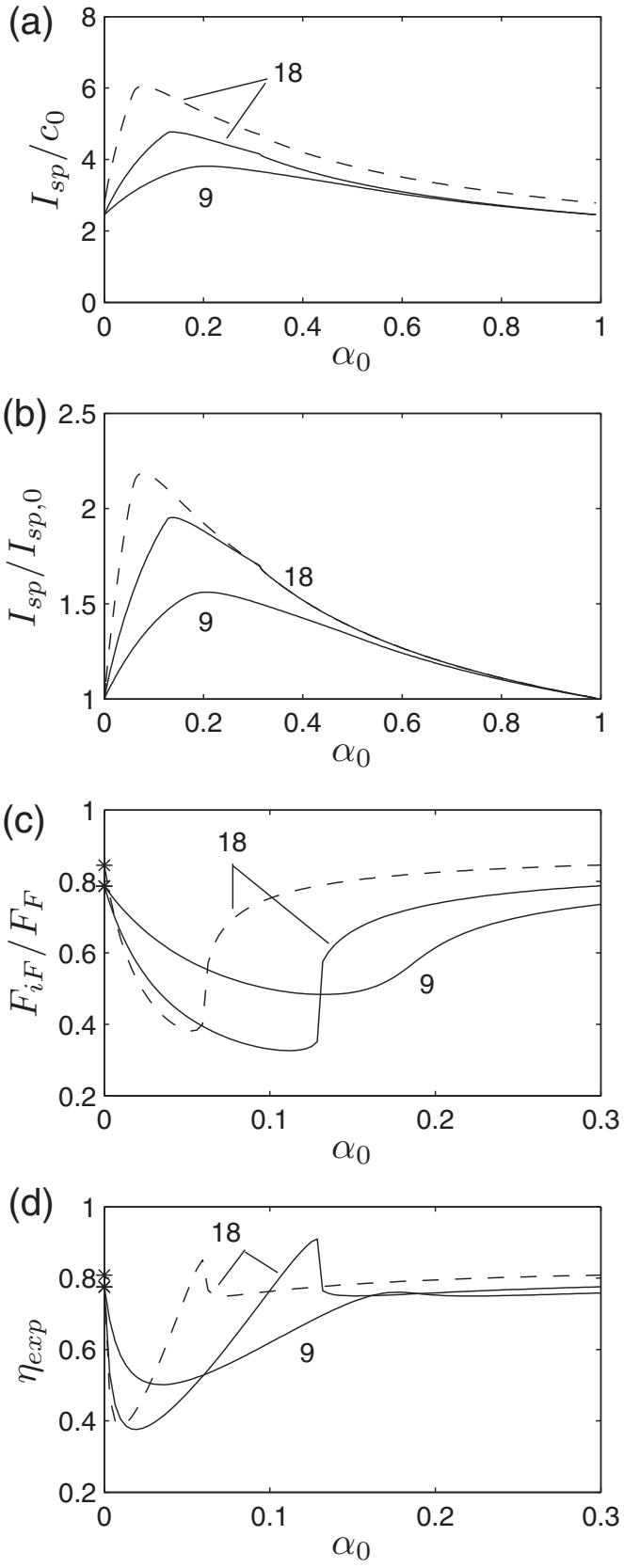

FIG. 8. Propulsive figures vs α_0, for $\tau=9$ and 18, and $\sigma=2$ (solid lines) and 4 (dashed lines). (a) Specific impulse coefficient, (b) specific impulse of a three-species plasma referenced to that of a simple plasma with the same T_0, (c) ion momentum contribution to the thrust, and (d) expansion efficiency. Asterisks in (d) represent values for a simple plasma. Notice that the horizontal scale in (c) and (d) differs from that of (a) and (b).

same useful power. For this class of plasmas, the thrust efficiency is factorized as

$$\eta = \eta_{loss}\eta_{exp}, \quad \eta_{loss} = P_{use}/P_d, \quad \eta_{exp} = I_{sp}^2/I_{sp,m}^2, \tag{27}$$

where $I_{sp,m}=(2P_{use}/\dot{m})^{1/2}$, and the expansion efficiency η_{exp} is the only factor that can be analyzed here. We find

$$1-\eta_{exp} = \frac{2\mu-1}{\mu(\mu+4a)} = \frac{2}{\mu} + O\left(\frac{1}{\mu^2}\right), \tag{28}$$

with $\mu=F_{iF}/F_{eF}$. If M_F is the Mach number at the end of the nozzle, one has $\mu<M_F^2$ for a three-species plasma and $\mu \simeq M_F^2$ when the hot population dominates downstream. Figure 8(c) plots the ion contribution to thrust, $F_{iF}/F_F=\mu(1+\mu)^{-1}$ and Fig. 8(d) plots η_{exp}. From these figures we conclude that, in general, a three-species plasma presents a lower expansion efficiency than a simple plasma, the deficit being maximum in the case of higher interest, when the steepened layer is in the divergent nozzle.

Apart from the efficiency of the 1D expansion, the thrust efficiency of plasmas with and without hot electrons can still differ because of power losses, due to either processes inside the source (ionization and wall heating) or 2D effects in the downstream part of the nozzle (radial energy and detachment). At present, all these processes are very poorly known for a three-species plasma.

The fact that $\eta_{exp}<1$ is due to the incomplete expansion of the plasma in the finite nozzle. Indeed, the isothermal assumption makes η_{exp} increase very slowly with σ. Adiabatic cooling of electrons[33] is likely to make $\eta_{exp}(\sigma)$ approach one much quicker, so that $I_{sp}\simeq I_{sp,m}$ independently of the plasma parameters, α_0 and τ. Then, the difference in thrust efficiency between plasmas with and without hot electrons would lie exclusively on aspects outside the scope of the present model.

The isothermal assumption also implies that, for $\sigma\to\infty$, $M_F(\sigma)\to\infty$. For plasmas with $\dot{m}$ and $P_{use}=\eta_{loss}P_d$ given, the plasma velocity tends to $I_{sp,m}$, and therefore, the upstream temperature satisfies $T_0(\sigma)\to 0$. This is consistent with the global energy balance that determines T_0 in a collisionless plasma (of course, the 1D model is not expected to apply for $\sigma\to\infty$). Then, for $\dot{m}$ and P_{use} given, the curves of Fig. 8(a) are not informing us on the variation of I_{sp} but of $T_0\eta_{exp}^{1/2} \approx T_0$, and the curves of Fig. 8(b) are depicting (approximately) the ratio $\sqrt{T_0/T_{0,0}}$, with $T_{0,0}$ the upstream temperature of the simple plasmas with the same P_{use}.

V. CONCLUSIONS

The presence of two electron populations in a fully-ionized collisionless plasma leads to an anomalous thermodynamic behavior, illustrated by an equivalent specific ratio lower than one (implying temperature increasing when density decreasing) and a nonmonotonic behavior of the Mach number. A steepened layer is formed around a local minimum of the Mach number and, for α_0 small, marks the transition from a region dominated by cold electrons to a region governed by hot electrons. A two-scale asymptotic analysis is able to distinguish between a quasineutral steepened layer

and a non-neutral double layer. This last one forms when the quasineutral solution presents several sonic points, and a regular crossing of all of them is impossible.

The three-species plasma has been assumed to expand in a convergent-divergent nozzle. For α_0 small, the steepened layer forms in the divergent nozzle, provided that the nozzle expansion ratio is high enough. As α_0 increases, the steepened layer moves toward the throat and the convergent nozzle. In this last case, all three-species effects are confined upstream of the nozzle throat and the downstream plasma is basically a simple one. The formation of the steepened layer in the downstream region of the nozzle leads to a large increment of the total potential fall, from $O(T_c/e)$ to $O(T_h/e)$, and therefore of the energy of ions.

The propulsive properties of the plasma/nozzle system, that is, thrust and specific impulse, are determined by the downstream plasma momentum flux and velocity. It is confirmed that there is no gain in plasma momentum across the DL, just conversion of electron momentum into ion momentum, so that the DL does not constitute a thrust mechanism, as claimed in the HDLT concept. The thrust mechanism in a helicon thruster is the axial Lorentz force between the plasma and the magnetic circuit, independently of whether the ion acceleration takes place in a very thin DL or gradually along the divergent nozzle.

A comparative propulsive analysis for simple and three-species plasmas has been carried out under the constraints of same useful power, mass flow, and finite magnetic nozzle. Although the study of the power losses related to plasma processes inside the source and in the 2D detachment region remains to be done, we have found no indication that the presence of a hot-electron tail makes the plasma more favorable for propulsion. Indeed, we find that, for any finite nozzle, the expansion efficiency is, in general, slightly lower for a three-species plasma than for a simple plasma.

The formation of a QSL in a three-species plasma has been confirmed by a 2D model of a magnetic nozzle.[40] There, the QSL is observed as a curved front with a pronounced peak of the ambipolar electric field and the parametric dependence of the QSL location and potential agrees with present results. The 2D model is purely quasineutral and could not be run within the CFDL parametric region. With respect to propulsive efficiency, the 2D model concludes that the plume efficiency, defined as the ratio of axial-to-total ion power, is slightly lower for a three-species plasma.

We acknowledge that the simple Boltzmann relation used for cold and hot electrons is the most delicate aspect of our model. First, the cold electron population is likely to be Maxwellian upstream of the nozzle throat but magnetic moment effects modify that character on the divergent nozzle.[33] Second and more relevant for the study here, there is no reliable knowledge of the upstream distribution function of hot electrons. Solutions with a CFDL have been found using monoenergetic populations of hot electrons[13,16] and polytropic laws for the two electron populations.[10] This would mean that the DL, being a local structure, is not much dependent on the details of the upstream distribution functions (as long as cold and hot electron energies are disparate). On the contrary, the downstream properties of the (collisionless) plasma, such as the final plasma velocity and the density profile, are certainly influenced by the hot-electron distribution function and the presence of intermediate energy barriers (related to either the DL, magnetic moments, or a moving plasma boundary[33]).

Finally, the present model can be easily extended to include the ionization and heating processes in the upstream side of the nozzle. Then, several conservation laws that are analytical in the present model would remain differential equations to be integrated numerically. However, as long as ionization and plasma heating are efficient (which is essential for a competitive thruster device), the plasma response in the divergent nozzle, which is the important region in our study, is not modified.

ACKNOWLEDGMENTS

This work was initiated under project 'Helicon Plasma Hydrazine Combined Micro', financed by the European Community (Seventh Framework Programme, Grant No. 218862), and could be finished thanks to the Air Force Office of Scientific Research, Air Force Material Command, USAF, under Grant No. FA8655-10-1-3085. Marginal funding came from the Gobierno de España (Plan Nacional de I+D, Project No. ESP2007-62694). The author thanks Professor Martínez-Sánchez for very fruitful discussions and Dr. Birkan for his support.

APPENDIX A: EXPANSION WITH AN INTERMEDIATE DOUBLE LAYER

The derivation here is extracted from Ref. 29, adding some explanatory details. The internal structure of the DL requires us to solve the Poisson Eq. (4) in the inner variable $\xi=(x-x_{DL})/\lambda_D$, with x_{DL} an inner point of the DL and $\lambda_D=\sqrt{\epsilon_0 T_c/e^2 n_0}$. Equation (4) yields the first integral

$$\frac{1}{2}\left(\frac{d\psi}{d\xi}\right)^2=\int_{\psi_A}^{\psi}(\overline{n_i}-\overline{n_c}-\overline{n_h})(\psi)d\psi\equiv U(\psi)-U(\psi_A) \tag{A1}$$

with

$$U(\psi,\overline{g_A};\alpha_0,\tau)=\sqrt{2\psi}\overline{g_A}+\overline{n_c}(\psi)+\tau\overline{n_h}(\psi), \tag{A2}$$

the (dimensionless) Sagdeev's potential. Since a non-neutral DL connects two quasineutral regions of the plasma, a steady DL inside any plasma must satisfy the following three pairs of conditions at its upstream and downstream boundaries (points A and B, respectively):[26,25] (a) plasma quasineutrality, $U'=0$; (b) asymptotically zero space-charge field, $U_B=U_A$ [in order to cancel the total DL charge and match with the much weaker ambipolar field of the quasineutral regions]; and (c) the sonic/supersonic Bohm condition, $U''\geq 0$, which assures the development of a nonoscillatory layer profile. In terms of the function $\overline{g}$, these *necessary* conditions imply that $\overline{g_A}=\overline{g_B}$, and $\overline{g}'_A,\overline{g}'_B\leq 0$. Physically, the last conditions imply that the ion flow cannot be subsonic at the entrance and exit of a *standard* DL.

A standard DL forms for $\alpha_{0,1}(\tau)<\alpha_0<\alpha_{0,3}(\tau)$ on the divergent nozzle. The ion flow is supersonic at both the DL

entrance and exit. For (τ, α_0) given, the DL is defined by three parameters: the ion flux $\overline{g_A}$ across it and the entrance and exit potentials ψ_A and ψ_B. These are obtained from the set of algebraic equations

$$\overline{g_A} = \overline{g}(\psi_A) = \overline{g}(\psi_B), \quad U_B(\psi_B, \overline{g_A}) = U_A(\psi_A, \overline{g_A}), \tag{A3}$$

and Eq. (17) yields the location of the DL. Figures 3(a)–3(b) of Ref. 29 plot the inner profiles of such DL. As α_0 is increased, the DL location moves upstream. The limit curve $\alpha_0 = \alpha_{0,3}(\tau)$ is determined from the additional condition $d\overline{g}/d\psi|_A = 0$ and corresponds to the case when the DL entrance reaches the throat and the ion flux at the DL entrance is sonic.

Reference 29 discusses that the fulfillment of all conditions for a standard DL is impossible in the parametric region $\alpha_{0,3}(\tau) < \alpha_0 < \alpha_{0,2}(\tau)$. Instead, an 'ill-ended' DL is formed, which is constituted by the usual monotonic region, from entrance A to an intermediate point C where ϕ is minimum and the ion flux is subsonic, followed by a (space-charged) rippled tail. This type of DL is illustrated in Figs. 3(c)–3(d) of Ref. 29 and has been reported also in the wall-collection models of Refs. 13, 15, and 16. Parameters $\overline{g_A}$, ψ_A, and ψ_C determining the monotonic part of the DL are obtained from

$$\overline{g_A} = \overline{g}(\psi_A), \quad \overline{g}'(\psi_A) = 0, \quad U_B(\psi_C, \overline{g_A}) = U_A(\psi_A, \overline{g_A}). \tag{A4}$$

Then, the electron density at point C is

$$\overline{n_{eC}} = (1 - \alpha_0)e^{-\psi_C} + \alpha_0 e^{-\psi_C/\tau} \tag{A5}$$

and, because of the potential barrier created around the minimum potential ψ_C, the electron density is constant in the rippled tail. This modifies the Sagdeev's potential there, that becomes $U = \sqrt{2\psi\overline{g_A}} - \psi\overline{n_{eC}}$.

Since the space-charge rippling is small and averages to zero in distances Δz, such that $\lambda_d \ll \Delta z \ll L$, it makes sense to consider the averaged plasma profiles downstream of the monotonic part of the DL. This requires us to define the 'exit' of the DL as a point B with averaged values in the rippled tail. It turns out that the potential ψ_B defining point B is

$$\psi_B = \overline{u_{iB}^2}/2 \equiv (\overline{g_A}/\overline{n_{eC}})^2/2. \tag{A6}$$

In the quasineutral region downstream of the DL, the electron densities of Eq. (15) are modified into

$$\overline{n_c} = (1 - \alpha_0)e^{\psi_{CB} - \psi}, \quad \overline{n_h} = \alpha_0 e^{(\psi_{CB} - \psi)/\tau}, \tag{A7}$$

with $\psi_{CB} = \psi_B - \psi_C$. Physically, these modifications are the consequence of the potential barrier for electrons at the rippled tail.

The DL with a rippled tail covers the whole parametric region $\alpha_{0,3} < \alpha_0 < \alpha_{0,2}$, but two subregions are distinguishable in terms of the location of the double layer: they are separated by the curve $\alpha_0 = \alpha_{0,4}(\tau)$ of Fig. 2. For $\alpha_{0,4} < \alpha_0 < \alpha_{0,2}$, the double layer is located in the convergent side of the nozzle, whereas for $\alpha_{0,3} < \alpha_0 < \alpha_{0,4}$, the whole DL is at the nozzle throat. The curve $\alpha_0 = \alpha_{0,4}(\tau)$ is obtained imposing that the exit of a DL reaches the throat from the convergent side, which means to impose the extra condition $\overline{g}'(\psi_B) = 0$, with the electron densities satisfying Eq. (A7).

[1] C. Charles and R. Boswell, Appl. Phys. Lett. **82**, 1356 (2003).
[2] T. Ziemba, J. Carscadden, J. Slough, J. Prager, and R. Winglee, *41st Joint Propulsion Conference*, Tucson, AR (American Institute of Aeronautics and Astronautics, Washington, D.C., 2005), p. 4119.
[3] O. Batishchev, IEEE Trans. Plasma Sci. **37**, 1563 (2009).
[4] D. Pavarin, F. Ferri, M. Manente, D. Curreli, Y. Guclu, D. Melazzi, D. Rondini, S. Suman, J. Carlsson, C. Bramanti, E. Ahedo, V. Lancellotti, K. Katsonis, and G. Markelov, *31st International Electric Propulsion Conference*, Ann Arbor, MI (Electric Rocket Propulsion Society, Fairview Park, OH, 2009), p. 205.
[5] A. Gurevich, L. Pariiskaya, and L. Pitaevskii, Sov. Phys. JETP **22**, 449 (1966).
[6] S. A. Andersen, V. O. Jensen, P. Nielsen, and N. D'Angelo, Phys. Fluids **12**, 557 (1969).
[7] E. Ahedo and M. Merino, Phys. Plasmas **17**, 073501 (2010).
[8] C. Charles and R. Boswell, Phys. Plasmas **11**, 1706 (2004).
[9] C. Charles, R. Boswell, and M. Lieberman, Appl. Phys. Lett. **89**, 261503 (2006).
[10] B. Bezzerides, D. W. Forslund, and E. L. Lindman, Phys. Fluids **21**, 2179 (1978).
[11] L. M. Wickens, J. E. Allen, and P. T. Rumsby, Phys. Rev. Lett. **41**, 243 (1978).
[12] A. Gurevich, D. Anderson, and H. Wilhelmsson, Phys. Rev. Lett. **42**, 769 (1979).
[13] L. Schott, Phys. Fluids **30**, 1795 (1987).
[14] K. Sato and F. Miyawaki, Phys. Fluids B **4**, 1247 (1992).
[15] A. Kono, J. Phys. D **32**, 1357 (1999).
[16] T. E. Sheridan, P. Chabert, and R. W. Boswell, Plasma Sources Sci. Technol. **8**, 457 (1999).
[17] G. Hairapetian and R. L. Stenzel, Phys. Fluids B **3**, 899 (1991).
[18] X. Sun, A. Keesee, C. Biloiu, E. Scime, A. Meige, C. Charles, and R. Boswell, Phys. Rev. Lett. **95**, 025004 (2005).
[19] S. A. Cohen, X. Sun, N. Ferraro, E. E. Scime, M. Miah, S. Stange, N. Siefert, and R. Boivin, IEEE Trans. Plasma Sci. **34**, 792 (2006).
[20] N. Plihon, P. Chabert, and C. S. Corr, Phys. Plasmas **14**, 013506 (2007).
[21] P. Zhu and R. W. Boswell, Phys. Fluids B **3**, 869 (1991).
[22] R. T. S. Chen and N. Hershkowitz, Phys. Rev. Lett. **80**, 4677 (1998).
[23] A. W. Degeling, T. E. Sheridan, and R. W. Boswell, Phys. Plasmas **6**, 1641 (1999).
[24] S. Tysk, C. Denning, J. Scharer, and K. Akhtar, Phys. Plasmas **11**, 878 (2004).
[25] L. Block, Astrophys. Space Sci. **55**, 59 (1978).
[26] M. A. Raadu, Phys. Rep. **178**, 25 (1989).
[27] V. Lapuerta and E. Ahedo, Phys. Plasmas **7**, 2693 (2000).
[28] A. Fruchtman, Phys. Rev. Lett. **96**, 065002 (2006).
[29] E. Ahedo and M. Martínez-Sánchez, Phys. Rev. Lett. **103**, 135002 (2009).
[30] F. F. Chen, Phys. Plasmas **13**, 034502 (2006).
[31] A. Fruchtman, G. Makrinich, and J. Ashkenazy, Plasma Sources Sci. Technol. **14**, 152 (2005).
[32] E. Ahedo, *31st International Electric Propulsion Conference*, Ann Arbor, MI (Electric Rocket Propulsion Society, Fairview Park, OH, 2009), p. 193.
[33] A. Arefiev and B. Breizman, Phys. Plasmas **15**, 042109 (2008); **16**, 055707 (2009).
[34] R. W. Moses, R. Gerwin, and K. Schoenberg, *Proceedings Ninth Symposium on Space Nuclear Power Systems*, Albuquerque, NM, 1992, AIP Conf. Proc. No. 246 (American Institute of Physics, Woodbury, NY, 1992), pp. 1293–1303.
[35] E. B. Hooper, J. Propul. Power **9**, 757 (1993).
[36] A. Arefiev and B. Breizman, Phys. Plasmas **12**, 043504 (2005).
[37] E. Ahedo and M. Merino, *46th Joint Propulsion Conference*, Nashville, TN (American Institute of Aeronautics and Astronautics, Washington, D.C., 2010), p. 6613.
[38] K. Schoenberg, R. Gerwin, R. Moses, J. Scheuer, and H. Wagner, Phys. Plasmas **5**, 2090 (1998).
[39] G. Sutton and O. Biblarz, *Rocket Propulsion Elements*, 7th ed. (Wiley, New York, 2001).
[40] M. Merino and E. Ahedo, *Proceedings of Space Propulsion 2010*, San Sebastián, Spain, 3–6 May 2010 (European Space Agency, Noordwijk, The Netherlands, 2010), p. 1841391; "Simulation of plasma flows in divergent magnetic nozzles," IEEE Trans. Plasma Sci. (submitted).

On electron inertia and current ambipolarity in magnetic nozzle models

IEPC-2011-050

Presented at the 32nd International Electric Propulsion Conference,
Wiesbaden, Germany
September 11–15, 2011

Eduardo Ahedo* and Mario Merino†
E.T.S. Ingenieros Aeronáuticos, Plaza Cardenal Cisneros, Madrid 28040, Spain

An axilsymmetric model of the supersonic plasma expansion in a divergent magnetic nozzle, which includes the relevant electron-inertia terms is presented. This generalized model presents the same mathematical structure and features than our extensively studied zero electron-inertia model. There is no room in the model for imposing current ambipolarity everywhere, and this is not fulfilled. The model confirms the trends obtained in a former linearized analysis about electron-inertia: this makes the plasma beam to diffuse outwards of the magnetic nozzle, thus hindering detachment. The generalized model has facilitated a quick revision of the electron-inertia detachment model of Hooper [J. Prop. Power 9, 757 (1993)] and the detection of a gross error in the manipulation of the equations, which leads to wrong solutions and conclusions. The error persists in recent followers of that model.

I. Introduction

A divergent magnetic nozzle, created by a longitudinal magnetic field, is being proposed as the acceleration stage for a magnetized plasma in advanced propulsion devices, such as the helicon thruster,[1–4] the applied-field magnetoplasmadynamic thruster,[5] and the VASIMR.[6] In order to understand the plasma physics in a propulsive magnetic nozzle we have being developing a two-dimensional(2D) plasma/nozzle model and its associated numerical code DIMAGNO. The model considers the stationary expansion of a fully-ionized, near-collisionless plasma (as the one we expect delivered from the production stage of a plasma thruster), with fully-magnetized electrons and partially-magnetized ions (which is the case to be expected for magnetic strengths of the order of 0.1 Tesla).

In a first group of works[7–11] we were devoted to analyze the main features of the plasma radial and axial expansion, the plasma currents, the thrust transmission, and the nozzle efficiency (i.e. the axial-versus-total energy flow). These studies have confirmed that a propulsive magnetic nozzle is able to both convert internal energy into axial directed energy and obtain additional thrust from the plasma beam, with the great benefit of no wall-contact and geometric versatility.

Then, in a second group of works, we have started to tackle the issue of plasma detachment from the nozzle,[12–14] which could be the penalty of using this, otherwise attractive, propulsive device. Since the nozzle magnetic lines close on themselves, once the plasma beam has been accelerated and before the turning point of the magnetic nozzle, the plasma jet needs to detach effectively from the magnetic lines. Experiments seem to confirm that (most of) the plasma detaches, but more measurements are needed to confirm this, detachment mechanisms are poorly known, and the efficiency of the detachment must be assessed.

Two detachment mechanisms of the plasma *from the guide magnetic field* have been modeled: magnetic-stretching detachment proposed by Arefiev and Breizman,[15,16] and electron-inertia detachment suggested by Hooper.[17] In the first case, the induced magnetic field would reinforce the applied field, thus stretching the effective magnetic nozzle. The plasma, by remaining attached to the nozzle resulting from the total magnetic

*Professor, eduardo.ahedo.upm.es (web.fmetsia.upm.es/ep2)
†PhD student, mario.merino@upm.es

field, would detach effectively *inwards* from the guide field nozzle. In the second case, Hooper claims that electron-inertia forces detach the plasma jet *inwards* from the guide-field nozzle. Resistive detachment[18] was also suggested as a third detachment mechanism, but no detailed model was developed.

In Ref. 13 we demonstrated that these three detachment mechanisms do not apply to a magnetic nozzle aimed for propulsion (i.e. with a near-sonic, hot plasma at its entrance). First, the induced magnetic field opposes the applied field and therefore reduces magnetization and increases the divergence of the effective nozzle. This has just been confirmed experimentally in Ref.[19] Second, a perturbation analysis showed that electron-inertia is a diffusive mechanism, comparable to resistivity, and both mechanisms detach the plasma plume *outwards* the magnetic streamtubes, therefore working against the axial expansion of the beam.

Current work is attempting mainly to unveil valid detachment mechanisms and, subsidiarily, to reinforce our disagreeing position with respect to magnetic-stretching and electron-inertia detachment theories. In Ref. 14 we show that plasma demagnetization, enhanced by the induced field, can be an effective detachment mechanism for a high density plasma. Here, it is the turn to deal directly with the model promoted by Hooper and to explain why we reach opposite conclusions to him. We will show that Hooper commits a mistake in the mathematical manipulation of the equations with fatal consequences, since it leads him to an ill-founded physical model and therefore to erroneous results and conclusions. Schmit and Fisch[20] and Little and Choueiri,[21,22] who tried to extend the model of Hooper to more general conditions, do not realize the mistake and are misled in their results too.

The central difference between Hooper's model and ours is that he *imposes* current ambipolarity everywhere whereas we show that its imposition makes the plasma model incompatible mathematically. Two other differences between the two models might be raised by someone to claim that both models are 'independent' and provide two 'independent truths'. The first one is that keeping electron-inertia is central in the derivation of Hooper's model, whereas for us electron-inertia is just a small effect, which does not modify the main features of the plasma/nozzle response. The second one is that Hooper considers only the case of a cold plasma at the nozzle entrance (a case of limited interest for a propulsive magnetic nozzle, since it misses its central role of incrementing thrust). Nonetheless, the cold-plasma case might still shed some right understanding on the detachment issue.

Here, we will proceed in the following way. First, we will derive the *nonzero* electron-inertia, hot-plasma model and we will demonstrate that that *zero* electron-inertia is just a regular limit of that model. Second, we will confirm that current ambipolarity is not fulfilled, *independently* of the presence or not electron-inertia effects. Third, we will show where lies the main mistake in Hooper's equations.

II. General model

A current-free, fully-ionized plasma jet is injected at the throat of a divergent magnetic nozzle created by both a external coil system *and* the magnetic field induced by plasma currents (which is solved as explained in Ref.14). In cylindrical coordinates (z, r, θ), the magnetic field is $\boldsymbol{B} = B_r \mathbf{1}_r + B_z \mathbf{1}_z$ and we adopt the convention $B_r, B_z > 0$. The cylindrical and magnetic frames of reference are $\{\mathbf{1}_z, \mathbf{1}_r, \mathbf{1}_\theta\}$ and $\{\mathbf{1}_\parallel, \mathbf{1}_\perp, \mathbf{1}_\theta\}$, with $\mathbf{1}_\parallel = \boldsymbol{B}/B = \cos\alpha \mathbf{1}_z + \sin\alpha \mathbf{1}_r$, $\mathbf{1}_\perp = -\sin\alpha \mathbf{1}_z + \cos\alpha \mathbf{1}_r$, and $\alpha(z, r)$ is the local magnetic angle. A magnetic streamfunction ψ exists, which satisfies

$$\nabla\psi = rB\mathbf{1}_\perp : \qquad \partial\psi/\partial z = -rB_r, \quad \partial\psi/\partial r = rB_z. \tag{1}$$

The plasma is assumed to satisfy the distinguished orderings

$$\lambda_{d0} \ll \ell_{e0} \ll R \ll \lambda_{ei0}, \qquad R\Omega_{i0}/u_{i0} = O(1) \tag{2}$$

where subscript 0 refers always to values at the center of the nozzle throat (located at $z = 0$); R is the plasma jet radius at the throat λ_d is the Debye length, ℓ_e is the electron gyroradius, λ_{ei} is the electron-ion collision mean-free-path, Ω_i is the ion gyrofrequency, and u_i is the longitudinal ion fluid velocity. These orderings imply that the plasma is quasineutral and near-collisionless, the magnetic field channels magnetized electrons (thus creating the nozzle effect) and ions are mildly or weakly magnetized (thus being tied to electrons mainly by the ambipolar electric field).[9]

A two-fluid model is adopted for the quasineutral plasma. Let $n \equiv n_i = n_e$ be the plasma density. For vectorial magnitudes, such as velocities $\boldsymbol{u}_k$ $(k = i, e)$ and current densities $\boldsymbol{j}_k$, it is convenient to separate the azimuthal component from the longitudinal ones, here denoted with a tilde: $\tilde{\boldsymbol{u}}_{\boldsymbol{i}} = \boldsymbol{u}_i - u_{\theta i}\mathbf{1}_\theta$, $\tilde{\boldsymbol{j}}_{\boldsymbol{e}} = \boldsymbol{j}_e - j_{\theta e}\mathbf{1}_\theta$,

etcetera. The fluid equations for ions are

$$\nabla \cdot n\tilde{\boldsymbol{u}}_{\boldsymbol{i}} = 0, \tag{3}$$

$$m_i \tilde{\boldsymbol{u}}_{\boldsymbol{i}} \cdot \nabla (r u_{\theta i}) = r e u_{\perp i} B, \tag{4}$$

$$m_i \tilde{\boldsymbol{u}}_{\boldsymbol{i}} \cdot \nabla \tilde{\boldsymbol{u}}_{\boldsymbol{i}} = -\nabla h_i - e\nabla\phi + \mathbf{1}_\perp e u_{\theta i} B + \mathbf{1}_r m_i u_{\theta i}^2 / r, \tag{5}$$

where ϕ is the ambipolar electric potential and $h_i \equiv n^{-1}\nabla(nT_i)$ is the barotropic function, with $h_i = T_i \ln n$ for isothermal ions and $h_i = T_{i0}\gamma_i(\gamma_i - 1)^{-1}(n/n_0)^{(\gamma_i - 1)}$ for polytropic ions. The rest of symbols are conventional. Notice that $\tilde{\boldsymbol{u}}_{\boldsymbol{i}} \cdot \nabla$ is the derivative along the (meridian-projected) ion streamlines. From Eq. (3) an ion streamfunction ψ_i exists, which satisfies

$$\partial\psi_i/\partial z = -rnu_{ri}, \quad \partial\psi_i/\partial r = rnu_{zi}. \tag{6}$$

Also, Eq. (1) and Eq. (4) yield the conservation of total ion angular momentum,

$$r m_i u_{\theta i} + e\psi = D_i(\psi_i), \tag{7}$$

with $D_i(\psi_i)$ determined from entrance conditions at the throat. This equation relates, at $z = 0$, the magnetic and ion streamtubes (i.e. $\psi = \text{const}$ and $\psi_i = \text{const}$) with the same cross section.

The fluid equations for electrons are

$$\nabla \cdot n\tilde{\boldsymbol{u}}_{\boldsymbol{e}} = 0, \tag{8}$$

$$m_e \tilde{\boldsymbol{u}}_{\boldsymbol{e}} \cdot \nabla (r u_{\theta e}) = -r e u_{\perp e} B, \tag{9}$$

$$0 = -\nabla h_e + e\nabla\phi - \mathbf{1}_\perp e u_{\theta e} B + \mathbf{1}_r m_e u_{\theta e}^2 / r. \tag{10}$$

The formulation is identical than for ions, except for the longitudinal inertia term $m_e \tilde{\boldsymbol{u}}_{\boldsymbol{e}} \cdot \nabla \tilde{\boldsymbol{u}}_{\boldsymbol{e}}$ in Eq. (10) is neglected, based on $m_e/m_i \ll 1$ and $\tilde{u}_e \sim \tilde{u}_i$. However, azimuthal inertia terms in Eqs. (9) and (10), involving $m_e u_{\theta e}$, are kept in order to recover the model of Hooper. Clearly these inertia terms are fully negligible if $u_{\theta e} \leq O(\tilde{u}_e)$. As in the case of ions: h_e is the electron barotropic function; there is an electron streamfunction ψ_e satisfying

$$\partial\psi_e/\partial z = -rnu_{re}, \quad \partial\psi_e/\partial r = rnu_{ze}; \tag{11}$$

and the conservation of total electron angular momentum reads

$$r m_e u_{\theta e} - e\psi = D_e(\psi_e), \tag{12}$$

with $D_e(\psi_e)$ determined from conditions at the throat.

The equation for plasma longitudinal momentum is the sum of Eqs. (5) and (10),

$$m_i \tilde{\boldsymbol{u}}_{\boldsymbol{i}} \cdot \nabla \tilde{\boldsymbol{u}}_{\boldsymbol{i}} = -\nabla(h_i + h_e) + \mathbf{1}_\perp e B (u_{\theta i} - u_{\theta e}) + \mathbf{1}_r \frac{m_i u_{\theta i}^2 + m_e u_{\theta e}^2}{r}, \tag{13}$$

and is used instead of Eq. (5), because it does not involve the electric field, $-\nabla\phi$.

Equations (3)-(5) and (8)-(10) constitute a *complete* set of 8 scalar equations for the 8 plasma variables $\boldsymbol{u}_i$, $\boldsymbol{u}_e$, n, and ϕ. We will show this set to be a well-posed mathematical problem with a unique solution (for given throat conditions). Therefore, any equation added to the model makes it incompatible (unless it is an automatic consequence of the other 8 equations and their boundary conditions). Equations (3) and (8) yield the electron conservation law

$$\nabla \cdot (\tilde{\boldsymbol{j}}_i + \tilde{\boldsymbol{j}}_e) = 0. \tag{14}$$

Hooper substitutes this *scalar* equation by the more restrictive *vectorial* equation

$$\tilde{\boldsymbol{j}}_i + \tilde{\boldsymbol{j}}_e = \mathbf{0}, \quad \text{i.e.} \quad \tilde{\boldsymbol{u}}_{\boldsymbol{i}} = \tilde{\boldsymbol{u}}_{\boldsymbol{e}}, \tag{15}$$

known as *current ambipolarity* condition. Clearly, this procedure leads to a 9-equation model with 8 variables, which is presumably incompatible. This reasoning is independent on whether we keep the inertial terms on Eqs. (9) and (10) or we drop them.

III. The massless electron model

Since $m_e/m_i \sim 10^{-4}$ (and unless we presume $u_{\theta e}$ to be very large) the *natural* 8-equation model to discuss is the one with $m_e/m_i \to 0$. This requires only to drop from the above general model one term in Eq. (9) and another one in Eq. (10). The massless electron model is the one we have analyzed extensively in previous works. We summarize next the most relevant *mathematical and physical* results we have achieved.

On the mathematical side we have, first, that Eq. (9) yields

$$u_{\perp e} = 0, \tag{16}$$

and the alternative Eq. (12) becomes

$$-e\psi = D_e(\psi_e). \tag{17}$$

They state that electron streamtubes are magnetic streamtubes everywhere (relating univocally ψ and ψ_e). Second, Eq. (8) and $\nabla \cdot \boldsymbol{B} = 0$ yield

$$u_{\parallel e} = G_e(\psi_e)B/n, \tag{18}$$

with $G_e(\psi)$ determined from throat conditions. Third, the projection of Eq. (10) along $\mathbf{1}_\parallel$ yields a Boltzmann-type law for the electric potential

$$-e\phi + h_e = H_e(\psi_e), \tag{19}$$

with $H_e(\psi_e)$ determined from throat conditions. Fourth, the projection of Eq. (10) along $\mathbf{1}_\perp$ yields the electron azimuthal velocity

$$u_{\theta e} = -\frac{1}{eB}\frac{\partial H_e}{\partial \mathbf{1}_\perp} \equiv -\frac{r}{e}\frac{dH_e}{d\psi}. \tag{20}$$

This equation states that, first, $u_{\theta e}$ is the combination of the $E \times B$ and the diamagnetic drifts and, second, the angular velocity of the electron flow, $u_{\theta e}/r$, is frozen in the streamtubes. Fifth, the substitution of these electron magnitudes into the 4 ion equations, yields an hyperbolic set of equations for supersonic ions, wherefrom $\boldsymbol{u}_i$ and n are determined. It is worth to stand out that the four conservation equations for magnetized electrons are standard and have a well-founded physical meaning.

The most relevant physical features extracted from our model are the following:

(1) Partially-magnetized ions are not fully-channeled by the magnetic/electron streamtubes so that *current ambipolarity is not satisfied*, even when it is imposed as entrance condition at the throat.

(2) Due to the separation between electron and ion streamtubes, a strong electric field along $\mathbf{1}_\perp$ is formed to comply with quasineutrality. This leads to a strong perpendicular rarefaction and makes *quasi-1D models of the nozzle little adequate.*

(3) The perpendicular electron force balance consists of *an expanding pressure force, a confining magnetic force, and a confining electric force.*

(4) The confining magnetic force on electrons is intimately related to the *electron azimuthal current $j_{\theta e}$ being diamagnetic* (i.e. running opposite to the coils azimuthal electric current).

(5) In general, *$j_{\theta e}$ consists of a volumetric contribution within the plasma beam and a surface contribution at the plasma/vacuum edge.*

(6) For ions without azimuthal rotation at the nozzle throat, the *ion azimuthal current $j_{\theta i}$ is paramagnetic.*

(7) It is readily derived from basic physics that *positive plasma beam acceleration and thrust contribution in the diverging nozzle are achieved with a net diamagnetic plasma current.* [Points (4) to (7) seem to have been rediscovered lately by Little and Choueiri.[22]]

(8) Maximum thrust gain is achieved for a *sonic plasma flow at the throat* (so that there is maximum internal energy to be converted into axial directed energy) and *weakly magnetized ions* (so that perpendicular rarefaction is maximum). This case coincides with a minimum contribution of ion paramagnetic currents.

(9) Plasma detachment via magnetic stretching, as proposed by Arefiev and Breizman,[15] is related to a dominance of paramagnetic plasma currents and therefore has no interest for propulsive magnetic nozzles. Instead, plasma detachment in these nozzles is facilitated by demagnetization, enhanced by induced field effects.[14]

IV. Model with electron-inertia

We return here to the general model with the two electron inertia terms in Eqs. (9) and (10). Since these two terms have the product $m_e u_{\theta e}$, the relevance of electron inertia is going to depend on the value of $u_{\theta e}$ at the nozzle throat. Three cases can be distinguished.

The first one corresponds to the plasma entering the divergent nozzle with $u_{\theta e}(z=0,r)=0$. In this case *the solution of the general model is the solution of the massless-electron model with* $u_{\theta e}=0$ *everywhere* (that is with $H_e=\text{const}$).

The second case corresponds to the plasma entering the divergent nozzle with a 'moderate' value of $u_{\theta e}(z=0,r)$, say $u_{\theta e}\sim u_i$. Then, the linear-perturbation analysis based on the solution for $m_e/m_i=0$, that we carried out in Ref.13, should be enough to assess electron-inertia effects. The main conclusion of that analysis is that electron inertia allows the development of an *outwards* velocity

$$u_{\perp e}\simeq m_e\frac{2u_{re}}{eB}\frac{u_{\theta e}}{r}. \tag{21}$$

This is the consequence of the diffusive character of electron inertia, which tends naturally to expand the plasma beam (instead of contracting it). Notice that since B is inversely proportional to the nozzle cross-section area, electron-inertia effects increase downstream proportionally to that area. [Our analysis of Ref.13 also showed that, in practical cases, electron-inertia is likely to be a more important effect than resistivity.]

Finally, the exact solution of the general model is presented next. This is likely to be needed for either large values of $u_{\theta e}$ or far downstream in the nozzle.

A. General analysis

When electron-inertia is included the solving of electron equations is less straightforward. The electron streamtubes differ from magnetic streamtubes and their shape must be determined. First, Eq. (12) yields $u_{\theta e}=[D_e(\psi_e)+e\psi]/(m_e r)$, that substituted into Eq. (10) leads to

$$0=\nabla(e\phi-h_e)-\mathbf{1}_\perp eB\frac{D_e(\psi_e)+e\psi}{m_e r}+\mathbf{1}_r\frac{[D_e(\psi_e)+e\psi]^2}{m_e r^3}. \tag{22}$$

After using Eq. (1) and some manipulation, this equation becomes

$$0=\nabla\left[e\phi-h_e-\frac{\big(D_e+e\psi\big)^2}{2m_e r^2}\right]+\frac{D_e+e\psi}{m_e r^2}\frac{dD_e}{d\psi_e}\nabla\psi_e. \tag{23}$$

The component of Eq. (23) parallel to electron streamtubes is

$$-e\phi+h_e+\frac{1}{2}m_e u_{\theta e}^2=H_e(\psi_e), \tag{24}$$

which is a recognizable generalization of Eq. (19). Then, the component of Eq. (23) perpendicular to electron streamtubes yields

$$\frac{D_e(\psi_e)+e\psi}{m_e r^2}\frac{dD_e}{d\psi_e}-\frac{dH_e}{d\psi_e}=0,$$

that is

$$e\psi=-D_e(\psi_e)+m_e r^2\frac{dH_e/d\psi_e}{dD_e/d\psi_e} \tag{25}$$

and

$$\frac{u_{\theta e}}{r}=\frac{dH_e/d\psi_e}{dD_e/d\psi_e}. \tag{26}$$

Equations (25) and (26) reduce, respectively, to Eqs. (17) and (20) in the massless-electron limit.

The main point here is that Eq. (25) is an implicit equation for the electron streamfunction $\psi_e\big(\psi(z,r),r\big)$ and therefore determines the shapes of the electron streamtubes without requiring the solution for the plasma density and the ion velocity. Once $\psi_e(z,r)$ is known, Eq. (26) yields $u_{\theta e}(z,r)$, which substituted in Eq. (13) allows the integration of the 4 ion hyperbolic equations and the determination of $\boldsymbol{u}_i$ and n. The last step is the determination of $\tilde{\boldsymbol{u}}_{\boldsymbol{e}}$ from Eq. (11).

Taking into account that $H_e(\psi_e)$ and $D_e(\psi_e)$ are expected to be negative and monotonic functions, the last term of Eq. (25) states that electron streamtubes separate *outwards* from magnetic streamtubes and the *separation increases with the nozzle cross-section area* (as predicted already by the perturbation analysis). Ion streamtubes are expected to continue separating *inwards* from magnetic streamtubes, so that *current ambipolarity is farther from being fulfilled when electron-inertia is added.*

A final observation is that $D_e(\psi_e) = \text{const}$ (and the constant can be set to 0 without loss of generality) is a singular case for expression (26). According to Eq. (12), it corresponds only to the particular conditions

$$u_{\theta e}(z=0,r) = \frac{e\psi(z=0,r)}{m_e r}. \tag{27}$$

and Eq. (26) imposes that $H_e(\psi_e) = \text{const} = 0$ too. The way to solve $\psi_e(\psi, r)$ for this very singular case has not been worked out completely since we believe it has no practical interest. First, it corresponds to a very particular spatial profile of $u_{\theta e}(z=0,r)$ at the throat. Second, the azimuthal velocity for this case seems extremely large: $u_{\theta e}/c_s \sim (R/\ell_{e0})(m_i/m_e)^{1/2}$ with c_s the plasma sound velocity.

V. On models with current ambipolarity

Once we have established and discussed the model with electron-inertia, we are ready to show where and why Hooper equations get wrong. Hooper assumes that electrons have no rotation when injected at the nozzle throat, i.e. $u_{\theta e}(z=0,r) = 0$, leading to $D_e(\psi_e) = -e\psi$ at $z = 0$. The *correct solution* for these conditions was derived before and has $u_{\theta e} = 0$ everywhere and electron streamtubes coincide with magnetic streamtubes while ion streamtubes do not, i.e. *there is neither current ambipolarity nor detachment.*

Instead, Hooper commits the gross mistake of treating the function $D_e(\psi_e)$ as a constant (his $-e\psi_0$) and thus *misses* the term with $dD_e/d\psi_e$ in Eq. (23). The consequence is fatal because he then misses Eq. (25), which is crucial for determining the electron streamtubes. The one-equation vacancy left by Eq. (25) misleads him to supplant it with the ambipolarity condition. The consequence is a nonphysical model, yielding conclusions widely opposed from those of the correct solution pointed out in the former paragraph.

The very only case where the model of Hooper could claim a possibility of being correct is for the singular conditions of Eq. (27), when Eq. (25) provides no information. Still we believe that current ambipolarity is not satisfied. Indeed, the solution that arises from adding current ambipolarity is rather weird. We illustrate it with the simple case of a cold plasma ($h_i = h_e = 0$) and a zero-divergence nozzle, having $B_r = 0$, $B_z = \text{const} = B_0$, $\psi = B_0 r^2/2$. Then, one has

$$u_{\theta e}(z,r) = u_{\theta e}(0,r) = \frac{eB_0}{2m_e} r, \qquad e\phi(z,r) = \frac{1}{2} m_e u_{\theta e}^2 = \frac{e^2 B_0^2}{8m_e} r^2. \tag{28}$$

This electric potential profile is not natural since it expands radially electrons instead of confining them as in the rest of cases. The effect of the unnatural radial electric field on the ion beam is to contract it until collapsing in a point. *This convergence of the ion beam would be the detachment mechanism claimed by Hooper.*

Schmit and Fisch[20] adopt the same cold plasma model of Hooper and discuss plasmas with non-zero injection angular velocity profiles. Little and Choueiri[21,22] extend the model of Hooper to include (in a simplified way) the electron pressure. Both works continue ignoring dD_e/ψ_e [and dD_i/ψ_i too] and adding current ambipolarity to the model.

VI. Conclusions

A model that generalizes our previous one by including the relevant electron-inertia terms has been derived and analyzed. It has been shown that the zero electron-inertia limit is a regular limit and a parametric continuation of solutions is expected to be continuous. The general model has the same mathematical structure and features than the zero inertia one. First, electron equations reduce to conservation equations, which are easily matched to the ion differential equations. Second, ion equations continue to be a set of hyperbolic differential equations to be solved with the method of characteristic surfaces. Third, the model does not leave room for imposing the current ambipolarity condition, and this is not fulfilled. This

non-fulfilment is by no means anecdotic, as results show. Two interesting properties of the zero-inertia model are preserved in the general model: (a) if the electron azimuthal current is zero at the entrance, it remains zero everywhere (except in the plasma/vacuum current sheet); and (b) the electron streamtubes and the electron longitudinal flux are determined exclusively from the electron equations. In addition, the general model confirms the two main trends of electron-inertia, obtained in our former linearized analysis:[13] (a) electron-inertia expands outwards the plasma beam and therefore is negative for detachment; and (b) although electron-inertia effects are expected quite small near the nozzle entrance, they grow downstream proportionally to the nozzle cross-section area.

Finally, it has been demonstrated that Hooper commits a mistake in the mathematical manipulation of the equations. The error is fatal since it eliminates one crucial electron equation from the model and leads him to fill the false vacancy with current ambipolarity. Consequently, the resulting solutions and conclusions are nonphysical.

Acknowledgments

This work has been sponsored by the Air Force Office of Scientific Research, Air Force Material Command, USAF, under grant number FA8655-10-1-3085. The U.S Government is authorized to reproduce and distribute reprints for Governmental purpose notwithstanding any copyright notation thereon. Additional support came from the Gobierno de España (Project AYA-2010-16699). E. Ahedo is very indebted to Prof. Martínez-Sánchez: the guidelines for our magnetic nozzle models were drafted out from intensive discussions between them in the summer of 2008.

References

[1]Ziemba, T., Carscadden, J., Slough, J., Prager, J., and Winglee, R., "High Power Helicon Thruster," *41th Joint Propulsion Conference, Tucson, AR*, AIAA 2005-4119, American Institute of Aeronautics and Astronautics, Washington DC, 2005.

[2]Charles, C., Boswell, R., and Lieberman, M., "Xenon ion beam characterization in a helicon double layer thruster," *Applied Physics Letters*, Vol. 89, 2006, pp. 261503.

[3]Batishchev, O., "Minihelicon Plasma Thruster," *IEEE Transaction on Plasma Science*, Vol. 37, 2009, pp. 1563–1571.

[4]Pavarin, D., Ferri, F., Manente, M., Curreli, D., Guclu, Y., Melazzi, D., Rondini, D., Suman, S., Carlsson, J., Bramanti, C., Ahedo, E., Lancellotti, V., Katsonis, K., and Markelov, G., "Design of 50W Helicon Plasma Thruster," *31th International Electric Propulsion Conference, Ann Arbor, Michigan, USA*, IEPC 2009-205, Electric Rocket Propulsion Society, Fairview Park, OH, 2009.

[5]Krülle, G., Auweter-Kurtz, M., and Sasoh, A., "Technology and application aspects of applied field magnetoplasmadynamic propulsion," *J. Propulsion and Power*, Vol. 14, 1998, pp. 754–763.

[6]Arefiev, A. and Breizman, B., "Theoretical components of the VASIMR plasma propulsion concepta," *Physics of Plasmas*, Vol. 11, No. 5, 2004, pp. 2942–2949.

[7]Ahedo, E. and Merino, M., "Two-dimensional plasma acceleration in a divergent magnetic nozzle," *44th Joint Propulsion Conference, Hartford, CT*, AIAA 2009-5361, American Institute of Aeronautics and Astronautics, Washington DC, 2008.

[8]Ahedo, E. and Merino, M., "Acceleration of a focused plasma jet in a divergent magnetic nozzle," *31th International Electric Propulsion Conference, Ann Arbor, Michigan, USA*, IEPC 2009-002, Electric Rocket Propulsion Society, Fairview Park, OH, 2009.

[9]Ahedo, E. and Merino, M., "Two-dimensional supersonic plasma acceleration in a magnetic nozzle," *Physics of Plasmas*, Vol. 17, 2010, pp. 073501.

[10]Merino, M. and Ahedo, E., "Two-dimensional magnetic nozzle acceleration of a two-electron component plasma," *Proceedings of Space Propulsion 2010, San Sebastián, Spain, May 3-6, 2010*, European Space Agency, Noordwijk, The Netherlands, 2010, pp. SP2010–1841391.

[11]Merino, M. and Ahedo, E., "Simulation of plasma flows in divergent magnetic nozzles," *IEEE Transactions Plasma Science (to appear in August)*, 2011.

[12]Ahedo, E. and Merino, M., "Preliminary assessment of detachment in a plasma thruster magnetic nozzle," *46th Joint Propulsion Conference, Nashville, TN*, AIAA 2010-6613, American Institute of Aeronautics and Astronautics, Washington DC, 2010.

[13]Ahedo, E. and Merino, M., "On plasma detachment in propulsive magnetic nozzles," *Physics of Plasmas*, Vol. 18, 2011, pp. 053504.

[14]Merino, M. and Ahedo, E., "Plasma detachment mechanisms in a magnetic nozzle," *Proceedings of 47th Joint Propulsion Conference, San Diego, CA*, AIAA 2011-5999, American Institute of Aeronautics and Astronautics, Washington DC, 2010.

[15]Arefiev, A. and Breizman, B., "Magnetohydrodynamic scenario of plasma detachment in a magnetic nozzle," *Physics of Plasmas*, Vol. 12, 2005, pp. 043504.

[16]Breizman, B. N., Tushentsov, M. R., and Arefiev, A. V., "Magnetic nozzle and plasma detachment model for a steady-state flow," *Physics of Plasmas*, Vol. 15, 2008, pp. 057103.

[17]Hooper, E. B., "Plasma Detachment from a Magnetic Nozzle," *Journal of Propulsion and Power*, Vol. 9, No. 5, 1993, pp. 757–763.

[18]Moses, R. W., Gerwin, R., and Schoenberg, K., "Resistive plasma detachment in nozzle based coaxial thrusters," *Proceedings Ninth Symposium on Space Nuclear Power Systems, Albuquerque, New Mexico, 1992*, AIP Conference Proceedings No. 246, American Institute of Physics, Woodbury NY, 1992, pp. 1293–1303.

[19]Roberson, B., Winglee, R., and Prager, J., "Enhanced diamagnetic perturbations and electric currents observed downstream of the high power helicon," *Physics of Plasmas*, Vol. 18, 2011, pp. 053505.

[20]Schmit, P. and Fisch, N., "Magnetic detachment and plume control in escaping magnetized plasma," *Journal of Plasma Physics*, Vol. 75, No. 03, 2009, pp. 359–371.

[21]Little, J. and Choueiri, E., "The Influence of Induced Currents on Magnetic Nozzle Acceleration and Plasma Detachment," *Proceedings of 46th Joint Propulsion Conference, Nashville, TN*, AIAA 2010-6615, American Institute of Aeronautics and Astronautics, Washington DC, 2010.

[22]Little, J. and Choueiri, E., "Plasma detachment and momentum transfer in magnetic nozzles," *Proceedings of 47th Joint Propulsion Conference, San Diego, CA*, AIAA 2011-6001, American Institute of Aeronautics and Astronautics, Washington DC, 2011.

Hybrid model simulation of a plasma plume in a magnetic nozzle

IEPC-2011-048

Presented at the 32nd International Electric Propulsion Conference,
Wiesbaden, Germany
September 11–15, 2011

Jaume Navarro* and Eduardo Ahedo†
E.T.S. Ingenieros Aeronáuticos, Plaza Cardenal Cisneros, Madrid 28040, Spain

The following research inquiries into the plasma expansion in a divergent magnetic nozzle using an axilsymmetric hybrid code. This code is derived from a previous one for Hall-effect thrusters. It is based on Particle-in-cell (PIC) methods for ions and neutrals, and anisotropic fluid model for electrons, assuming they are strongly magnetized. The PIC subcode provides a map of densities and fluxes of heavy species. Likewise, the code assumes the plasma to be quasineutral. Ion streamtubes are found to detach from electron/magnetic streamtubes, thus agreeing with results from a fluid code of our own. The behavior of the magnetic nozzle on the plasma plume expansion is contrasted with simulations of an unmagnetized plasma plume.

I. Introduction

Some propulsion devices propose the divergent magnetic nozzle as an efficient mechanism to accelerate the plasma, generated upstream, inside the thruster discharge chamber, like the Helicon thruster,[1–4] the applied-field magnetoplasmadynamic thruster,[5] and the VASIMR.[6] Merino and Ahedo[7–11] have carried out studies of supersonic plasma expansion along the divergent magnetic nozzle. Most of the results have been obtained with DIMAGNO, the numerical code associated to a two-dimensional fluid plasma/nozzle model. They analyzed the plasma radial and axial expansion, the plasma currents and the main magnetic nozzles performances in terms of thrust gain and thrust efficiency.

The present investigation tries to make inquiries on the resourcefulness of an axilsymmetric hybrid code to simulate the plasma expansion inside a divergent magnetic nozzle. The hybrid model physical and mathematical bases were summarized by Parra et al.,[12] and it solves the most important aspects of Hall-effect thrusters performances. Some modifications have been introduced since 2005 in order to simulate other physical processes, such as the improvement of the plasma-wall interaction models,[13,14] the Bohm condition fulfillment in the transition between the quasineutral domain and the non-neutral plasma sheath near the wall,[15] and other improvements related to numerical algorithms.

The former hybrid code has been reorganized to figure out the new topology of the present problem, the divergent magnetic nozzle. Required changes affect both the electron fluid subcode and the PIC algorithms. Besides, the new version is able to simulate the expansion of an unmagnetized plasma, neglecting the effects of the magnetic nozzle. Subsequently, it provides the opportunity to draw a comparison between each acceleration mechanism.

In the current step of development, electrons will be take for granted to be isothermal. However, a previous analysis of the problem gives us enough information to consider the non-isothermal case. At the moment, it is being built up, but it might require substantial modifications on the numerical scheme on the former electron fluid subcode due to numerical instabilities.

This study also confirms that current ambipolarity is not fulfilled everywhere inside the plasma expansion in a divergent magnetic nozzle topology. The fulfillment of this conjecture presents some incompatibilities with basic laws such as charge conservation.[16]

*PhD student, jaume.navarro@upm.es
†Professor, eduardo.ahedo@upm.es (web.fmetsia.upm.es/ep2)

This article is structured in the following way. In a fist place, we will summarize the former hybrid code important modifications. In a second place, the key points of the plasma model expansion in a divergent magnetic nozzle will be derived. In a third place, a plasma expansion simulation through a divergent magnetic nozzle will be compared with the plasma expansion without magnetic nozzle effects. Finally, a summary of the main conclusions and future improvements will be announced.

II. Modifications on the former hybrid code

In order to clarify the most important variations, a brief discussion about the original hybrid code is necessary to understand all introduced changes. The code can be divided into two very different parts: the PIC subcode, and the electron subcode. The first one provides the plasma density n_e distribution and ion current densities $\boldsymbol{j}_i$ to the second one. Consequently, the electron subcode returns the electron temperature T_e, the electric potential ϕ, and the perpendicular electric current $I_\perp$ through each magnetic surface. The three last plasma variables are one-dimensional, constant along each magnetic surface and inputs for the PIC subcode.

It is also necessary to emphasize that each subcode uses different meshes to do computations on it (Fig. 1). The electron subcode mesh is derived from the magnetic field. This field is stationary. A low-beta plasma is considered, so that the induced magnetic field, due to plasma currents, can be neglected when compared with the applied field. The field particularities allow us to get the magnetic streamfunction. Each magnetic line (or magnetic surface, if axilsymmetry is assumed) constitutes a node for the electron subcode, and all fluid dynamics equations will be projected on them. In addition, referring to the PIC subcode, we could distinguish two meshes: the $r-z$ mesh and the computational grid. The first one is a cylindrical prism lengthwise section where particles are moved according to electromagnetic and inertial forces. Also, the computational grid is a rectangular auxiliary mesh, which is necessary for weighting PIC algorithms. Both electrons, as well as the PIC meshes, were prepared to deal with a very restrictive topology of conventional Hall thrusters, such as the SPT-100. The greatest effort carried out in this project, in terms of software development, has consisted on making it more flexible and adapting all subroutines to the new proposal.

The most important modifications are listed below.

1. **Boundary conditions** were intrinsically implemented in the former hybrid code. To give an example, observing the computational grid, all the escaped ions from the computational domain through the bottom or top boundaries were recombined automatically because the code assumed these boundaries to be walls. New conditions are extremely different now. The $r-z$ and its linked computational grid will assume right and top boundary to be vacuum, bottom boundary to be the axis of symmetry and left boundary to be, either wall or plasma injector (magnetic nozzle throat).

2. **Axis of symmetry** is included into the domain. It is the bottom boundary of the PIC mesh. Reducing the miscalculation tolerance between each particle position in the $r-z$ plane and its position in the computational grid is a required change to avoid inconsistencies of numerical weighting algorithms.

3. **Particle injection subroutine** requires significant modifications. The new version makes possible to introduce the density profile of the plasma along the panels that make up the injection section. This section can be located along a chosen range of panels in the left boundary.

4. **Electron mesh**, defined by the magnetic topology, was simple for a common Hall thruster. Every line intercepts both, bottom and top PIC boundaries, always finding wall conditions at the end of each line, wich make the process of stream function discretization to be easier, but some difficulties in the anode region (left boundary of PIC subcode) appeared. Magnetic lines can indistinctly intercept all PIC boundaries now. The last magnetic line coincides with the axis of symmetry. The new topology requires redefining all the boundary conditions at the end of each magnetic stream line depending on the PIC boundary that is intercepted.

5. **The electron temperature solver**, based on the solution of the electron energy equation is provisionally blocked because T_e is assumed constant.

6. **Ionization subroutines** are also blocked to simplify the plasma model. Furthermore, we will only take into account simple ions.

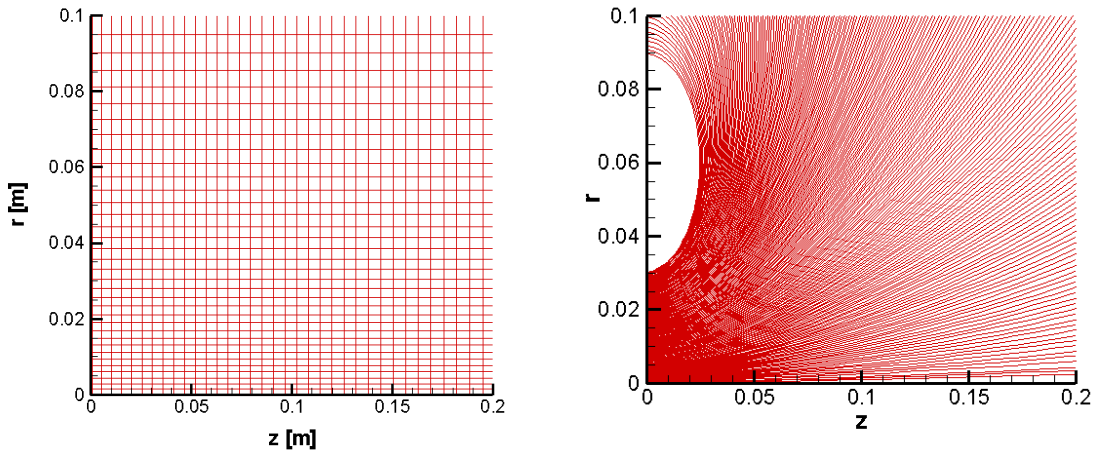

Figure 1. PIC $r-z$ mesh (left) and magnetic mesh (right)

III. Plasma model in a magnetic nozzle

First of all, we summarize the process to obtain the magnetic mesh from the magnetic field topology. This field, created by a coil system, is solved during the pre-process using a commercial FEM code. The zero-vorticity and zero-divergence of the magnetic field, $\nabla \times \boldsymbol{B}$ and $\nabla \cdot \boldsymbol{B}$ respectively, let us to assure the magnetic stream function λ exists and satisfies,

$$\frac{\partial \lambda}{\partial z} = -rB_r \qquad \frac{\partial \lambda}{\partial r} = rB_z \tag{1}$$

where B_z and B_r are the magnetic field components expressed on a cylindrical reference frame $\{\mathbf{1}_z, \mathbf{1}_r, \mathbf{1}_\theta\}$. The magnetic reference frame will be $\{\mathbf{1}_\perp, \mathbf{1}_\parallel, \mathbf{1}_\theta\}$ in which $\mathbf{1}_\parallel = \boldsymbol{B}/B = \cos\alpha \mathbf{1}_z + \sin\alpha \mathbf{1}_r$, $\mathbf{1}_\perp = \sin\alpha \mathbf{1}_z - \cos\alpha \mathbf{1}_r$ and $\alpha(r,z)$ is the local magnetic angle. Each different λ value, belongs to a different magnetic streamline, in which λ, T_e, $I_\perp$, and the thermalized potential ϕ_0 (defined below) are constant. Differential control volumes are defined for each streamline. The streamline revolution around the axis of symmetry, defines a magnetic surface.

Further, we will submit the electron fluid dynamics equations, basically, mass conservation and momentum equation. In this case, energy equation is omitted because T_e is constant.

$$\frac{\partial n_e}{\partial t} + \nabla \cdot (n_e \boldsymbol{u}_e) = \dot{n}_e \tag{2}$$

$$n_e m_e \left(\frac{\partial \boldsymbol{u}_e}{\partial t} + \boldsymbol{u}_e \cdot \nabla \boldsymbol{u}_e \right) = -\nabla p_e - e n_e (\boldsymbol{E} + \boldsymbol{u}_e \times \boldsymbol{B}) + \boldsymbol{M} \tag{3}$$

Equation 2 can be combined with the ion continuity equation, which has the same form. Afterwards, assuming the hypothesis of quasineutral plasma ($n_e \approx n_i$) and the lack of ionization processes, it yields the charge conservation law,

$$\nabla \cdot \boldsymbol{j} = 0, \tag{4}$$

where $\boldsymbol{j}$ is the electric current density.

Analyzing the electron momentum equation, some assumptions should be taken. $\boldsymbol{M}$ include all collisional effects and it can be written $\boldsymbol{M} = -n_e m_e \nu_e \boldsymbol{u}_e$, where ν_e is the effectively electron collision frequency and takes into account *electron-ion* and *electron-neutral* collisions. This frequency can also include other plasma physical processes related to the plasma wall interaction, virtual cathode considerations and anomalous diffusion. In this work, anomalous diffusion and virtual cathode contribution are not taken into account. The inertial term can be neglected due to the significant difference between electron mass, and ion mass $m_e/m_i \ll 1$. Moreover, this convective term is lower than the electromagnetic force, on the right side of the equation,

$$\|n_e m_e \boldsymbol{u}_e \cdot \nabla \boldsymbol{u}_e\| / \|e n_e \boldsymbol{u} \times \boldsymbol{B}\| \sim r_L u_e / R v_{te} \ll 1.$$

Here, r_L is the Larmor electron gyroradius, R the magnetic nozzle throat radius and v_{te} the electron thermal velocity. Electron pressure p_e can be written as a function of its temperature $p_e = n_e T_e$, and the electric field $\boldsymbol{E}$ derives from a scalar potential $\boldsymbol{E} = -\nabla\phi$. This last assumption comes from both $\nabla \times \boldsymbol{E} = 0$ and $\nabla \cdot \boldsymbol{E} = 0$ because *(i)* we neglect $\boldsymbol{B}$ field fluctuations in time and *(ii)* assume that plasma is quasineutral. After all these assumptions, momentum equation is reduced to

$$\mathbf{0} = -T_e \nabla n_e + e n_e \nabla\phi - e n_e \boldsymbol{u}_e \times \boldsymbol{B} - n_e m_e \nu_e \boldsymbol{u}_e \tag{5}$$

Electron momentum equation can be projected according $\mathbf{1}_\parallel$ direction obtaining,

$$0 = -T_e \frac{\partial n_e}{\partial \mathbf{1}_\parallel} + e n_e \frac{\partial \phi}{\partial \mathbf{1}_\parallel} \tag{6}$$

Note the collisional term in the Eq. 6 has been scorned in collating with the expected pressure gradients,

$$\frac{\| n_e m_e \nu_e \boldsymbol{u}_{e\parallel} / B \|}{\| T_e \partial n_e / \partial \mathbf{1}_\parallel \|} \sim \frac{u_{e\parallel} R}{v_{te} \lambda_{col}} \ll 1$$

In the last expression, λ_{col} is the electron collision mean-free-path and we characterize these orderings inside the plasma: $\lambda_D \ll r_L \ll R \ll \lambda_{col}$; λ_D is the Debye length. Equation 6 can be integrated, yielding the Boltzmann relation

$$\phi(r,z) = \phi_0(\lambda) + \frac{T_e(\lambda)}{e} \ln\left(\frac{n_e(r,z)}{n_{ref}}\right); \tag{7}$$

$\phi_0(\lambda)$ is the thermalized potential and n_{ref} is any reference density. The Boltzmann relation determines the electric potential in terms of one-dimensional variables (T_e and ϕ_0) and the plasma density distribution determined by the PIC subcode.

Now, we project momentum equation on $\mathbf{1}_\perp$ and $\mathbf{1}_\theta$ respectively,

$$- T_e \frac{\partial n_e}{\partial \vec{1}_\perp} + e n_e \frac{\partial \phi}{\partial \vec{1}_\perp} + e n_e u_{e\theta} B - \nu_e m_e n_e u_{e\perp} = 0 \tag{8}$$

$$- e n_e u_{e\perp} B - \nu_e m_e n_e u_{e\theta} = 0 \tag{9}$$

After some algebraic manipulation, these two equations allow us to obtain expressions for $\boldsymbol{u}_{e\perp}$ and $\boldsymbol{u}_{e\theta}$,

$$u_{e\theta} = -\beta_e u_{e\perp}, \tag{10}$$

$$u_{e\perp} = \frac{r}{\beta_e} \frac{\partial \phi_0(\lambda)}{\partial \lambda}; \tag{11}$$

$\beta_e = \Omega_{ce}/\nu_e$ is the Hall parameter, and Ω_{ce}, is the electron gyrofrequency. We assume again constant temperature and moreover $\beta_e \gg 1$. Note that equation 11 is the Ohm´s law here.

A. Plasma conditions in the magnetic nozzle throat

In a Hall effect thruster, we usually consider that mass injection section coincides with the anodic wall of this device. Likewise, only neutral particles are injected through this boundary. Conditions are extremely different now. First of all, a free-current and fully-ionized plasma jet is injected at the magnetic nozzle throat. And the key point is the equilibrium between magnetic pressure, which confines the plasma, and plasma pressure, which tries to expand it,

$$0 = -T_e \partial_r n_e - e n_e u_{e\theta} B_\parallel. \tag{12}$$

The balance between these forces is achieved thanks to the plasma behavior upstream the nozzle, in the plasma source. In conclusion, the radial electric field must be zero along the magnetic nozzle throat. This condition combined with the Boltzmann relation yields an important constrain for the thermalized potential along all magnetic streamlines that goes through the throat section,

$$\phi_0 = -\frac{T_e}{e} \ln \frac{n_e}{n_{ref}}\bigg|_{z=0}. \tag{13}$$

Therefore, $\phi_0(\lambda)$ is defined by the radial distribution of the plasma density at the throat. For the simulations here, this plasma distribution is assumed to be parabolic, $n_e(r) = A(1-(r/R)^2)+B$. A and B are numerical constants and depend on some parameters such as the desired mass flow, the averaged ion speed at the throat and the ion density background. Ion velocity will be sonic at the throat, taking ion sound speed defined as $c_s = \sqrt{T_e/m_i}$, where m_i is the simple ion mass.

As a consequence of all concepts explained before, the determination of ϕ_0 and $I_\perp$ must be divided into two parts, depending on the region of the magnetic mesh that we consider. The first zone is defined by all magnetic streamlines that intercept the magnetic nozzle throat, whereas the second one is composed by the rest of streamlines. In this research, we have realized that is necessary to use different methodologies to solve each region due to the variability of the physical constrains.

B. Solving the internal region

As it has been announced, in the internal region, $\phi_0(\lambda)$ is determined by equation 13. As a result, $I_\perp(\lambda)$ must be obtained assuring the fulfillment of the charge conservation law (Eq. 4) in each magnetic differential volume. This restriction implies that current ambipolarity condition has not been assumed everywhere. To note this result, we will project Eq. 4 on the magnetic mesh, and after some algebraic operations it commutes to

$$\frac{\partial I_\perp(\lambda)}{\partial \lambda} = -\left.\frac{2\pi j}{(B\cos\alpha)}\right|_0 - \left.\frac{2\pi j}{(B\cos\alpha)}\right|_1 \tag{14}$$

This shows how the variation on the perpendicular current through each magnetic surface is caused by the loss or gain of net charge current at the domain boundaries. Subscript 0 and 1 refers to plasma properties just at the magnetic streamlines boundaries, being 0 the boundary located closest to the left bottom corner of the PIC domain (magnetic throat). Current densities j are positive according to the orthogonal outward vector for the PIC domain boundary. α is the angle between the mentioned vector and the local vector $\mathbf{1}_\perp$.

In all expressions $I_\perp(\lambda)$ is defined as the integral of the density current along the magnetic surface. Naturally, it needs to be contributed by both, the perpendicular current of ions and electrons.

$$I_\perp(\lambda) = \iint_{S(\lambda)} (\boldsymbol{j}\cdot\boldsymbol{u}_\perp)dS = \iint_{S(\lambda)} (\boldsymbol{j}_i\cdot\boldsymbol{u}_{i\perp}) + (\boldsymbol{j}_e\cdot\boldsymbol{u}_{e\perp})dS = \int_{\Gamma(\lambda)} 2\pi r e n_e(\boldsymbol{u}_i - \boldsymbol{u}_e)\cdot\boldsymbol{u}_\perp d\chi = I_{i\perp}(\lambda) + I_{e\perp}(\lambda) \tag{15}$$

Here the ion contribution $I_{i\perp}(\lambda)$ is obtained by the PIC subcode, whereas $I_{e\perp}(\lambda)$ depends on the reduced Ohm law (Eq. 11) resulting in

$$I_{e\perp}(\lambda) = -\int \frac{2\pi e n_e r^2}{\beta_e} d\chi \left(\frac{\partial \phi_0}{\partial \lambda}\right). \tag{16}$$

As a consequence, $\partial_\lambda I_\perp(\lambda) \neq 0$. Concerning the current ambipolarity condition, it can be imposed only at one of the two ends. In this study, it is forced at the throat and, from the charge conservation, the current density downstream, $\boldsymbol{j}|_1$, fulfills

$$j|_1 = -\frac{\partial I_\perp(\lambda)}{\partial \lambda}\frac{B\cos\alpha}{2\pi}. \tag{17}$$

On the other hand, note that the free-current plasma condition must be globally accomplished. This constrain provides an expression to control the committed error in the internal region,

$$\epsilon_c = -I_\perp(\lambda_V) + \int_{axis}^{\lambda_V} (\boldsymbol{j}(\lambda)\,\boldsymbol{dS}(\lambda))\,|_1 \simeq 0; \tag{18}$$

λ_V is the upper magnetic borderline of the plasma beam at the throat. In the simulations below, the error (ϵ_c) in the free-current constrain is lower than 1% in comparison to the equivalent ion current injected at the throat, $e\dot{m}_i/m_i$.

C. On the transitional boundary and the external region

When this project was started, we expected a gentle enough transition of plasma properties at the nominal plasma jet edge, between the internal region and the near-vacuum region. But our preliminary results

show this transition not to be as gradual as we expected. The essential problem remains on the charge conservation law fulfillment on the outside region, and the lack yet of convincing models to estimate the current density at the top vacuum boundary of the domain. Also, if the wall, located at the left side, is made of dielectric material, the total current through this surface must be zero, and this boundary condition is not accomplished by the current model.

As a preliminary approach we assume constant the perpendicular current through all the streamlines in the outside region. This hypothesis and the result of $I_{i\perp}$ obtained by the PIC subcode allows us to compute $I_{e\perp}$, but then we find out that Eq. 16 for the thermalized potential leads to nonphysical results. This problem is more acute because of the low value reached by the perpendicular electron diffusivity outside the dense jet. This diffusivity follows this behavior because of the magnetic field intensity increases whereas the electron collision frequency tends to decrease. Consequently, the Hall parameter becomes higher and, according to equation 16, the required gradients of ϕ_0 to assure this electron perpendicular current are extremely high. In spite of the main problem, the charge conservation law fulfillment, according to the complete generalized Ohm law for $u_{e\perp}$, a non-isothermal model with a plasma temperature cooling outwards should contribute to a better performance of the current model. Adding anomalous turbulence would also help. These improvements will be tested in the next stage of this research. Another aspect to consider is the density parabolic profile imposed at the throat. It implies a high gradient of ϕ_0 close to the transition boundary due to the deep drop of the plasma density. Gentler profiles, such as Gaussian ones, could make easier the transition and the behavior of the thermalized potential at this transition region.

IV. Simulation results

This section presents and discuss the most interesting results so far. First, the plasma density distribution will be compared with the case in which there is not a magnetic nozzle. Then, the ion velocity vector distribution will be presented. Next, the contribution of the perpendicular electron current will be compared with ion and total currents. Afterwards, ion momentum axial contribution will be shown, in order to prove that the magnetic nozzle is an efficient device to accelerate a plasma jet. Finally, the distribution of the electromagnetic force generated by the azimuthal currents will be drawn in order to be compared with recent studies with DIMAGNO. Results have been obtained with the following parameters. Magnetic field axial intensity at the throat was 1000 Gauss. The injected ion mass flow was $\dot{m}_i = 5 \cdot 10^{-6} kg/s$. The electron temperature is 20eV. Plasma maps corresponds to results averaged over 40000 time-steps, equivalent to 0.4 milliseconds.

Figure 2 shows the plasma density distribution, for the cases with and without magnetic nozzle. The behavior is clearly different. It is also shown magnetic streamlines and ion streamlines (indeed their projection on a meridian plane). The nozzle effect is clearly illustrated and also the ion trend to detach downstream from the magnetic streamlines. In the unmagnetized case the plasma is accelerated diffusively and some ion streamlines go backwards to the left dielectric wall, where ions are recombined. Figure 3 complements the previous ones with the maps of radial and axial ion velocities. Figure 4 plots the ion azimuthal velocity, which is quite smaller than both the other two ion components and the electron azimuthal current, confirming both weak ion magnetization and thrust transmission to be dominated by the electron current.[9]

Figure 5 presents the perpendicular currents through magnetic surfaces as a function of the magnetic coordinate (λ). The perpendicular electron current is small due to strong magnetization. Again the much higher ion current indicates the low ion magnetization. The constant total electric current in the near-vacuum region is just an imposition, with no physical basis and will be revised.

Figure 6(left) shows the axial component of the ion momentum flux. It shows how an important gain is obtained compared with the reference value at the throat $F_0 = \dot{m}_i \bar{u}_i \sim 0.025N$. Finally, Fig. 6(right) shows the large azimuthal electron current at the plasma edge due to the diamagnetic drift caused by density gradients there. The electromagnetic force density $j_\theta B_r$ is the responsible of the momentum gain. The map distribution is much like the one shown by Merino and Ahedo.[11]

V. Conclusions

Hybrid code capabilities to simulate the magnetic nozzle performances and acceleration mechanisms have been analyzed. Obtained results show that the magnetic nozzle offers the advantage of guiding the plasma axially and confine it more efficiently. Our conclusions agree with the obtained results using the DIMAGNO

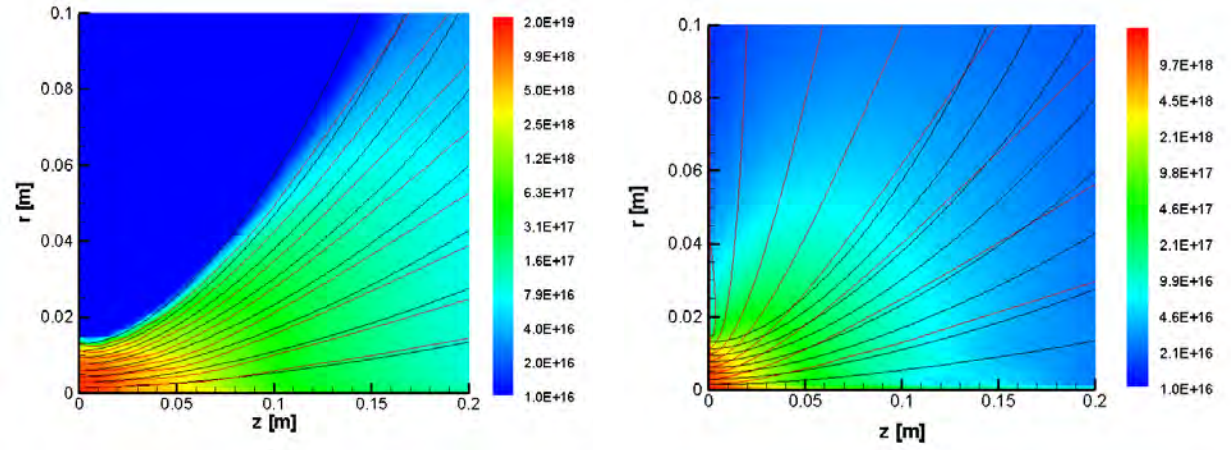

Figure 2. Plasma density distribution (in part/m^3) with magnetic nozzle effects (left) and without them (right). Magnetic streamlines are in black and ion streamlines are in red.

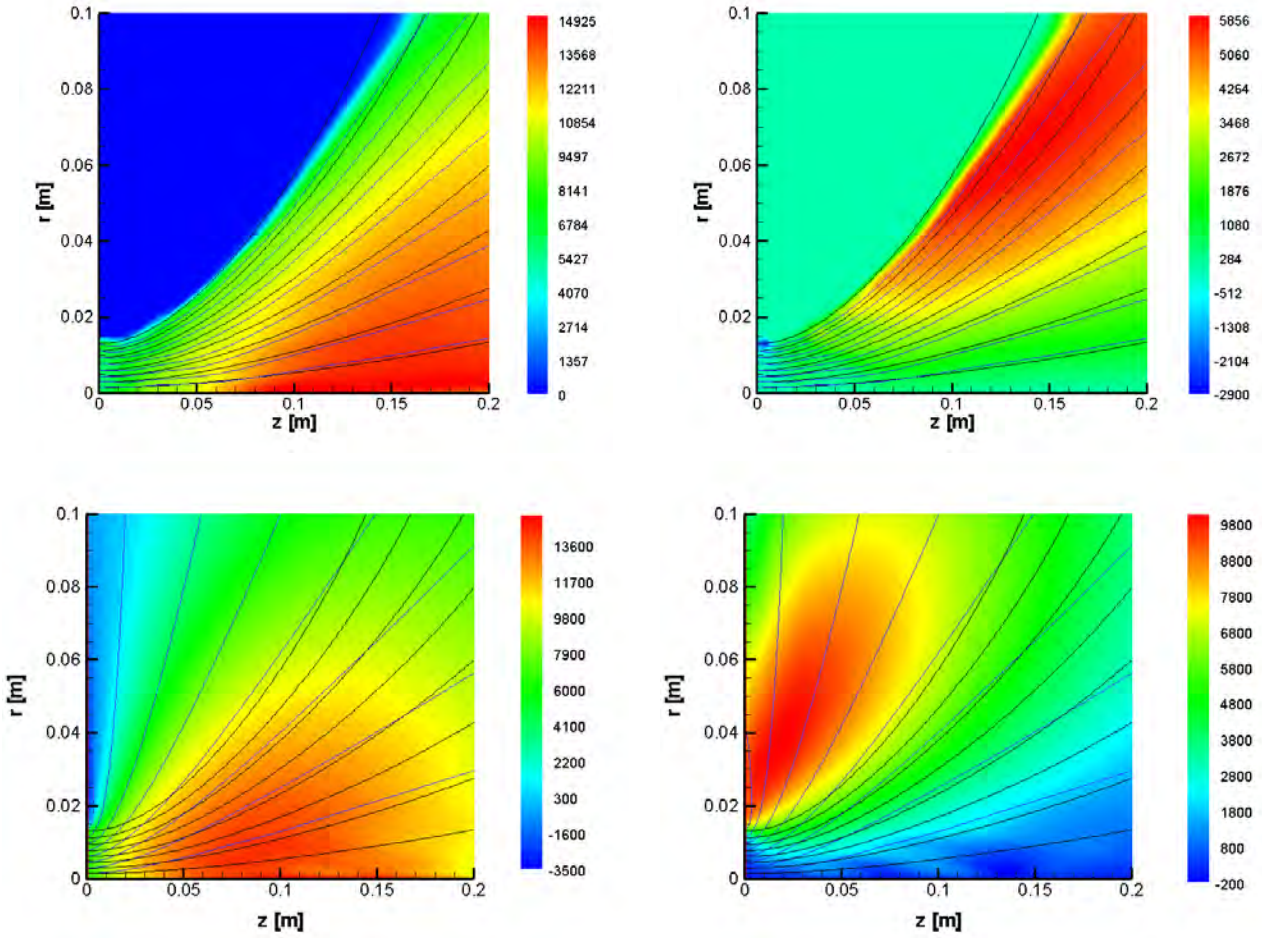

Figure 3. Ion axial (left) and radial (right) velocity (in m/s) with magnetic nozzle effects (up) and without them (down). Magnetic streamlines are in black and ion streamlines are in blue.

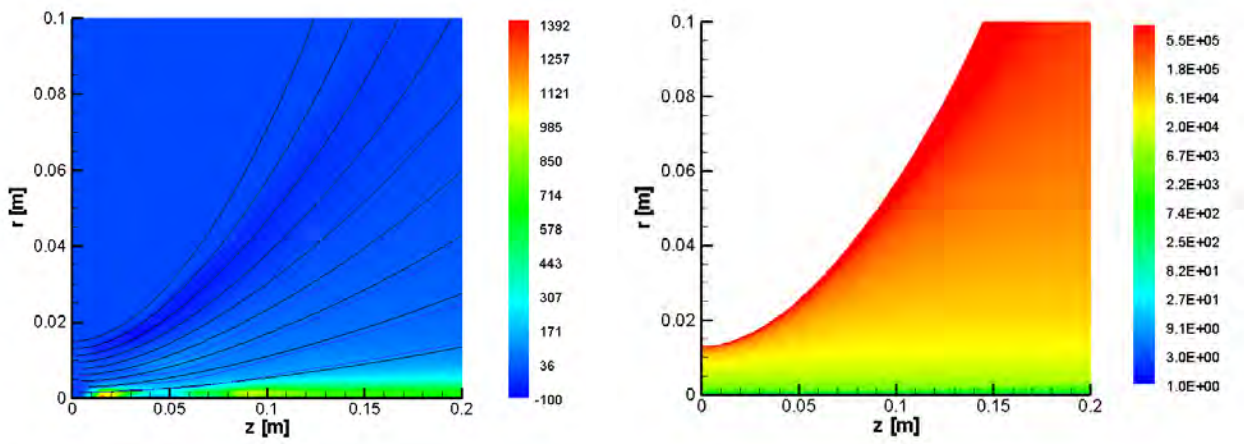

Figure 4. Ion azimuthal velocity (in m/s) with magnetic nozzle effects (left). Electron azimuthal velocity (in m/s) in the internal region (right).

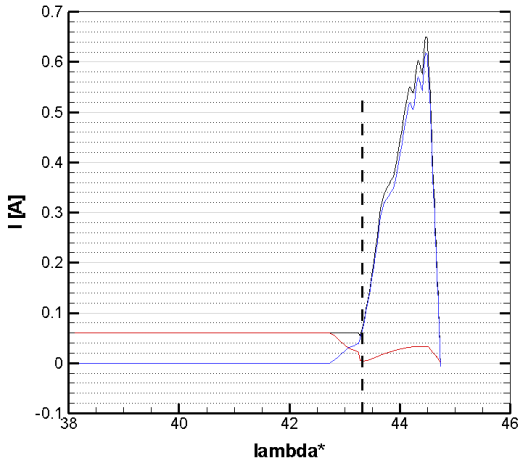

Figure 5. Perpendicular currents [A] through the magnetic surfaces as a function of the magnetic dimensionless coordinate (λ^*). Dashed vertical line separates the internal from the external region. The internal one is associated with high values of λ and it is located at the right side of the dashed line where perpendicular current is important. Outside, total current is forced to be constant. Total current is in black, ion current is in blue and electron current is in red.

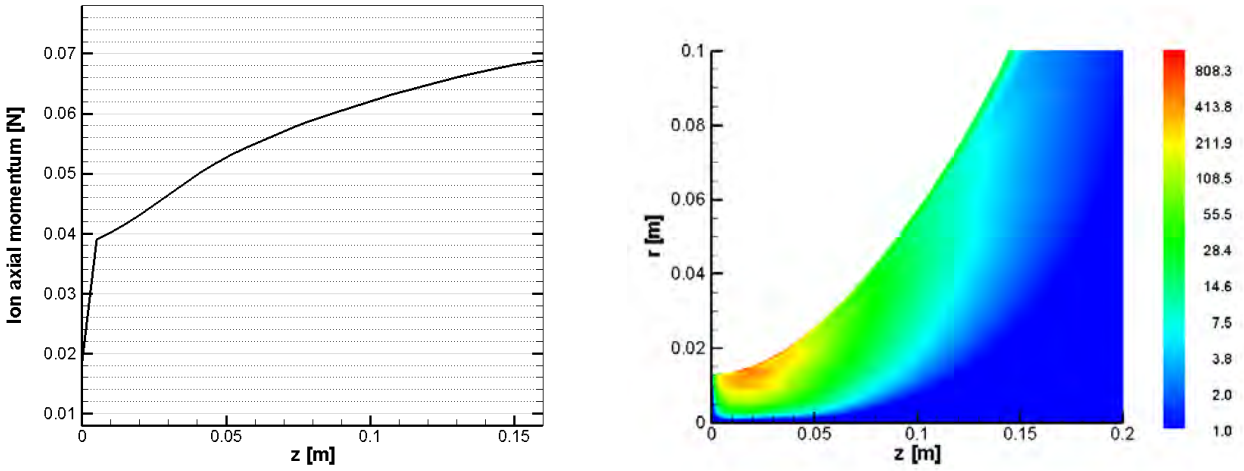

Figure 6. Ion momentum axial distribution [N] (left). Electromagnetic force per unit volume $j_\theta B_r \mathbf{1}_z [N/m^3]$ (right).

code. The comparison of plasma jets with and without magnetic effects is very illuminating too

Preliminary results indicate that the present model is more accurate in the plasma beam region, while the plasma beam edge and the near-vacuum external region, with very low plasma densities, require improvements in both PIC and electron-fluid subcodes. The following steps will be undertaken. First, the introduction of advanced algorithms on the PIC subcode for dealing with low plasma densities. Second, the development of a consistent model to assure the fulfillment of the charge conservation law and make it compatible with the existent electron diffusivity in the near-vacuum area. Third, the application of the non-isothermal model, by solving the electron energy equation.

Acknowledgments

This work was supported by the Gobierno de España under Project No. AYA2010-16699.

References

[1]Ziemba, T., Carscadden, J., Slough, J., Prager, J., and Winglee, R., "High Power Helicon Thruster," *41th Joint Propulsion Conference, Tucson, AR*, AIAA 2005-4119, American Institute of Aeronautics and Astronautics, Washington DC, 2005.

[2]Charles, C., Boswell, R., and Lieberman, M., "Xenon ion beam characterization in a helicon double layer thruster," *Applied Physics Letters*, Vol. 89, 2006, pp. 261503.

[3]Batishchev, O., "Minihelicon Plasma Thruster," *IEEE Transaction on Plasma Science*, Vol. 37, 2009, pp. 1563–1571.

[4]Pavarin, D., Ferri, F., Manente, M., Curreli, D., Guclu, Y., Melazzi, D., Rondini, D., Suman, S., Carlsson, J., Bramanti, C., Ahedo, E., Lancellotti, V., Katsonis, K., and Markelov, G., "Design of 50W Helicon Plasma Thruster," *31th International Electric Propulsion Conference, Ann Arbor, Michigan, USA*, IEPC 2009-205, Electric Rocket Propulsion Society, Fairview Park, OH, 2009.

[5]Krülle, G., Auweter-Kurtz, M., and Sasoh, A., "Technology and application aspects of applied field magnetoplasmadynamic propulsion," *J. Propulsion and Power*, Vol. 14, 1998, pp. 754–763.

[6]Arefiev, A. and Breizman, B., "Theoretical components of the VASIMR plasma propulsion concepta," *Physics of Plasmas*, Vol. 11, No. 5, 2004, pp. 2942–2949.

[7]Ahedo, E. and Merino, M., "Two-dimensional plasma acceleration in a divergent magnetic nozzle," *44th Joint Propulsion Conference, Hartford, CT*, AIAA 2009-5361, American Institute of Aeronautics and Astronautics, Washington DC, 2008.

[8]Ahedo, E. and Merino, M., "Acceleration of a focused plasma jet in a divergent magnetic nozzle," *31th International Electric Propulsion Conference, Ann Arbor, Michigan, USA*, IEPC 2009-002, Electric Rocket Propulsion Society, Fairview Park, OH, 2009.

[9]Ahedo, E. and Merino, M., "Two-dimensional supersonic plasma acceleration in a magnetic nozzle," *Physics of Plasmas*, Vol. 17, 2010, pp. 073501.

[10]Merino, M. and Ahedo, E., "Two-dimensional magnetic nozzle acceleration of a two-electron component plasma," *Proceedings of Space Propulsion 2010, San Sebastián, Spain, May 3-6, 2010*, European Space Agency, Noordwijk, The Netherlands, 2010, pp. SP2010–1841391.

[11]Merino, M. and Ahedo, E., "Simulation of plasma flows in divergent magnetic nozzles," *IEEE Transactions Plasma Science (to appear in August)*, 2011.

[12]Parra, F., Ahedo, E., Fife, M., and Martínez-Sánchez, M., "A two-dimensional hybrid model of the Hall thruster discharge," *Journal of Applied Physics*, Vol. 100, 2006, pp. 023304.

[13]Parra, F. and Ahedo, E., "Improvement of the plasma-wall interaction model on a hybrid fluid-PIC simulation of a Hall thruster," Presented at the 1st AIAA-Pegasus Student Conference, Toulouse, France.

[14]Antón, A., Escobar, D., and Ahedo, E., "Contour algorithms for a Hall thruster hybrid code," *42th Joint Propulsion Conference, Sacramento, CA*, AIAA-2006-4834, American Institute of Aeronautics and Astronautics,Washington, DC, 2006.

[15]Ahedo, E., Santos, R., and Parra, F., "Fulfilment of the kinetic Bohm criterion in a quasineutral particle-in-cell model," *Physics of Plasmas*, Vol. 17, 2010, pp. 073507.

[16]Ahedo, E. and Merino, M., "Current Ambipolarity and Plasma Detachment on a Magnetic Nozzle," *32th International Electric Propulsion Conference, Wiesbaden, Germany*, IEPC 2011-050, Electric Rocket Propulsion Society, Fairview Park, OH, 2011.

46th AIAA/ASME/SAE/ASEE Joint Propulsion Conference & Exhibit
25 - 28 July 2010, Nashville, TN

AIAA 2010-6613

Preliminary assessment of detachment in a plasma thruster magnetic nozzle

E. Ahedo * and M. Merino †

E.T.S. Ingenieros Aeronáuticos, Universidad Politécnica de Madrid, Spain

A magnetic nozzle model for the supersonic expansion of a collisionless, low-beta plasma characterizes the plasma flow for propulsive applications. Thrust gain in the nozzle is achieved by an azimuthal current developed in the plasma. That current is necessarily diamagnetic in character, which disagrees with the current direction assumed in existing theories for resistive, inertial-based, and MHD self-field detachment.

I. Introduction

A divergent magnetic nozzle, created by a longitudinal magnetic field is being proposed as an acceleration mechanism for a magnetized plasma in advanced propulsion devices, such as the applied-field magnetoplasmadynamic (AFMPD) thruster,[1] the helicon thruster,[2,3] and the VASIMR.[4] There is a clear analogy between the dynamics of a magnetized plasma in a magnetic nozzle and a neutral gas in a solid (deLaval) nozzle: the plasma flow is tied to the magnetic streamlines and a regular sonic transition occurs at the magnetic throat.[5] Nonetheless, plasma dynamics in a magnetic nozzle are more complex than gas dynamics in a solid nozzle. Depending on each particular thruster type, different plasma conditions and acceleration mechanisms take place.[6]

Once the plasma has been accelerated in the magnetic nozzle, the detachment of the plasma from the guiding magnetic lines is crucial. Otherwise, part of the plasma would turn back towards the thruster walls and the thruster efficiency will be ruined. Resistive detachment,[7] electron-inertia detachment,[8] and self-field detachment[9–11] are the main mechanisms that have been envisaged up to date.

We have recently published a two-dimensional(2D) model of the expansion of a collisionless, electron-magnetized, low-beta, current-free plasma in a divergent magnetic nozzle.[12,13] The plasma response was investigated in terms of the nozzle/plasma divergence rate, the magnetic strength on ions, and the upstream plasma conditions. Whereas average axial plasma profiles agree well with those estimated from a simple one-dimensional model, a strong radial nonuniformity develops downstream. Relevant 2D aspects are highlighted, such as the development of azimuthal and longitudinal plasma currents and the dual character of the magnetic nozzle, consisting of an electrothermal plasma acceleration and an electromagnetic thrust transmission.

The present paper uses the above 2D nozzle model to carry out a first assessment of the several plasma detachment mechanisms and the existing theories on them. Sections 2 and 3 give a summary of the model of Ref. 12 and those results that are relevant to discuss detachment. Section 4 is devoted to the detachment mechanisms.

II. The divergent nozzle model

Let us consider a guide longitudinal magnetic field, created by a simple current loop of intensity I_L, flowing along $\mathbf{1}_\theta$, and located at $(z,r)=(0,R_L)$. [notice that the guide field generated by more complex magnetic

*Professor; Senior AIAA member; e-mail: eduardo.ahedo@upm.es.
†PhD Student.

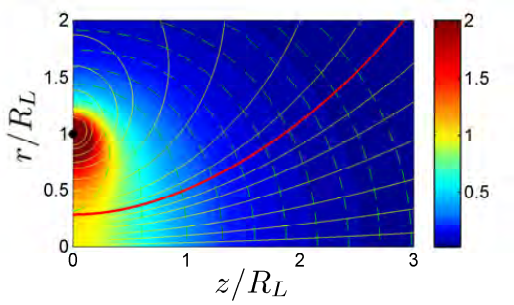

Figure 1. Magnetic field created by a single current loop, placed at $(z, r) = (0, R_L)$. The background color shows the magnetic field intensity. Solid lines are magnetic streamlines. Dashed lines are $B =$ const lines. The red thick line shows the magnetic streamline used as outer plasma edge line in the simulations.

circuits tend to reduce themselves to that of a single loop downstream.] The magnetic streamfunction of the guide field is[14]

$$\psi(z,r) = \frac{\mu_0 I_L}{4\pi}\sqrt{(R_L+r)^2+z^2}\,\mathbf{F}(m), \tag{1}$$

with

$$\mathbf{F}(m) = (2-m)\mathbf{K}(m) - 2\mathbf{E}(m), \qquad m = \frac{4R_L r}{(R_L+r)^2+z^2}, \tag{2}$$

and $\mathbf{K}(m)$ and $\mathbf{E}(m)$ the complete elliptic integrals of first and second kind, respectively.[15] The magnetic field $\boldsymbol{B} = B_r\mathbf{1}_r + B_z\mathbf{1}_z$ (with $B_r, B_z > 0$) is obtained from

$$\partial\psi/\partial z = -rB_r, \quad \partial\psi/\partial r = rB_z, \tag{3}$$

and $B_0 \equiv B_z(0,0) = \mu_0 I_L/(2R_L)$. The cylindrical and magnetic frames of reference are $\{\mathbf{1}_z, \mathbf{1}_r, \mathbf{1}_\theta\}$ and $\{\boldsymbol{b}, \mathbf{1}_\perp, \mathbf{1}_\theta\}$, with $\boldsymbol{b} = \boldsymbol{B}/B = \cos\alpha\mathbf{1}_z + \sin\alpha\mathbf{1}_r$, and $\mathbf{1}_\perp = -\sin\alpha\mathbf{1}_z + \cos\alpha\mathbf{1}_r$. where $\alpha(z,r)$ is the local magnetic angle. Figure 1 shows the magnetic lines created by the current loop.

A current-free, fully-ionized plasma jet of radius R, with $R < R_L$, is injected sonically at the nozzle throat, located at $z = 0$, flowingin the direction of the guide magnetic field. We assume the distinguished orderings

$$\lambda_{d0} \ll \ell_{e0} \ll R \ll \lambda_{ei0}, \tag{4}$$

$$m_e/m_i \ll 1, \tag{5}$$

$$R\Omega_{i0}/u_{i0} = O(1) \tag{6}$$

$$\beta_0 \equiv \frac{\mu_0 n_0 T_0}{B_0^2} \ll 1, \tag{7}$$

where subscript 0 refers always to values at the center of the nozzle throat, λ_d is the Debye length, ℓ_e is the electron gyroradius, λ_{ei} is the electon-ion collision mean-free-path, Ω_i is the ion gyrofrequency, and u_i is the macroscopic ion longitudinal velocity. These orderings imply the following plasma features:

(1) the plasma is quasineutral and near-collisionless;

(2) electrons are massless and the electron streamtubes are the magnetic streamtubes;

(3) ions are from mild- to weakly magnetized;

(4) the plasma-vacuum edge V, $r = R_V(z)$ is the magnetic streamsurface of cross-section radius R at the throat, that is $R_V(z)$ is defined implicitly by $\psi(z, R_V(z)) = \psi(0, R)$;

(5) the induced magnetic field (i.e. the self-field), $\boldsymbol{B}^*$, is negligible.

	low-beta plasma[2]	'high'-beta plasma[9]
B(G)	1000	200
$n(\mathrm{m}^{-3})$	$7 \cdot 10^{18}$	$2 \cdot 10^{19}$
R(mm)	10	100
T_e(eV)	20	20
c_e(m/s)	$1.9 \cdot 10^6$	$1.9 \cdot 10^6$
c_s(m/s)	$6.9 \cdot 10^3$	$6.9 \cdot 10^3$
λ_d(mm)	$1.3 \cdot 10^{-2}$	$7.3 \cdot 10^{-3}$
ℓ_e(mm)	0.11	0.53
$\Omega_i(\mathrm{s}^{-1})$	$2.4 \cdot 10^5$	$4.8 \cdot 10^4$
$\Omega_e(\mathrm{s}^{-1})$	$1.8 \cdot 10^{10}$	$3.5 \cdot 10^9$
$c_s/R(\mathrm{s}^{-1})$	$6.9 \cdot 10^5$	$0.69 \cdot 10^5$
$\nu_{ei}(\mathrm{s}^{-1})$	$2.9 \cdot 10^6$	$7.8 \cdot 10^6$
β	$2.8 \cdot 10^{-3}$	0.2
ℓ_e/R	$1.1 \cdot 10^{-2}$	$5.3 \cdot 10^{-3}$
λ_{d0}/R	$1.3 \cdot 10^{-3}$	$7.3 \cdot 10^{-4}$
χ	6160	450

Table 1. Typical argon plasma parameters at the nozzle throat based on data from the helicon thruster experiments of Batischev[2] and Winglee et al.;[9] The Hall parameter χ is based on e-i resistivity only.

Figure 1 plots the magnetic field of a current loop and the edge of the plasma jet to be simulated here. Table 1 presents experimental values of the main plasma parameters for two plasmas created in helicon sources.

Following Ref.12, electrons are assumed isothermal and ions cold; then, plasma equations consist of both differential and conservation equations. The equations for the ion azimuthal momentum, the electron momentum, and the electron continuity yield the following conservation relations:

$$rm_i u_{\theta i} + e\psi = D_i(\psi_i), \tag{8}$$

$$u_{\perp e} = 0, \tag{9}$$

$$-e\phi + T_e \ln n = H_e(\psi), \tag{10}$$

$$\frac{u_{\theta e}}{r} = -\frac{1}{e}\frac{dH_e}{d\psi}. \tag{11}$$

$$u_{\parallel e} n/B = G_e(\psi), \tag{12}$$

where: the ion total angular momentum, $D_i(\psi_i)$, is constant on each ion streamtube, ψ_i= const (with $\nabla\psi_i = -rn\boldsymbol{u}_i \times \mathbf{1}_\theta$); and the electron-to-magnetic flux ratio, G_e, and the electron total enthalpy, H_e, are constant on each electron/magnetic streamtube. Ion continuity and the longitudinal plasma momentum

provide the three partial differential equations

$$u_{ri}\frac{\partial \ln n}{\partial r}+u_{zi}\frac{\partial \ln n}{\partial z}+\frac{\partial u_{ri}}{\partial r}+\frac{\partial u_{zi}}{\partial z}=-\frac{u_{ri}}{r}, \tag{13}$$

$$u_{ri}\frac{\partial u_{ri}}{\partial r}+u_{zi}\frac{\partial u_{ri}}{\partial z}+c_s^2\frac{\partial \ln n}{\partial r}=-(u_{\theta e}-u_{\theta i})\Omega_i\cos\alpha+\frac{u_{\theta i}^2}{r}, \tag{14}$$

$$u_{ri}\frac{\partial u_{zi}}{\partial r}+u_{zi}\frac{\partial u_{zi}}{\partial z}+c_s^2\frac{\partial \ln n}{\partial z}=(u_{\theta e}-u_{\theta i})\Omega_i\sin\alpha, \tag{15}$$

where $c_s=\sqrt{T_e/m_i}$ is the sound speed, and electron momentum equation has been employed to eliminate the electric potential. These ion equations, provided that the plasma is not subsonic, are integrated with the method of characteristics.[16]

For the ion and electron velocities and currents, it is convenient to separate the azimuthal components from the longitudinal ones, here denoted with a tilde, $\tilde{}$. For example,

$$\tilde{\boldsymbol{u}}_{\boldsymbol{i}}=\boldsymbol{u}_i-u_{\theta i}\mathbf{1}_\theta,\quad \tilde{\boldsymbol{j}}_{\boldsymbol{i}}=\boldsymbol{j}_i-j_{\theta i}\mathbf{1}_\theta,\quad \tilde{\boldsymbol{j}}_{\boldsymbol{e}}=-\left(\boldsymbol{j}_e-j_{\theta e}\mathbf{1}_\theta\right),$$

etcetera. The electric current density is thus $\tilde{\boldsymbol{j}}=\tilde{\boldsymbol{j}}_{\boldsymbol{i}}+\tilde{\boldsymbol{j}}_{\boldsymbol{e}}$. Prior to integration, the energy T_e, the sound speed c_s, the length R, the density $n_0=n(0,0)$, and the magnetic field B_0, are used to non-dimensionalize all plasma magnitudes. Dimensionless variables will be expressed with a hat: $\hat{n}=n/n_0$, $\hat{\phi}=e\phi/T_e$, etcetera. The plasma Mach number is defined from the ion longitudinal velocity: $M=\tilde{u}_i/c_s$.

The boundary conditions at the nozzle throat, $\hat{z}=0$ and $0\le\hat{r}\le 1$, discussed in Ref.12 are:

$$\hat{u}_{zi}=M_0, \tag{16}$$

$$\hat{u}_{ze}=\hat{u}_{zi}, \tag{17}$$

$$\hat{u}_{ri}=\hat{u}_{re}=0, \tag{18}$$

$$\hat{\phi}=0, \tag{19}$$

$$\hat{n}=J_0(a_0\sigma\hat{r}), \tag{20}$$

$$\hat{j}_{\theta e}=-\hat{\Omega}_{i0}^{-1}a_0J_1(a_0\sigma\hat{r}),\quad \hat{u}_{\theta e}=-\hat{j}_{\theta e}/\hat{n}, \tag{21}$$

$$\hat{u}_{\theta i}=0, \tag{22}$$

with M_0 as the Mach number at the throat, J_0 and J_1 as the Bessel functions of the first kind, $a_0=2.405$ the first zero of J_0, and σ a parameter measuring both the Hall current and the radial non-uniformity of the plasma density at the throat: $\sigma=0$ yields $\hat{n}=1$ and $\hat{u}_{\theta e}=0$ at the throat.

The model depends on four dimensionless parameters: two are related to the plasma conditions, M_0 and σ, and two characterize the divergent magnetic nozzle, R_L/R measuring the nozzle divergence rate, and Ω_{i0} measuring the magnetic strength. The most physical choice for M_0 is $\simeq 1$; σ depends much on how the plasma is created and there are qualitative differences, commented below, between $\sigma=0$ (i.e. uniform jet) and $\sigma\approx 1$ (i.e. strongly non-uniform jet); for practical cases, Ω_{i0} is less than or about $O(1)$, and the solution depends weakly on it; at least, in the acceleration region, there is not a qualitative effect of R_L/R on the solution. Unless stated otherwise, results shown here are for $M_0=1.05$, $\hat{\Omega}_{i0}=1$, and $R_L/R=3.5$. The integration is carried out between $\hat{z}=0$ and a downstream section $\hat{z}=\hat{z}_F=14$ near the turning point of tube V (i.e. where B_z changes sign). This means that only the main acceleration region is being simulated.

III. Main results on plasma acceleration

A. Current ambipolarity

The fact that ions are partially magnetized implies that the divergence of the ion streamtubes is lower than the divergence of the electron/magnetic streamtubes, except at the nozzle axis, and at the edge of the plasma jet, where the ambipolar electric field, set up by quasineutrality, forces the ion streamtube there to coincide

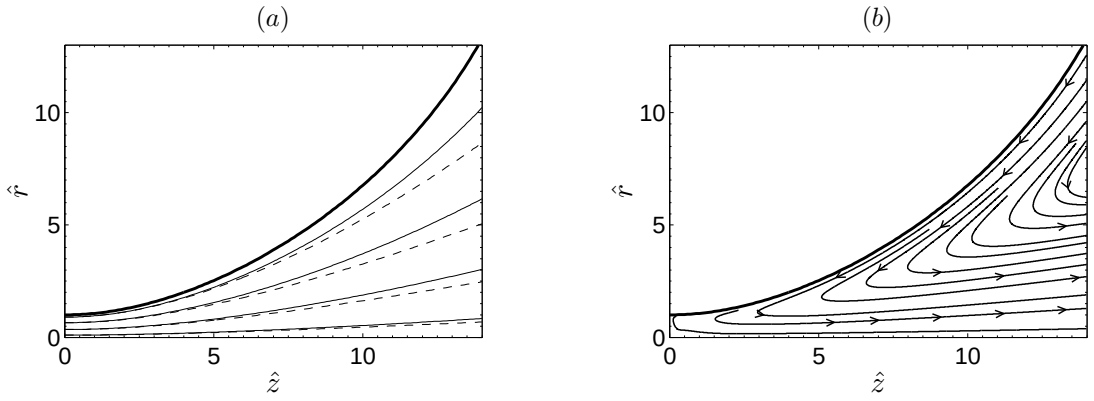

Figure 2. (a) Electron (solid) and ion (dashed) streamtubes in the magnetic nozzle. (b) Lines of longitudinal electric current, $\tilde{j} = \tilde{j}_i + \tilde{j}_e$. (Taken from Ref. 12)

with that of electrons. Figure 2(a) shows ion and electron streamtubes. Although the local separation angle between ion and electron streamtubes is small, the separation is cumulative along z for a pair of ion and electron streamtubes with the same cross-section at the nozzle throat.

Equation (17) imposes the current ambipolarity condition, $\tilde{j}(z,r) = 0$, at the nozzle throat, thus assuring that the plasma is current-free in the nozzle, that is

$$I(z) = 2\pi \int_0^{R_V(z)} drrj_z(r) = 0. \tag{23}$$

However, the plasma response shows that current ambipolarity is not preserved downstream, i.e. $\tilde{j}(z,r) \neq 0$ outside the throat. This is a consequence of the ion/electron separation and means the formation of longitudinal electric currents, with $\tilde{j}$ of the order of $\tilde{j}_i$ and $\tilde{j}_e$, within the plasma jet. Figure 2(b) shows the electric current lines.

The failure of current ambipolarity is intrinsic to the present model, as we discussed in Ref.12. It means that the combination of quasineutrality, a global current-free plasma, and current ambipolarity at one nozzle section is not enough to assure current ambipolarity everywhere. Indeed, there is a simple mathematical argument that denies the fulfilment of current ambipolarity: the exchange of the *scalar* current conservation equation, $\nabla \cdot \tilde{\boldsymbol{j}} = 0$ (a combination of the ion and electron continuity equations) by the *vectorial* equation $\tilde{\boldsymbol{j}} = \mathbf{0}$ adds one scalar equation to the model. Consequently, the model is likely to become incompatible, unless one of the original plasma equations is satisfied automatically or it is just ignored. This last case is what we believe Hooper[8] does in his detachment model, commented below. He assumes current ambipolarity and seems to ignore the central equation (11), that establishes that $u_{\theta e}$ is created by magnetic drifts.

B. Hall current and 2D plasma expansion

The evolution of the plasma jet is depicted in Fig. 3 for different cases. As it can be seen, Mach number increases as electric potential drops and the plasma accelerates. Plasma density focalizes around the nozzle axis. The different simulations show that slightly larger radial gradients are obtained for weaker ion magnetization. Red lines correspond to the results for a simple 1D paraxial model.

Equations (14) and (15) detail the radial and axial forces driving the plasma, once the ambipolar electric field has been canceled out. The only *external* force acting on the plasma longitudinal plane is the product of the azimuthal current with the magnetic field, and thus its presence is essential both for plasma confinement and acceleration. For weak- and mildly magnetized ions, $u_{\theta i}$ can be neglected and only the electrons

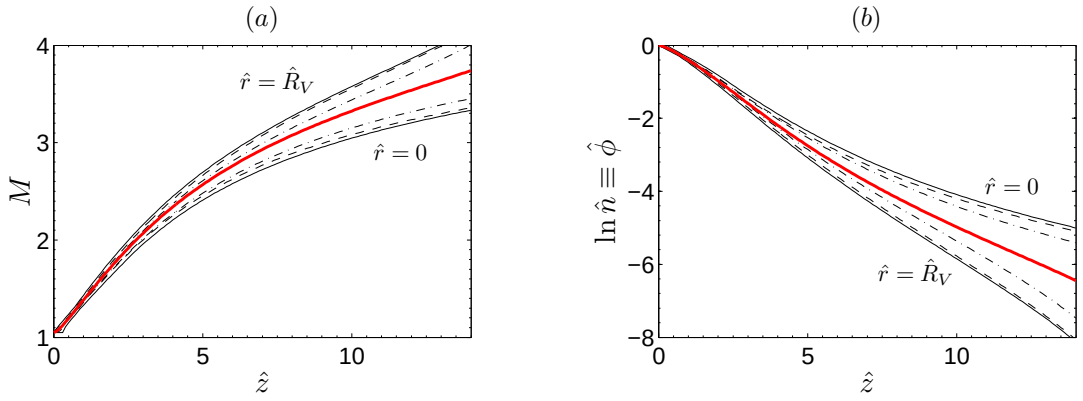

Figure 3. (a) Mach number and (b) electric potential and plasma density along the plasma jet axis and edge for different simulations with $\sigma = 0$, $\hat{\Omega}_{i0} = 0.01$(solid), 10 (dashed), and 100 (dash-and-dot). The red lines is the solution of the 1D paraxial model. (Taken from Ref. 12)

contribute to the azimuthal current, $j_\theta \simeq -enu_{\theta e}$, and hence to the magnetic force. Let us consider the general case of a non-uniform jet ($\sigma \neq 0$), when the plasma enters the divergent nozzle with a non-zero, radially-distributed, azimuthal current, Eq. (21).

The radial equation (14) shows the competition between the *expanding* pressure gradient and the *confining* magnetic force. These are balanced exactly at the nozzle throat but the pressure gradient tend to dominate downstream, forcing the radial expansion of the plasma. For guide fields with $B_z > 0$, a confining magnetic force requires that $u_{\theta_e} > 0$ and $j_\theta < 0$, i.e., that the azimuthal plasma current runs in the *opposite* direction to the current in the thruster magnetic circuit (if the sign of $\boldsymbol{B}$ is reversed, so is that of j_θ). The electron momentum equations, (10) and (11), show us that the electron azimuthal (or Hall) current is the difference between the diamagnetic current (caused by the pressure gradient) and the $\boldsymbol{E} \times \boldsymbol{B}$ current, the last one being of opposite direction.

The axial equation (15) shows that the pressure gradient and the magnetic force constitute the *electrothermal and Hall acceleration* mechanisms, respectively. The *plasma axial momentum* at a section $z = \text{const}$ is $F(z) = F_i(z) + F_e(z)$, with

$$F_i = 2\pi \int_0^{R_V(z)} drrnm_i u_{zi}^2, \quad F_e = 2\pi \int_0^{R_V(z)} drrnT_e, \tag{24}$$

the ion and electron contributions, respectively. Combining the axial momentum equations of ions and electrons, in order to eliminate the ambipolar electric field, and integrating the resultant equation in a volume $\mathcal{V}(z)$ bounded by the throat, a generic axial cross-section downstream the nozzle, and the lateral area $A_V(z)$ of the plasma jet, the plasma axial momentum is expressed as

$$F(z) = F_0 + F_v(z) + F_s(z), \tag{25}$$

with $F_0 = F(0)$ as the momentum at the nozzle throat, and

$$F_v = \int_{\mathcal{V}(z)} d\mathcal{V}\ (-j_\theta)B_r, \quad F_s = \int_{A_V(z)} dA\ (-J_\theta)B_r, \tag{26}$$

as the two contributions of the axial magnetic force in the divergent nozzle.[12] $F_v(z)$ is generated by the Hall current density within the plasma beam, and $F_s(z)$ is due to the diamagnetic Hall current (per unit of length),

$$J_\theta(z) = -(p_e/B)|_{\left(z,R_V(z)\right)}, \tag{27}$$

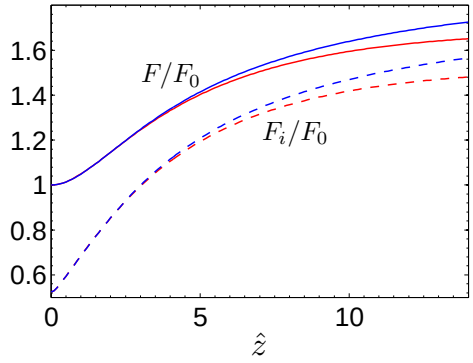

Figure 4. $F_i(z)$ **(dashed) and** $F(z)$ **(solid) for two different simulations: red lines for** $\sigma = 0$ **and blue lines for** $\sigma = 0.9$**. All thrusts have been normalized with** $F(0)$**, the value at the nozzle throat. At the sonic transition,** $\tilde{u}_i = \sqrt{T_e/m_i}$**, and thus** $F_i(0) = F(0)/2$**.**

that develops in a layer of thickness about the electron gyrodiameter, generated by the pressure gradient at the plasma-vacuum edge; for $\ell_e \ll R$, this layer is seen here as a discontinuity.

In the case of a uniform plasma jet at the entrance, one has $j_{\theta e} = 0$ at $z = 0$. Equation (11) states that the electron azimuthal frequency is conserved in each streamtube. Therefore, $j_{\theta e} = 0$ everywhere (yielding $F_v(z) = 0$) and all the Hall current is concentrated in the plasma-vacuum edge. In a highly non-uniform jet, the pressure at the plasma-vacuum edge is small and $F_v \gg F_s$.

C. Gains and losses in a magnetic nozzle

Equation (25) illustrates the main function of a divergent magnetic nozzle within a plasma thruster: to produce a gain in plasma momentum and therefore in thrust. Following Ref. 10, a nozzle efficiency can be defined as the ratio between the plasma momentum downstream and the plasma momentum at the throat. In the simulations presented in Ref.12, the nozzle efficiency between the throat and $z = z_F$ was about a 200%. Figure 4 plots the axial evolution of $F_i(z)$ and $F(z)$, with an efficiency of 60% in this short nozzle.

The plasma momentum gain in the nozzle is achieved by the axial magnetic force, $-j_\theta B_r$, which must be positive. This requires again the Hall current to run opposite to the azimuthal current in the external circuit (i.e. $j_\theta < 0$ for $B_r > 0$). Simulations show, however, that the small ion azimuthal (swirl) current runs in the opposite direction, thus leading to a radial expansion and to an axial deceleration. Hence, the gneration of these parasital currents should be kept to a minimum. Figure 5(a) sketches the azimuthal currents in the external circuit and the plasma beam and the mutual force between them for a plasma thruster. A second characteristic of the nozzle is to convert the internal energy into directed axial energy. For sonic conditions at the nozzle throat one has $F_i(0) = F_e(0) = F_0/2$, whereas $F_e \ll F_i$, far downstream, as seen in Fig. 4.

An unavoidable penalty of using a magnetic nozzle for plasma acceleration is the divergence created in the plasma beam. In Ref.12, we defined the plume efficiency, η_{plume}, as the ratio between the radial and the total power in the ion beam. The simulations showed the plume efficiency was about an 80% for a highly-non-uniform jet and 60-70% for a uniform jet at z_F. Further studies on magnetic nozzle optimization should look for improving the plume efficiency.

The second and potentially strong penalty of a magnetic nozzle is detachment. Once the magnetic force of the nozzle becomes residual, the attachment of the plasma to the magnetic streamtubes is a serious issue (certainly, at this point we would like that the magnetic nozzle became 'screened' somehow). The detachment process is treated in the next Section.

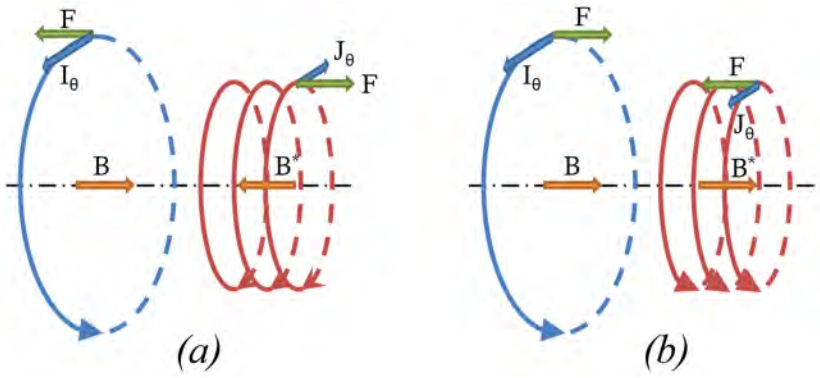

Figure 5. (a) Sketch of the azimuthal currents in the external circuit and the plasma beam, the magnetic fields they create, and the mutual force between them, for a plasma thruster. (b) Same than before for the configuration proposed in the detachment theories of Refs. 8–10.

IV. Plasma detachment

The above plasma-nozzle model has considered the triple asymptotic limit

$$R/\lambda_{ei} \to 0, \quad m_e/m_i \to 0, \quad \beta \to 0, \tag{28}$$

corresponding to a collisionless, electron-massless, and zero-beta plasma. Consequently, the model cannot reproduce the resistive, inertial, and self-field mechanisms of detachment. Nonetheless, the solution of our asymptotic model can be used to understand the onset of the three detachment mechanisms when the corresponding parameter is small but non-zero.

A. Self-field detachment

The detachment via the induced magnetic field has been suggested by Arefiev and Breizman[10,17] and by Winglee and coworkers.[9] Arefiev and Breizman propose a magnetohydrodynamic(MHD) detachment scenario in which the plasma flow stretches the magnetic field lines to infinity. Detachment takes place after the energy density of the expanding magnetic field drops below the kinetic energy density of the plasma. Winglee et al. insist on the idea that plasma currents induced downstream from the magnetic nozzle, lead to magnetic fields that have a smaller divergence than the original vacuum magnetic field, so that the following plasma will be more collimated than the proceeding plasma, and the beam propagates over extended distances.

Unfortunately, the direction of the plasma azimuthal currents required for above scenario, with a stretching of the magnetic field, is not the correct one for the beam in a plasma thruster. Figure 5(b) sketches the current topology for the field-stretching scenario. The induced magnetic field, B^*, is created by the azimuthal current of the plasma, which acts as a solenoid. In order that B^* strengthens the guide field B, both fields must have the same direction at the beam axis, which requires the plasma Hall current to run in the same direction than the external current. It is well known that two parallel currents running in the same direction attract each other, so that the mutual force decelerates the plasma beam and produces negative thrust in the magnetic device. Indeed, Arefiev and Breizman[10,17] obtain a nozzle efficiency below 1.

Therefore, the detachment theory for a propulsive plasma via the induced magnetic field, needs to be reconsidered. The first point to stand out is that the induced field is going to increase the divergence of the resulting magnetic field. This feature, negative for detachment, in principle, could be positive if it demagnetizes the plasma (but this has not been proven yet). As a first insight on the characteristics of the the resultant magnetic field, let us consider a low-beta plasma with a uniform profile ($\sigma = 0$) at the throat. In this case, all the plasma Hall current is concentrated in a sheet at the plasma-vacuum edge, $r = R_V(z)$. Equation (27) yields the azimuthal current (per unit of length), J_θ. This current sheet can be considered as

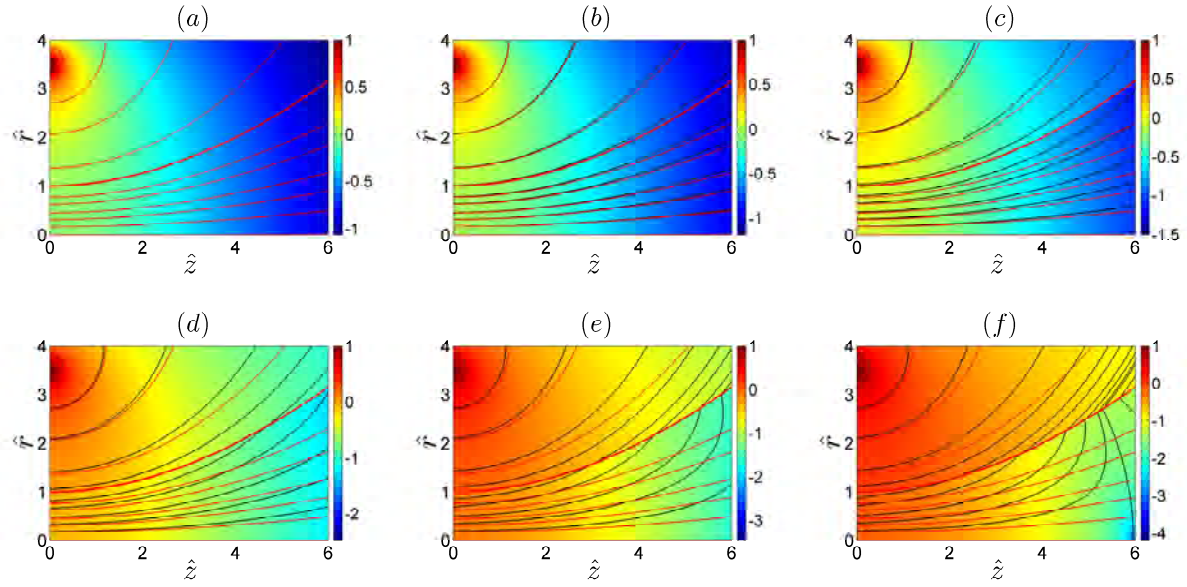

Figure 6. Total (induced plus guide) magnetic field for a magnetic nozzle and a uniform plasma at the throat. Background color corresponds to $\log_{10}(B+B^*)/B_0$. The induced magnetic field is computed from the plasma currents obtained from the $\beta_0 = 0$ case (hence results are not self-consistent). These currents are concentrated at the plasma-vacuum edge, resulting in a configuration similar to a expanding solenoid. The values of β_0 in the displayed figures are (a) $\beta_0 = 0$ (negligible induced field; the original, applied magnetic field only); (b) $\beta_0 = 0.05$; (c) $\beta_0 = 0.15$; (d) $\beta_0 = 0.25$; (e) $\beta_0 = 0.4$; and (f) $\beta_0 = 0.5$. A number of magnetic streamlines have been plotted for the unaltered guide field (red) and the total field (black). The unaltered nozzle edge is displayed as a red thick line.

a continuous sequence of differential current loops, each one of intensity $dI = J_\theta dz/\cos\alpha_V$. The magnetic streamfunction induced by these differential loops, located at (z', r'), is

$$\psi^*(z,r) = \frac{\mu_0}{4\pi}\int_0^{z_F} dz' \frac{J_\theta(R_V)}{\cos\alpha_V}\sqrt{(r+R_V)^2+(z-z')^2}\,\mathbf{F}(m) \tag{29}$$

with

$$R_V \equiv R_V(z'), \quad \alpha_V \equiv \alpha_V(z'), \quad m = \frac{4R_V r}{(r+R_V)^2+(z-z')^2}. \tag{30}$$

The induced longitudinal magnetic field and streamfunction satisfy

$$\nabla\psi^* = rB^*\mathbf{1}_\perp, \quad \text{i.e.} \quad \partial\psi^*/\partial z = -rB_r^*, \quad \partial\psi^*/\partial r = rB_z^*. \tag{31}$$

Using the same normalization than in Sec. 2 and $\hat{B} = B/B_0$, one has

$$\hat{\psi}^*(\hat{z},\hat{r}) = -\frac{\beta_0}{4\pi}\int_0^{z_F} d\hat{z}' \left.\frac{\hat{p}_e}{\hat{B}\cos\alpha}\right|_V \sqrt{(\hat{r}+\hat{R}_V)^2+(\hat{z}-\hat{z}')^2}\,\mathbf{F}(m) \tag{32}$$

where the dependence on $\beta_0 = \mu_0\frac{n_0 T_e}{B_0^2}$ and the negative character of the induced magnetic streamfunction and field must be stood out.

Figures 6 (a) to (f) show the total magnetic field for different values of β_0, where ψ^* and B^* have been computed from the plasma currents obtained in the solution with $\beta = 0$. This, of course, is not a consistent solution: an iterative process needs to be carried out, in order to recalculate the plasma response including the total magnetic field, until the plasma currents and the assumed induced field match correctly. At any

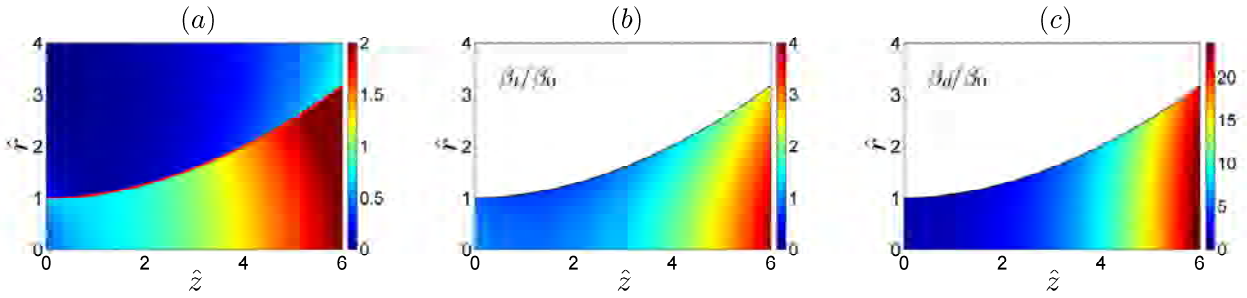

Figure 7. (a) Ratio between the induced and applied magnetic field, $B^*/(\beta_0 B)$. (b) Thermal and (c) dynamic beta-parameters.

rate, Fig. 6 guides us on some aspects of the plasma response that can be expected. The current sheet behaves similarly to a solenoid, inducing a larger magnetic field inside than outside. Nonetheless, both the inner and outer magnetic field are modified by the presence of the plasma currents.

As it has been pointed out, the induced magnetic field opposes the applied one, increasing the divergence of the total magnetic field, and its relative intensity is proportional to β_0. With $\beta_0 = 0.15$, the magnetic nozzle divergence has already increased a 30%. The fact that plasma currents exist until far downstream suggests that, for any β_0, the induced magnetic field will eventually cancel the applied field at the axis, giving rise to a saddle point in the magnetic streamfunction and a separatrix surface which is born from it, corresponding to $\psi = 0$. This is first visible in the displayed range of Fig.6 for $\beta_0 = 0.5$. Unquestionably, the existence of such a feature in the magnetic field will severely alter the plasma response, as the plasma would become effectively unmagnetized about the saddle point, and the near-radial separatrix magnetic surface could block the downstream flow of the quasineutral, still magnetized plasma. We are currently working on the iterative solution of the plasma-jet/induced-field problem. This will allow us to understand which is the consistent plasma response and the plausible detachment mechanism.

Figure 7(a) plots the induced-to-applied magnetic field ratio, B^*/B, the induced magnetic field becoming gradually more important downstream. Figures 7(b) and (c) plot the 'thermal' and 'dynamic' beta parameters,

$$\beta_t = \mu_0 \frac{nT_e}{B^2}, \quad \beta_d = \mu_0 \frac{nm_i \tilde{u}_i^2}{B^2}. \tag{33}$$

Although these two parameters increase downstream, neither of them seems proportional to the induced-to-applied magnetic field ratio.

B. Diffusive detachment

The central idea here is that either resistivity[8] or electron-inertia[7] allow the plasma to diffuse *radially inwards* across the guide field lines. The key equation for diffusive detachment is the one for electron azimuthal momentum, which including resistivity and inertia, is

$$\frac{m_e}{r} \tilde{\boldsymbol{u}}_{\boldsymbol{e}} \cdot \nabla (r u_{\theta e}) + m_e \nu_{ei} u_{\theta e} = e u_{\perp e} B. \tag{34}$$

with $\nu_{ei} \equiv c_s/\lambda_{ei}$ the Coulomb collision frequency,

$$\nu_{ei} = 1.15 \cdot 10^6 \mathrm{s}^{-1} \cdot \frac{n_0 \hat{n}}{10^{18} \mathrm{m}^{-3}} \frac{\ln \Lambda}{12.5} \left(\frac{10 \mathrm{eV}}{T_e} \right)^{3/2} = \nu_{ei0} \hat{n} \tag{35}$$

Let us define an *effective Hall parameter*,

$$\chi = \frac{\Omega_e}{\nu_{ei} + \nu_{iner}}, \tag{36}$$

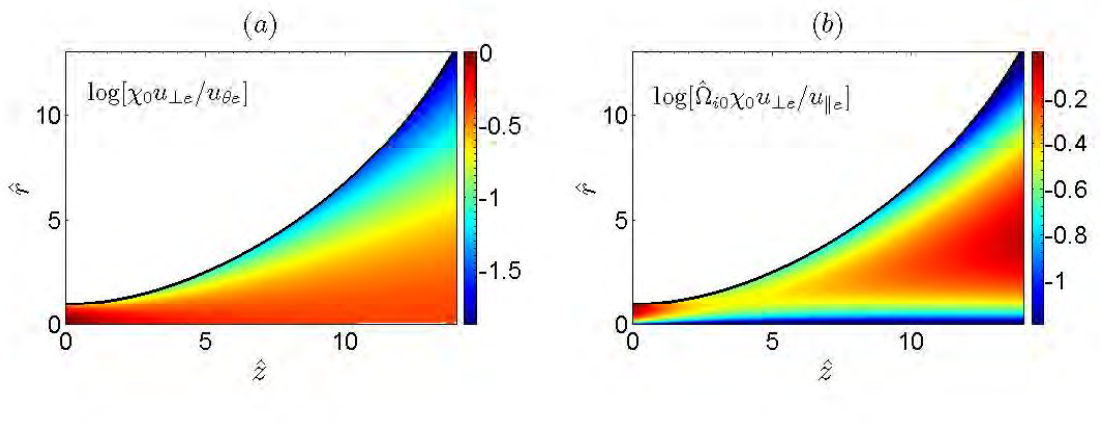

Figure 8. Diffusion caused by resistivity effects only. (a) Evolution of the inverse of the Hall parameter, $\log_{10}(\chi_0 u_{\perp e}/u_{\theta e}) = \log_{10}(\chi_0/\chi)$**. (b) Diffusion of electron streamtubes from magnetic streamtubes measured through** $u_{\perp e}/u_{\parallel e}$**.**

with $\Omega_e = eB/m_e$ as the electron gyrofrequency and

$$\nu_{iner} = \tilde{\boldsymbol{u}}_{\boldsymbol{e}} \cdot \nabla \ln u_{\theta_e} + \frac{u_{re}}{r} \tag{37}$$

as an effective frequency for inertia effects. Then, the perpendicular electron velocity satisfies

$$u_{\perp e} = \chi^{-1} u_{\theta e}. \tag{38}$$

and, of course, we are assuming that $\chi \gg 1$.

In order to illustrate the diffusive detachment, we have computed diffusion created by e-i resistivity (i.e. keeping $m_e/m_i \to 0$). For an isothermal plasma and ignoring the small change of $\ln \Lambda$, we have $\nu_{ei} \simeq \nu_{ei0}\hat{n}$ and $\chi = \chi_0 \hat{B}/\hat{n}$, with subindex 0 referring to values at the throat. Figure 8 plots the ratios $u_{\perp e}/u_{\theta e} \equiv \chi^{-1}$ and $u_{\perp e}/u_{\parallel e}$ in a rather universal way: the last ratio measures (the tangent of) the detachment angle. According to Table 1, practical values of χ_0 are of the order of 10^3 whereas we expect $\hat{\Omega}_{i0} \leq O(1)$. Therefore resistive detachment is very small, at least for isothermal electrons and no anomalous resistivity. This and an adiabatic electron fluid (with ν_{ei} decreasing slower than n) are considered by Moses et al.[7]

But the real main point regarding resistive diffusion is that $u_{\theta e} > 0$ for a propulsive plasma (and $j_{\theta e} < 0$) so that $u_{\perp e} > 0$ and electron streamtubes are *more divergent* than magnetic streamtubes. Therefore, resistive diffusion in a propulsive plasma constitutes a *divergent* detachment mechanism and not a convergent one, which is the desired type of detachment mechanism. Resistive diffusion, at least while electrons continue to be strongly-magnetized, is an additional issue for the axial ejection of a plasma beam from the magnetic nozzle.

We do not show it here, but inertia-based diffusion also yields ν_{iner}, Eq. (37), positive and therefore a divergent detachment. This disagrees flagrantly with Hooper,[8] who postulates a model similar to ours and predicts inertia-based, convergent detachment. A detailed discussion of his model is out of the limits of this paper. We believe that by assuming current ambipolarity, that implies $u_{\perp e} = u_{\perp i}$, he is forcing $u_{\perp e} < 0$: clearly ion streamtubes diverge less than magnetic streamtubes. Then, Eq. (38), which should determine $u_{\perp e}$ is in fact determining $u_{\theta e}$ and making it negative.

V. Conclusions

The magnetic nozzle model worked out in Ref.12 has been used to evaluate existing detachment theories. A central point in propulsive applications is that for the nozzle to yield a gain in plasma axial momentum

and thrust, the plasma beam must develop an azimuthal diamagnetic current that induces a magnetic field opposed axially to the guide field. This scenario disagrees with the one suggested in the stretching self-field detachment theory.

Regarding resistive and inertia-based diffusion, it is shown that both make the electrons diverge from the magnetic streamlines instead of converge, which, again, is a behaviour opposite to the one claimed by present theories.

Therefore, detachment theories for magnetic nozzles in plasma thrusters require to be reconsidered fully.

Acknowledgments

This work was financed by the Gobierno de España (Project ESP-2007-62694). Part of it was carried out as preparation of the proposal 'Magnetic nozzles for plasma thrusters: acceleration, thrust, and detachment mechanisms', submitted to Dr. Mitat Birkan of US Air Force Office of Scientific Research and Dr. Brad Thompson of European Office of Aerospace Research & Development.

References

[1]G. Krülle, M. Auweter-Kurtz, and A. Sasoh, J. Propulsion and Power **14**, 754 (1998).

[2]O. Batishchev, IEEE Transaction on Plasma Science **37**, 1563 (2009).

[3]D. P. F. Ferri, M. Manente, D. Curreli, Y. Guclu, D. Melazzi, D. Rondini, S. Suman, J. Carlsson, C. Bramanti, E. Ahedo, V. Lancellotti, K.Katsonis, and G. Markelov, Design of 50W Helicon Plasma Thruster, in *31th International Electric Propulsion Conference, Ann Arbor, Michigan, USA*, IEPC 2009-205, Electric Rocket Propulsion Society, Fairview Park, OH, 2009.

[4]A. Arefiev and B. Breizman, Physics of Plasmas **11**, 2942 (2004).

[5]S. A. Andersen, V. O. Jensen, P. Nielsen, and N. D'Angelo, Phys. Fluids **12**, 557 (1969).

[6]A. Sasoh, Physics of Plasmas **1**, 464 (1994).

[7]R. W. Moses, R. Gerwin, and K. Schoenberg, Resistive plasma detachment in nozzle based coaxial thrusters, in *Proceedings Ninth Symposium on Space Nuclear Power Systems, Albuquerque, New Mexico, 1992*, AIP Conference Proceedings No. 246, pp. 1293–1303, American Institute of Physics, Woodbury NY, 1992.

[8]E. B. Hooper, Journal of Propulsion and Power **9**, 757 (1993).

[9]R. Winglee, T. Ziemba, L. Giersch, J. Prager, J. Carscadden, and B. R. Roberson, Physics of Plasmas **14**, 063501 (2007).

[10]A. Arefiev and B. Breizman, Physics of Plasmas **12**, 043504 (2005).

[11]C. A. Deline, R. D. Bengtson, B. N. Breizman, M. R. Tushentsov, J. E. Jones, D. G. Chavers, C. C. Dobson, and B. M. Schuettpelz, Physics of Plasmas **16**, 033502 (2009).

[12]E. Ahedo and M. Merino, Physics of Plasmas **17**, 073501 (2010).

[13]M. Merino and E. Ahedo, Two-dimensional magnetic nozzle acceleration of a two-electron component plasma, in *Proceedings of Space Propulsion 2010, San Sebastián, Spain, May 3-6, 2010*, SP2010-1841391, European Space Agency, 2010.

[14]J. Jackson, *Classical Electrodynamics*, Wiley, New York, 1999.

[15]M. Abramowitz and I. Stegun, *Handbook of Mathematical Functions*, Dover, New York, 1965.

[16]M. Zucrow and J. Hoffman, *Gas dynamics* , Wiley, New York, 1976.

[17]B. N. Breizman, M. R. Tushentsov, and A. V. Arefiev, Physics of Plasmas **15**, 057103 (2008).

47th AIAA/ASME/SAE/ASEE Joint Propulsion Conference & Exhibit
31 July - 03 August 2011, San Diego, California

AIAA 2011-5999

Plasma detachment mechanisms in a magnetic nozzle

M. Merino* and E. Ahedo†

Universidad Politécnica de Madrid, 28040 Madrid, Spain

An axisymmetric model of the supersonic expansion of a collisionless, totally ionized plasma in a divergent magnetic nozzle and the DIMAGNO simulation code are being used to study the plasma detachment from the guiding magnetic field, taking into account the effects of the induced magnetic field generated by the plasma electric currents. The azimuthal electric currents carried by the plasma from the discharge chamber or created within the nozzle are the central feature for both thrust generation and plasma detachment. These currents are mainly electronic and have a globally diamagnetic character, as their induced field lowers the total field around the axis and increases nozzle divergence rate. This paper focuses on the role of the plasma-generated magnetic field and the detachment issue, particularized for the case of a helicon thruster (although conclusions extracted herein might be easily generalizable to other thruster types). A viable alternative detachment mechanism based on plasma self-demagnetization is investigated.

I. Introduction

Propulsive Magnetic Nozzles (PMN) are the fundamental acceleration device of advanced plasma thrusters currently being developed. PMN are being used to guide, control and accelerate a plasma beam in the helicon thruster,[1–4] the VASIMR,[5] and the Applied-Field MagnetoPlasmaDynamic Thruster.[6] It is also a secondary element of the Diverging Cusped Field Thruster[7] and some configurations of the Cylindrical Hall Thruster.[8]

The fundament of these devices lies on the possibility of controlling the expansion of a plasma into vacuum with an imposed magnetic field of appropriate geometry and mild intensity, strong enough to have electrons magnetized. Accomplishing this allows to nozzle the plasma without magnetizing ions—which would require a magnetic field several orders of magnitude stronger,—since electrons pull ions via the ambipolar electric field that ensues. A PMN exhibits a thermoelectric character, as it converts the thermal energy present in the plasma (provided electrically by the plasma source) into directed kinetic energy of ions, in close resemblance to a traditional de Laval nozzle with a supersonic neutral gas.[9] On the other hand, the PMN can be termed a electromagnetic device, since the external forces that channel the plasma and convey the produced thrust back to the engine are purely magnetic.

The discussion presented in this paper is based on the two-dimensional, two-fluid model of a collisionless, quasineutral and totally-ionized plasma flow in a divergent PMN introduced in Ref. 10. The model assumes that electrons are fully magnetized, and allows any degree of ion magnetization. This is typically the situation with the helicon thruster, which consists of a helicon plasma source ending in a PMN, such as the HPH.com thruster being developed in Europe.[4] In a helicon source, most of the energy is deposited on the electrons, while ions remain relatively cold. A plasma with these characteristics constitutes the reference case for this study, although most of the results obtained therewith are readily generalizable or adaptable to more complex plasmas.

With the help of this model, we performed a parametric investigation of the evolution of the plasma in the PMN and characterized its propulsive performances when the plasma density is low enough to neglect the induced magnetic field it creates, i.e., when the plasma beta, $\beta = \mu_0 n T_e / B^2 \ll 1$. We showed that the confinement and acceleration of the plasma is governed by the presence of azimuthal electric currents in the plasma, which (1) are mainly electron-based, (2) posses a globally diamagnetic character with respect to the external magnetic field in order to produce thrust and (3) are proportional to the internal energy of

*Student, AIAA Student Member (mario.merino@upm.es)
†Professor, AIAA Member

the plasma. When cold ions do not rotate initially their contribution to azimuthal currents is paramagnetic, which was found to negligible for the parametric range explored (at least up to the magnetic nozzle turning point). It was seen that the plasma response is strongly 2D, and that many important aspects such as these azimuthal electric currents, or the not-fulfillment of local current ambipolarity in the longitudinal plane, are only recoverable with a two-dimensional model.

Building upon these results, a preliminary investigation of the issue of plasma detachment from the applied field was carried out in Refs. 11,12. The relevance of achieving plasma detachment in a PMN once it has been accelerated strives in the closed nature of magnetic streamlines, which poses a major concern about the use of PMN for space propulsion. Without proper separation from the field, the magnetized plasma would return onto the thruster along field lines, ruining thrust and endangering sensitive spacecraft surfaces and equipment. A competitive PMN requires the bulk of the plasma to detach well before the turning point of the magnetic lines, keeping attachment losses (which might be unavoidable) to a minimum.

Arguably, the ability of a mild magnetic field to deflect 180 deg an energetic plasma beam must be limited. However, the mechanisms that allow the plasma to detach are complex and controversial, and they are still not well understood. A number of detachment theories have been proposed in the last years: firstly, it has been claimed that plasma electric currents could be strong enough to modify the geometry of the magnetic field and stretch the magnetic lines to infinity, effectively avoiding the problem of detachment, as the plasma would carry the magnetic field with it instead of turning back.[13] However, as we demonstrated in Ref. 12, this scenario implicitly requires the azimuthal currents to be *paramagnetic* so that plasma-induced magnetic field reinforces the applied one axially and avoids the magnetic lines to turn back. This is unfortunately not the case for a PMN, where the azimuthal plasma currents are are dominantly *diamagnetic* at least up to the turning point.

Secondly, plasma resistivity[14] and electron inertia effects,[15] although small in the largest part of the plasma volume, have also been proposed as plausible detachment mechanisms, which would allow electrons to diffuse across the magnetic field lines, allowing the plasma beam to continue its downstream motion without turning back. However, we have shown that these diffusive-detachment mechanisms lead to *divergent detachment* in a PMN, meaning that the plasma plume would diverge faster than the magnetic field, which is an undesired situation. It follows that resistivity (and electron inertia) effects should be kept to a minimum to avoid the additional, uncontrolled plasma divergence. The reason why these detachment mechanisms produce divergent detachment is again related to the plasma currents being diamagnetic.

The diamagnetic nature of the plasma has been recently confirmed experimentally.[16] Indeed, the applied and the induced magnetic fields need to repel each other to produce thrust, requiring a diamagnetic character of the latter.

Two new detachment mechanisms which do observe this requirement for thrust were suggested in Ref. 12. Firstly, it is observed from the simulations that for low ion magnetization, the plasma near the vacuum becomes strongly rarefied, as most of the ion flux diverges much less than the magnetic field. This is a consequence of ions being already detached from the field and the ambipolar electric field not being able to significantly alter their trajectories without further rarefaction. This is highly beneficial for propulsion, as radial efficiency losses are kept much lower than if ions followed magnetic lines, and it can be regarded as a naturally-occurring *self-separation* detachment. Related to this, an interesting possibility to be explored is the appearance of non-neutral effects due to the low density near the plasma-vacuum transition, which could participate in the development of the plasma-vacuum edge and allow its detachment from the field.

The second plausible detachment mechanism is plasma demagnetization fostered by the self-induced field. This *self-demagnetization* detachment is motivated again by the diamagnetic character of the plasma currents: the induced magnetic field that they create competes with the applied one, lowering the intensity of the field downstream. If conditions are appropriate, the resulting magnetic field might become weak enough for electrons to become unmagnetized, meaning that plasma would be able to detach from the magnetic field.

This paper is dedicated to the investigation of the second detachment mechanism. The model of Ref. 10 is extended to include the induced magnetic field as described in section II, in order to allow the study of plasma flows with $\beta > 0$. The self-consistent magnetic field is calculated with an iterative method. Then, section III presents the simulation results for the induced magnetic field and derived quantities, which provide the necessary elements for the discussion of detachment in section IV. There, the self-separation and self-demagnetization mechanisms are analyzed within the limits of the present model. Finally, the main conclusions of this work are gathered in section V. An appendix details the procedure used to calculate the

applied and induced magnetic fields.

II. Plasma model and integration

The 2D model developed in Ref. 10 is extended here to include the induced magnetic field. A quasineutral, collisionless plasma, formed by cold ions and hot Maxwellian, isothermal electrons ($T_e = \text{const}$), streaming out of an helicon source at ion-sonic velocity, is subject to the action of a total magnetic field $\boldsymbol{B} = \boldsymbol{B}_a + \boldsymbol{B}_p$, resulting from the superposition of an applied, external magnetic field $\boldsymbol{B}_a$, and the plasma-induced magnetic field $\boldsymbol{B}_p$ created by the electric currents present in the plasma. It is assumed that electron inertia plays a negligible role, and that electrons are completely magnetized so that they remain in their initial streamtube ($\boldsymbol{u}_e = u_{\parallel e}\mathbf{1}_\parallel + u_{\theta e}\mathbf{1}_\theta$, with $\mathbf{1}_\parallel$ and $\mathbf{1}_\theta$ the unit vectors in the direction parallel to $\boldsymbol{B}$ and the azimuthal direction. Analogously, $\mathbf{1}_\perp = \mathbf{1}_\theta \times \mathbf{1}_\parallel$ is defined). The equations that govern the flow,[10] expressed in cylindrical coordinates (z, r, θ) centered at the nozzle throat, are summarized below:

$$u_{zi}\frac{\partial \ln n}{\partial z} + u_{ri}\frac{\partial \ln n}{\partial r} + \frac{\partial u_{zi}}{\partial z} + \frac{1}{r}\frac{\partial (r u_{ri})}{\partial r} = 0, \tag{1}$$

$$u_{zi}\frac{\partial u_{zi}}{\partial z} + u_{ri}\frac{\partial u_{zi}}{\partial r} + c_s^2\frac{\partial \ln n}{\partial z} = -\left(u_{\theta i} - u_{\theta e}\right) B_r, \tag{2}$$

$$u_{zi}\frac{\partial u_{ri}}{\partial z} + u_{ri}\frac{\partial u_{ri}}{\partial r} + c_s^2\frac{\partial \ln n}{\partial r} = \left(u_{\theta i} - u_{\theta e}\right) B_z + \frac{u_{\theta i}^2}{r}, \tag{3}$$

$$r m_i u_{\theta i} + e\psi = D_i\left(\psi_i\right), \tag{4}$$

$$T_e \ln n - e\phi = H_e\left(\psi\right), \tag{5}$$

$$u_{\theta e} = -\frac{r}{e}\frac{\partial H_e}{\partial \psi}, \tag{6}$$

$$\frac{n u_{\parallel e}}{B} = G_e\left(\psi\right). \tag{7}$$

The longitudinal components of the different magnetic fields can be expressed through a streamfunction ψ_k, where the subindex k indicates the applied (a), plasma (p) and total (no subindex) fields, with

$$\frac{\partial \psi_k}{\partial r} = r B_{zk};\ \frac{\partial \psi_k}{\partial z} = -r B_{rk}. \tag{8}$$

Equations 1–7 need to be complemented with Ampère's equation in order to include the induced magnetic field:

$$\nabla \times \boldsymbol{B}_p = \mu_0\left(\boldsymbol{j}_i - \boldsymbol{j}_e\right) = \mu_0 e n\left(\boldsymbol{u}_i - \boldsymbol{u}_e\right). \tag{9}$$

In the previous equations $c_{si} = \sqrt{T_e/m_i}$ is the sound velocity of ions, and $D_i\left(\psi_i\right)$, $H_e\left(\psi\right)$, $G_e\left(\psi\right)$ are functions of the ion streamline function ψ_i and total magnetic field streamfunction ψ that can be evaluated given the initial conditions. These expressions can be normalized using T_e (electron temperature, energy units), m_i (ion mass), e (element charge), R (plasma radius at nozzle throat) and n_0 (plasma density at the centerline at the throat). A hat is used to denote dimensionless variables, e.g. $\hat{\phi} = e\phi/T_e$, $\hat{B} = eRB/\sqrt{T_e m_i}$, $\hat{n} = n/n_0$. Notice that Eq. 9 can then be re-written as

$$\nabla \times \hat{\boldsymbol{B}}_p = \beta_0 \hat{B}_{a0}^2 \hat{n}\left(\hat{\boldsymbol{u}}_i - \hat{\boldsymbol{u}}_e\right), \tag{10}$$

where $\beta_0 = \mu_0 n_0 T_e / B_{a0}^2$ is the plasma beta at the origin.

Aside from the geometry of the imposed magnetic field $\boldsymbol{B}_a$ (here created by a set of two solenoids, as detailed in the appendix, the resulting model depends on (1) the magnitude of this field at the origin, B_{a0}, which controls the degree of ion magnetization. Notice that $\hat{B}_{a0} \simeq \hat{B}_0 = \hat{\Omega}_{i0} = R\Omega_{i0}/c_s$, the dimensionless ion gyrofrequency at the origin. A typical helicon xenon thruster with $R = 10$ cm, $T_e = 20$ eV and $B_{a0} = 200$ G has $\hat{B}_{a0} = 0.38$. For practical devices, $\hat{B}_{a0}$ is expected to range from 0.1 or lower to 1 (Refs. 2, 3). Additionally, the plasma response is dependent on (2) the plasma density, electric potential, and velocity profiles at the nozzle throat, and (3) β_0, which determines the relative importance of the induced magnetic field with respect to the applied one. In previous work, it was assumed that $\beta_0 \ll 1$, and the induced magnetic field effects were neglected.

In this article, we are concerned with the role of the induced magnetic field in the plasma response, which is governed by β_0. The influence of ion magnetization and plasma profiles was already studied in Ref. 10; therefore, for the present study, simulations will use $B_{a0} = 0.1$ and the non-uniform density profile characteristic of helicon sources described in the mentioned reference.

Inclusion of the elliptic Ampère's equation (Eq. 10) ruins the hyperbolic character of Eqs. 1–3, upon which our solution method is based. To deal with this, a new iterative scheme to obtain the self-consistent solution of the plasma response with the induced magnetic field that it generates has been implemented into a new version of our DIMAGNO code,[10,17] which has been restructured into a new object-oriented architecture for improved flexibility (OO-DIMAGNO). The ability to calculate the induced magnetic field frees the previously-existing constrain of $\beta_0 \ll 1$ that assured a negligible induced field.

The scheme is based on solving the plasma and the magnetic field separately. Firstly, the plasma response for a fixed magnetic field, which initially is just the applied field $\boldsymbol{B}_a$, is obtained. Taking advantage of the supersonic character of the plasma flow, equations 1–7 are numerically integrated with the Method of Characteristics (MoC), which reduces the partial differential equations (Eqs. 1–3) to ordinary differential equations along the three families of characteristic lines in the meridian plane of the nozzle (two Mach line families and the ion streamlines). Adequate propagation and intersection of these characteristics allows then to calculate the plasma response. This makes DIMAGNO a fast and accurate code for calculating the plasma response in the PMN, displaying greater performances than other finite difference schemes.[18,19]

Knowing this first version of the plasma flow, the induced field $\boldsymbol{B}_p^1$ due to the plasma electric currents is calculated. This field is then used to correct the total field of the next iteration, $\boldsymbol{B} = \boldsymbol{B}_a + \boldsymbol{B}_p^1$. A new induced field results from this iteration, $\boldsymbol{B}_p^2$. This iterative process is repeated until convergence of the induced magnetic field ψ_p function is reached everywhere in the computational domain. The solutions obtained in this way readily converge to the self-consistent flow and magnetic field (absolute error in ψ_p/B_{a0} diminishes about one order of magnitude per iteration for small values of β_0). A detailed description of the calculation of the applied and induced magnetic field is described in the appendix.

III. Induced magnetic field

Diamagnetic azimuthal currents are a key element of a PMN, as they produce the radial confining force $j_\theta B_{za} < 0$ that compensates for the radial pressure gradient $-T_e \partial \ln n/\partial r > 0$, but also the axial accelerating force $-j_\theta B_{ra} > 0$. As shown in Eq. 17 of the appendix, these forces are proportional to $j_\theta B_{a0} \sim T_e$, which manifests that propulsive performances largely depend on the internal energy. An intuitive way to express this is that the plasma pressure "pushes" against the magnetic field lines as if they were the virtual walls of a solid nozzle, so that the expansion is directed mostly axially, producing thrust. For the same reasons, the presence of paramagnetic currents is detrimental for propulsion.

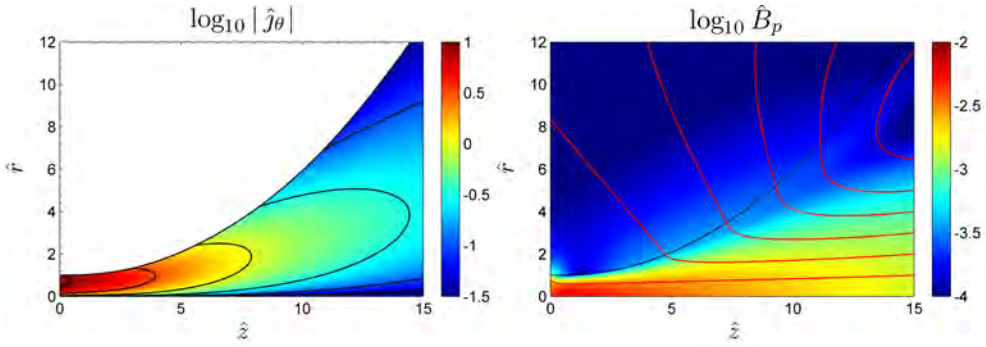

Figure 1. Magnitude of the azimuthal currents (left), $\log_{10}|\hat{j}_\theta|$ and their induced magnetic field (right) when $\beta_0 = 0.1$. The currents are diamagnetic ($j_\theta < 0$ for $B_{za} > 0$ at the axis). Black contour lines in steps of 0.5 of the magnitude $\log_{10}|\hat{j}_\theta|$ are displayed. Red lines show the direction of the induced magnetic field, which opposes the applied one at the axis. Plasma-vacuum line (dashed black) has been plotted for reference.

As explained in the previous section, these currents give rise to a longitudinal induced magnetic field, which opposes the applied one. Azimuthal plasma currents and their induced field are shown in figure 1 for a representative case. It is seen that j_θ is larger closer to the nozzle throat, and diminishes as the plasma

expands downstream. The induced magnetic field is stronger about the nozzle centerline, and its direction is almost-axial in most of the plasma domain.

The consequences of this induced field are twofold: (1) the opening of the magnetic streamtubes (producing a faster-diverging nozzle) and (2) the weakening of the total field. Figure 2 shows the magnitude of these effects in the total magnetic field for different values of β_0. These results agree qualitatively with the predictions of a previous first-order perturbation analysis.[11]

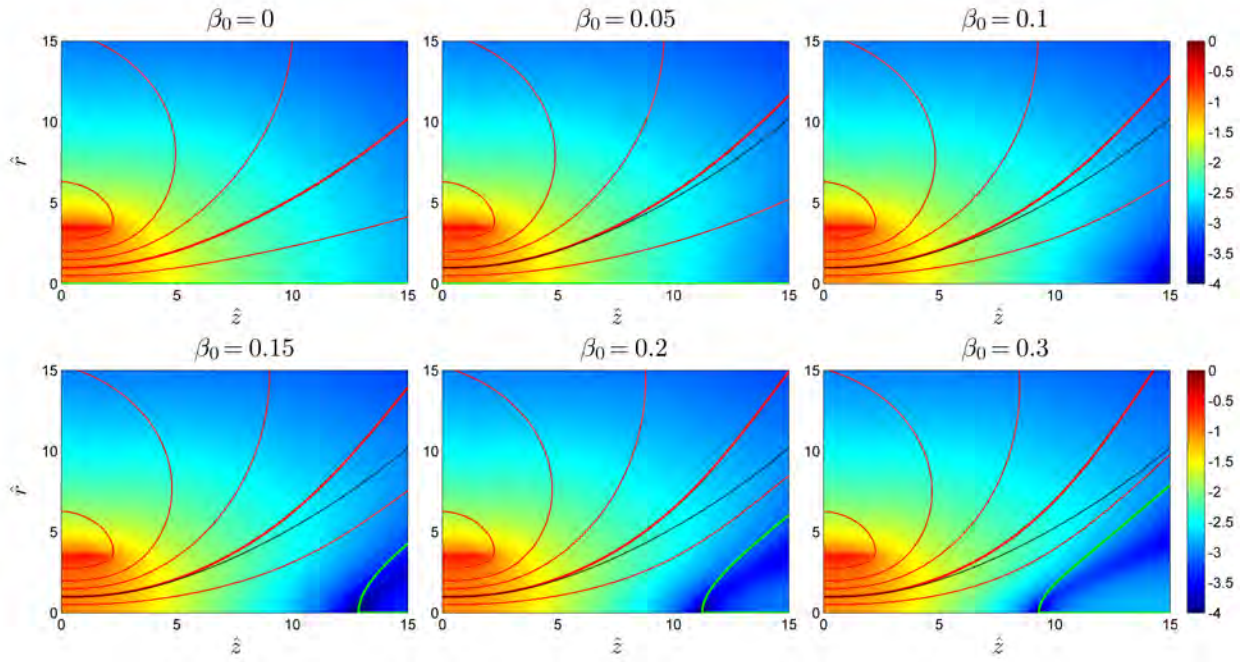

Figure 2. Self-consistent total magnetic field $\boldsymbol{B} = \boldsymbol{B}_a + \boldsymbol{B}_p$ for different values of β_0. The background color indicates the intensity of the field in logarithmic scale, $\log_{10} \hat{B}$. Red lines show magnetic streamlines, the thicker one being the plasma-vacuum edge in the simulations (it passes through $\hat{z} = 0$, $\hat{r} = 1$). The black dashed line serves to compare this to the corresponding line of the initial applied magnetic field, $\boldsymbol{B}_a$. The green line, when present, displays the magnetic separatrix, $\psi = 0$.

These results show that larger values of β_0 cause weaker total magnetic fields downstream. An interesting feature of these figures is the existence of a region of very low magnetic field around the axis, that moves upstream as β_0 increases. This hints that the induced magnetic field can become an outstanding mechanism to lower the total field magnitude enough to allow electron demagnetization for moderate β_0. Additionally, some of the simulations exhibit a saddle-point within this zone where the field actually cancels out, followed by a separatrix surface that extends downstream and divides the magnetic field in two disconnected regions, *internal* (upstream) and *external* (downstream). The existence of a point where $B = 0$ has been observed in recent experiments by Roberson *et al.*[16] Since our current model cannot predict the electron currents that might exist beyond the separatrix line (where $\psi < 0$), we have taken $j_{\theta e} = 0$ in this region. The actual magnetic field may therefore differ in this zone and its neighborhood for the simulations with larger β_0. We are currently working to properly model flow and currents in the demagnetized plasma.

The strong alteration of the geometry and intensity of the magnetic nozzle seen in figure 2 has profound implications in the behavior of the plasma and its detachment from the field: firstly, thruster performances are affected. The additional divergence of the field causes a decrease of the plume efficiency η_{plume}, which quantifies the radial kinetic losses,[10]

$$\eta_{plume}(z) = \frac{P_{zi}(z)}{P_i(z)} = \frac{\int_{A(z)} m_i n u_{zi}^3 / 2dA}{\int_{A(z)} m_i n u_i^2 u_{zi} / 2dA}, \tag{11}$$

where $P_{zi}(z)$ and $P_i(z)$ are, respectively, the ion axial and total power traversing section $A(z)$ (plane perpendicular to the axis at position z). Figure 3 displays (1) the thrust gain $\kappa_{noz}(z) = F(z)/F(0) - 1$,

with $F(z) = \int_{A(z)} \left(nu_{zi}^2 + nT_e\right) dA$ the thrust (ion momentum plus electron pressure) achieved at section $A(z)$, and (2) the plume efficiency $\eta_{plume}(z)$ for different values of β_0. These results manifest that while κ_{noz} remains almost unaffected (although a small decrease for the same nozzle aperture $\hat{r}$ seems to occur), η_{plume} decreases as β_0 increases.

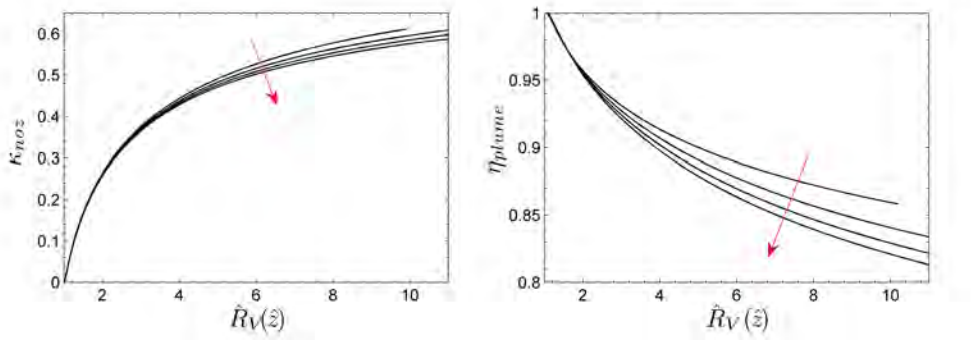

Figure 3. Nozzle performances $\kappa_{noz}(z)$ (left) and $\eta_{plume}(z)$ (right) plotted against the value of the nozzle radius R_V at that each z-section, for $\beta_0 = 0$, 0.05, 0.1 and 0.15 (direction of increasing values of β_0 denoted with arrows).

Secondly, as the plasma moves downstream, it approaches the low-B region and the separatrix surface. There, the plasma near the axis and the plasma near the nozzle edge can behave differently. The weaker field near the axis enhances demagnetization of electrons, which become effectively free of the influence of the applied magnetic field, and thus are able to traverse the separatrix surface and continue downstream. Subsequent development of the plasma beam is then dominated by the residual plasma pressure and plasma currents/induced field. The flow thereafter might then be described in an approximate way with e.g. self-similar plasma plume expansion models.[20]

On the other hand, the influence of the induced magnetic field near the nozzle edge is modest, and depending on the plasma properties, B might be still strong enough for electrons to remain attached. Since the topology of the magnetic field near the separatrix is severely altered, electrons which are unable to traverse this feature will be pulled outwards by the deflected magnetic streamlines. The large slip between ion and electron velocities in this region could give rise to considerable longitudinal currents that might further complicate the flow.

The transition from one behavior to the other, and the plasma dynamics in the external magnetic field behind the separatrix, cannot be determined with the current model, since it is based upon the assumption of magnetized electrons. However, as discussed in the next section, a first estimation of demagnetization can be performed based on the value of the electron Larmor radius ℓ_e, showing that plasma *self-demagnetization* can be a viable detachment mechanism for the bulk of the plasma beam.

IV. Plasma detachment via demagnetization

The model of section II is based upon the fundamental assumption

$$\lambda_D \ll \ell_e \ll R, \tag{12}$$

i.e., that the Debye length λ_D is the smallest scale in the problem, and that electron Larmor radius ℓ_e is smaller than the macroscopic gradient length (which is $\sim R$, the initial nozzle radius). As long as this scale ordering is fulfilled, electrons can be assumed to be magnetized, and their movement can be approximately studied with the gyrocenter trajectories, which coincide with magnetic streamlines. This hypothesis might fail due to two reasons. First, for very low plasma densities, λ_D might increase and become $\lambda_D \sim \ell_e$, in which case non-neutral effects would strongly alter the orbital motion of electrons about the magnetic streamlines. This phenomenon would destroy their clean helical movement and/or pull their gyrocenters out of their magnetic line, hence producing the demagnetization of electrons. Second, the magnetic field might become low enough to allow $\ell_e \sim R$, with the gyroradius becoming of the order of the macroscopic gradient length, resulting in analogous consequences. Here, our attention is focused in this second possibility for attaining demagnetization.

It is important to note that, although ions are normally unmagnetized (their gyrofrequency at the origin, $\hat{\Omega}_{i0}$, is typically $\hat{\Omega}_{i0} \sim 0.1$–$1$ or lower in present helicon thrusters), the reason why the plasma remains attached to the magnetic field is the fact that electrons are magnetized, forcing the whole plasma to adapt to the geometry of the magnetic field. Therefore, achieving electron demagnetization is crucial to free the plasma from the field.

Success of the PMN as a plasma accelerator device is conditioned to being able to detach at least the *bulk* of the plasma beam. Fortunately, most of the plasma flux is concentrated about the nozzle axis: there is a strong rarefaction taking place near the plasma edge, related to the *self-separation* of ion and electron streamtubes downstream (illustrated in figure 4). Self-separation[12] is due to ions not being magnetized, and the ambipolar electric field being insufficient to deflect ion trajectories enough (except at the plasma edge to have quasineutrality fulfilled there). This indicates that even in the worst scenario where electrons in the near-edge region remained completely magnetized even after the turning point of magnetic streamlines, they would constitute only a small fraction of the ion flux, and therefore they would not degrade nozzle performances substantially, as long as the core flow is able to detach successfully.

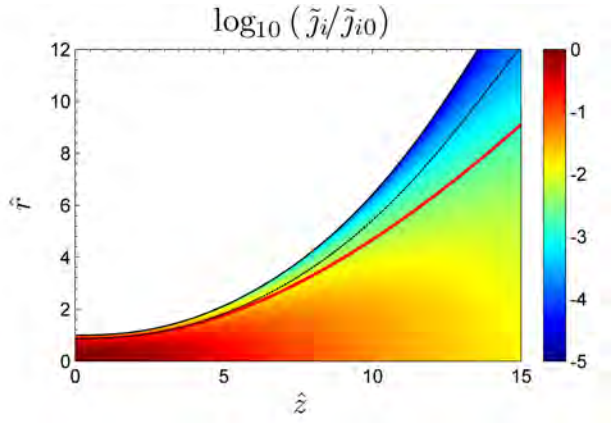

Figure 4. Logarithm of the ion flux in the longitudinal plane, normalized with its value at the origin $\log_{10}(\tilde{\jmath}_i/\tilde{\jmath}_{i0})$, with $\tilde{\jmath}_i = n\sqrt{u_{zi}^2 + u_{ri}^2}$. In this simulation, $\beta_0 = 0.15$. The streamtube containing 95% of the total ion flux (which passes through $\hat{r} = 0.86$, $\hat{z} = 0$) has been plotted in red. The dashed black line denotes the position of the magnetic streamline that coincides initially with this tube, showing that strong self-separation occurs, and the largest part of the plasma flux does not diverge as much as the magnetic field.

Having discarded diffusion and field-stretching as viable detachment mechanisms for a PMN,[11,12] we now propose demagnetization of electrons as a means to release the plasma from the magnetic field. Clearly, as the magnetic nozzle diverges, the magnitude of the magnetic field B/B_0 decays as $\sim 1/\hat{R}_V^2$ (with R_V the local nozzle radius). This means that $\ell_e/\ell_{e0} \sim \hat{R}_V^2$, and therefore the electron Larmor radius increases fast as the nozzle opens. Typical helicon thrusters,[2,3] have $\hat{\ell}_{e0}$ in the range $\sim 10^{-2}$–10^{-3}, meaning that the electron flow starts to demagnetize roughly at $R_V \simeq 10$–30.

Central to this process is the promoted demagnetization in the low-B region, as ℓ_e increases substantially. The value of the electron Larmor radius normalized with its value at the origin, ℓ_e/ℓ_{e0}, is portrayed in figure 5. It is apparent that thanks to the induced field, plasma can reach $\ell_e \sim R$ much earlier for even small values of β_0. Larger values of this parameter increase this effect. This is hence an effective mechanism to facilitate the demagnetization (and thus detachment) of the core of the plasma beam, which contains most of the ion flux. Once demagnetized, the plasma plume will continue to expand under the action of its residual pressure and fields.

Figure 5 also reveals that demagnetization near the plasma edge is not significantly augmented by the plasma induced field, meaning that it will occur approximately at the same zone as in the $\beta_0 = 0$ case. Again, the small ion flux in this region has a negligible contribution to thrust, and therefore performances would not be noticeably penalized if its detachment occurs further downstream. It might be unavoidable, however, to lose a small fraction of flux due to unsuccessful detachment, which PMN design should minimize. As mentioned above, study of the behavior of the near-edge plasma will require to take into account non-neutral effects.

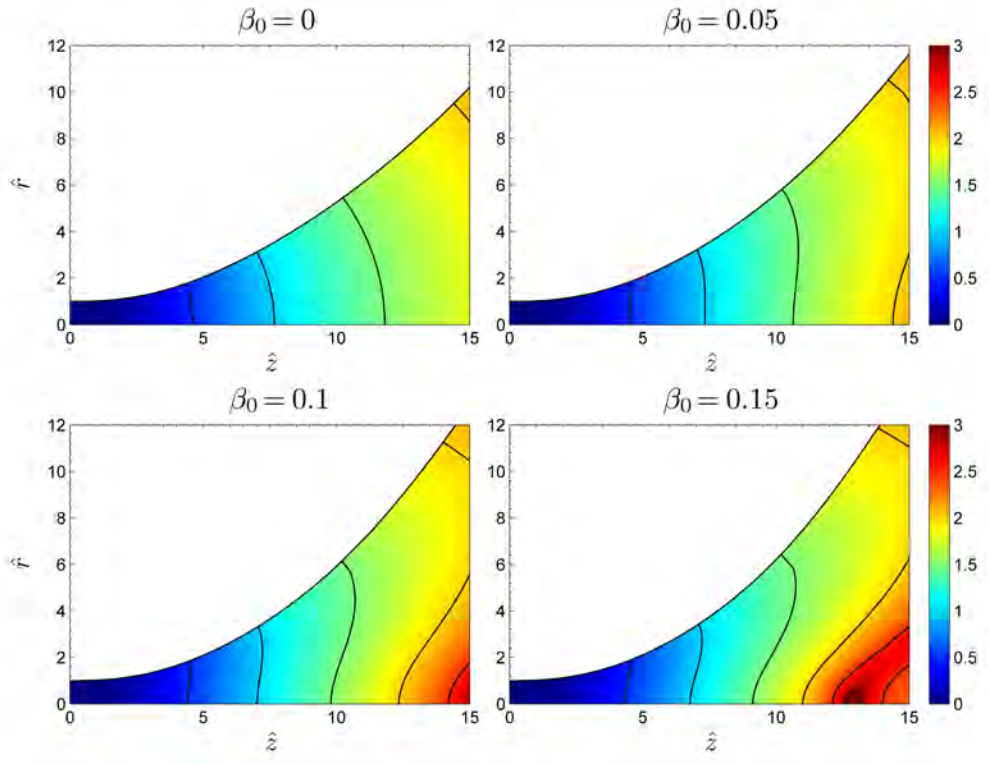

Figure 5. Logarithm of Larmor radius of electrons normalized with its value at the origin, $\log_{10}(\ell_e/\ell_{e0})$. Contour lines of this magnitude in steps of 0.5 are shown in black.

V. Conclusions

By extending our two-dimensional magnetic nozzle model to include the plasma-generated magnetic field, we have confirmed and quantified (1) the increase of nozzle divergence and (2) the diminishing of field intensity induced by the plasma diamagnetic currents. These effects do take place even for very low values of the plasma beta parameter at the origin, β_0. A region of low magnetic field forms about the axis, and it moves upstream for increasing values of β_0. A zero-field point and a separatrix surface occurs in this region for moderate β_0, separating internal and external magnetic fields.

The induced magnetic field is regarded as an excellent mechanism to promote self-demagnetization of the bulk of the plasma beam and attain its detachment. Once the plasma enters the external field region (after separatrix), it can be considered in practice free from the influence of the applied magnetic field. The evolution of the plasma plume thereafter is governed by its residual pressure, currents and fields.

The peripheral plasma carries a very small fraction of the total flux, thanks to the intense rarefaction and self-separation of ion and electron streamtubes close to this border. Induced field does not accelerate demagnetization here, but it can still occur naturally further downstream, as the nozzle opens and B decreases.

Critical parameters for this process are the initial Larmor Radius-to-nozzle radius ratio, $\hat{\ell}_{e0}$, which defines how much B/B_{a0} needs to decrease in order to achieve demagnetization, and β_0, as it controls the position and shape of the low-B region. Correct design of a PMN will take all these phenomena into account and optimize the value of these parameters in order to detach most of the plasma before the nozzle turning point. In this way, the fraction of plasma lost due to over-attachment and the radial losses can be minimized.

These conclusions are the result of an ongoing research effort, and many aspects of the plasma-field interaction remain our current object of study. Particularly, three points are highlighted: (1) the behavior of the plasma in the low-B region and downstream from the separatrix line. Our current model, based upon perfect electron magnetization, cannot describe a quasi-magnetized plasma. In this highly-complex flow, electron inertia effects (as well as resistivity) need to be taken into account. We are currently working to

include these phenomena into the model.

Additionally, (2) the longitudinal currents arising from the large ion-electron separation in this region might further complicate the flow, and the effects of their azimuthal induced field need to be assessed.

Future work also addresses (3) the investigation of non-neutral effects near the plasma edge, which could play a central role in the detachment of the near-edge plasma flow. This involves the definition of a more precise demagnetization criterion than $\ell_e \sim R$ or $\ell_e \sim \lambda_D$, such as a more refined critical characteristic length and the quantification of electron streamline separation from magnetic streamlines.

Appendix: Calculation of the Magnetic field

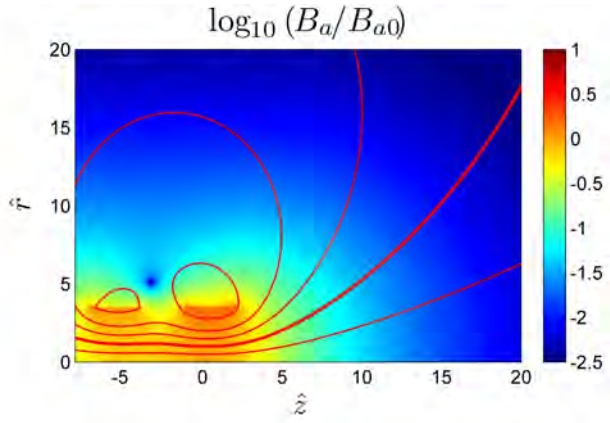

Figure 6. Magnetic Field created by the two solenoids, configuration representative for a Helicon thruster. The solenoids have a radius $\hat{r} = 3.5$, and run from $\hat{z} = -7$ to -4, and from -1 to 2. The field has been normalized with its value at the origin, B_{a0}. The intensity in the first and second solenoids are in a 4:6 ratio, to provide a stronger field at the open end of the helicon tube. Red lines denote selected magnetic streamlines. The thicker one constitutes the last plasma streamline in the simulations, i.e., the plasma-vacuum edge, and passes through $\hat{z} = 0$, $\hat{r} = 1$.

The applied magnetic field $\boldsymbol{B}_a$ used for the simulations is generated by two coaxial solenoids, as depicted in figure 6. This configuration is typical of the helicon plasma sources being used for helicon thrusters under development, and is representative of the HPH.com thruster.[4] By using two sets of coils, the resulting magnetic field is quasi-axial inside the helicon quartz tube, and opens at the end to conform a divergent PMN. The magnetic streamfunction ψ_a and the components B_{za}, B_{ra} of the axisymmetric field can be calculated with the analytical solution of the magnetic field of a single current loop,[21] summing over each loop L:

$$\psi_a = \sum_L \frac{\mu_0 I_L}{4\pi} \sqrt{(r+r_L)^2 + (z-z_L)^2} \left[(2-m_L)\,\mathbf{K}(m_L) - 2\mathbf{E}(m_L) \right], \tag{13}$$

$$B_{za} = \sum_L \frac{\mu_0 I_L}{2\pi} \frac{1}{\sqrt{(r+r_L)^2 + (z-z_L)^2}} \left[\mathbf{K}(m_L) - \frac{r^2 - r_L^2 + (z-z_L)^2}{(r-r_L)^2 + (z-z_L)^2} \mathbf{E}(m_L) \right], \tag{14}$$

$$B_{ra} = -\sum_L \frac{\mu_0 I_L}{2\pi r} \frac{(z-z_L)}{\sqrt{(r+r_L)^2 + (z-z_L)^2}} \left[\mathbf{K}(m_L) - \frac{r^2 + r_L^2 + (z-z_L)^2}{(r-r_L)^2 + (z-z_L)^2} \mathbf{E}(m_L) \right], \tag{15}$$

where $\mathbf{K}(m)$ and $\mathbf{E}(m)$ are the complete elliptic integrals of the first and second kind,[22] z_L, r_L denote the intersection of loop L with a meridional plane, I_L is the current on each loop (constant for a solenoid), and

$$m_L = \frac{4 r_L r}{(r+r_L)^2 + (z-z_L)^2}. \tag{16}$$

The induced magnetic field $\boldsymbol{B}_p$, on the other hand, arises from the plasma response, as electric currents create their own magnetic field. Both azimuthal and longitudinal electric currents exist in the PMN. Since we are interested here in the longitudinal induced field, we are concerned with azimuthal plasma currents,

because they are the only ones generating B_{zp}, B_{rp}. These electric currents are predominantly electron-based, if the plasma has no initial rotation.[10]

The magnitude of the induced field relative to the applied one is characterized by the local plasma beta β, which is proportional to its value at the origin: $\beta = \mu_0 n T_e / B_a^2 = \beta_0 \hat{n} \hat{B}_{a0}^2 / \hat{B}_a^2$. This dependence with β_0 can be seen from the electron momentum equation, $0 = -T_e \nabla \ln n + e\nabla\phi - e u_{\theta e} B \mathbf{1}_\perp$, particularized at the nozzle throat where $\phi = 0$, and Eq. 10:

$$j_\theta \sim \frac{T_e}{B_{a0}}; \quad B_p \sim \beta_0 B_{a0}. \tag{17}$$

Ideally, one would attempt to calculate the induced magnetic field simultaneously with the plasma response, by solving Ampère's equation (Eq. 10), which can be rewritten in terms of the streamfunction ψ_p (B_{zp} and B_{rp} then follow from definitions in Eq. 8),

$$\frac{1}{r}\frac{\partial^2 \psi_p}{\partial z^2} + \frac{\partial}{\partial r}\left(\frac{1}{r}\frac{\partial \psi_p}{\partial r}\right) = \beta_0 B_{a0}^2 n \left(u_{\theta e} - u_{\theta i}\right) \tag{18}$$

together with the plasma equations. The field thus obtained would then be added to the applied field to obtain the total magnetic field, $\boldsymbol{B} = \boldsymbol{B}_a + \boldsymbol{B}_p$. However, as mentioned in the text, this would break the hyperbolic character of the problem, since Eq. 10 is elliptic in nature (i.e., plasma currents at a given position influence the whole domain), and would force us to abandon the numerous advantages in terms of accuracy and speed associated to the MoC upon which DIMAGNO is based. This argument motivates the iterative approach used to obtain the solution.

A favorable method to calculate the induced magnetic field after concluding each plasma iteration is based on the analytical solution of a single current loop, Eq. 13–15. The obtained distribution of azimuthal current density, $j_\theta dz dr = n\left(u_{\theta i} - u_{\theta e}\right) dz dr$, is discretized at the nodes of a rectangular grid of $M \times N$ points covering the simulation region. Each node is then treated as a current loop, and the field it creates at the middle points of the grid is calculated analytically using expressions analogous to Eqs. 13–15, producing the "influence matrix" of that current loop in the calculation domain.

The influence of currents inside the plasma source, e.g. an helicon tube, is neglected. This is justified by the small radius of the plasma currents at this point, which means their influence has a limited range, in a region where the applied magnetic field dominates even for moderate values of β_0. Indeed, as it can be appreciated in figure 1, the effect is restricted to a local "leakage" of induced field at the throat region, that would not occur if source currents would be taken into account. Notwithstanding, the influence of these currents is negligible downstream, where detachment and the features under study take place. Similarly, currents beyond a chosen final integration section $z = z_{MAX}$ need also to be neglected. For the simulations presented in this work, $z_{MAX} = 20$ was used. It has been checked numerically that the solution for $z \lesssim 15$ is sufficiently insensitive to the inclusion of currents beyond $z = 20$.

Apart from being based on an analytical solution, this approach has the benefit of avoiding the need to use approximate boundary conditions for the calculation domain, which is the main inconvenient of methods based on directly solving Ampère's equation (Eq. 18) numerically, and it also avoids the necessity to numerically differentiate in ψ_p to obtain B_{zp} and B_{rp}, since the magnetic field components can be obtained simultaneously in the same analytical fashion.

By re-using the influence matrix of each loop in a column in an appropriate way, this algorithm has a computational cost in terms of time of the order $O\left(MN^2\right)$.

Acknowledgments

This work was sponsored by the Air Force Office of Scientific Research, Air Force Material Command, USAF, under grant number FA8655-10-1-3085. Additional support came from the Gobierno de España (Project AYA-2010-16699). The authors thank I. Martínez for helping with some of the computations.

References

[1]Charles, C., Boswell, R. W., and Lieberman, M. A., "Xenon ion beam characterization in a helicon double layer thruster," *Applied Physics Letters*, Vol. 89, No. 26, 2006, pp. 261503.

[2]Ziemba, T., Carscadden, J., Slough, J., Prager, J., and Winglee, R., "High Power Helicon Thruster," *41st AIAA/ASME/SAE/ASEE Joint Propulsion Conference & Exhibit*, AIAA, Washington DC, 2005.

[3]Batishchev, O., "Minihelicon Plasma Thruster," *IEEE Transactions on Plasma Science*, Vol. 37, No. 8, Aug. 2009, pp. 1563–1571.

[4]Pavarin, D., Ferri, F., Manente, M., Curreli, D., Güçlü, Y., Melazzi, D., Rondini, D., Suman, S., Carlsson, J., Bramanti, C., Ahedo, E., Lancellotti, V., and Markelov, G., "Design of 50 W Helicon Plasma Thruster," *31st International Electric Propulsion Conference*, Electric Rocket Propulsion Society, Fairview Park, OH, 2009.

[5]Chang-Diaz, F., "An overview of the VASIMR engine: High power space propulsion with RF plasma generation and heating," *AIP Conference Proceedings*, Vol. 595, AIP, Melville, NY, 2001.

[6]Krülle, G., Auweter-kurtz, M., and Sasoh, A., "Technology and Application Aspects of Applied Field Magnetoplasmadynamic Propulsion," *Journal of Propulsion and Power*, Vol. 14, No. 5, 1998, pp. 754–763.

[7]Courtney, D. and Martinez-Sanchez, M., "Diverging Cusped-Field Hall Thruster (DCHT)," *30th International Electric Propulsion Conference*, Electric Rocket Propulsion Society, Fairview Park, OH, 2007.

[8]Raitses, Y., Smirnov, A., and Fisch, N., "Cylindrical Hall Thrusters," *37th AIAA Plasmadynamics and Lasers Conference*, AIAA, Washington DC, 2006.

[9]Andersen, S., Jensen, V., Nielsen, P., and D'Angelo, N., "Continuous supersonic plasma wind tunnel," *Physics of Fluids*, Vol. 12, No. 3, 1969, pp. 557–560.

[10]Ahedo, E. and Merino, M., "Two-dimensional supersonic plasma acceleration in a magnetic nozzle," *Physics of Plasmas*, Vol. 17, No. 7, 2010, pp. 073501.

[11]Ahedo, E. and Merino, M., "Preliminary assessment of detachment in a plasma thruster magnetic nozzle," *46th AIAA/ASME/SAE/ASEE Joint Propulsion Conference & Exhibit*, AIAA, Washington DC, 2010.

[12]Ahedo, E. and Merino, M., "On plasma detachment in propulsive magnetic nozzles," *Physics of Plasmas*, Vol. 18, No. 5, 2011, pp. 053504.

[13]Arefiev, A. V. and Breizman, B. N., "Magnetohydrodynamic scenario of plasma detachment in a magnetic nozzle," *Physics of Plasmas*, Vol. 12, No. 4, 2005, pp. 043504.

[14]Moses Jr, R., Gerwin, R., and Schoenberg, K., "Resistive plasma detachment in nozzle based coaxial thrusters," *AIP Conference Proceedings*, Vol. 246, AIP, Melville, NY, 1992.

[15]Hooper, E. B., "Plasma detachment from a magnetic nozzle," *Journal of Propulsion and Power*, Vol. 9, No. 5, Sept. 1993, pp. 757–763.

[16]Roberson, B. R., Winglee, R., and Prager, J., "Enhanced diamagnetic perturbations and electric currents observed downstream of the high power helicon," *Physics of Plasmas*, Vol. 18, No. 5, 2011, pp. 053505.

[17]Merino, M. and Ahedo, E., "Simulation of plasma flows in divergent magnetic nozzles," *IEEE Transactions on Plasma Science (accepted)*, 2011.

[18]Zucrow, M. J. and Hoffman, J. D., *Gas Dynamics, volume I*, John Wiley & sons, 1976.

[19]Zucrow, M. J. and Hoffman, J. D., *Gas Dynamics, volume II*, Vol. M, John Wiley & sons, 1977.

[20]Merino, M., Ahedo, E., Bombardelli, C., Urrutxua, H., and Peláez, J., "Hypersonic Plasma Plume Expansion in Vacuum and Preliminary Assessment of Magnetic Effects," *to be presented in the 32nd International Electric Propulsion Conference*, No. IEPC-2011-086, Electric Rocket Propulsion Society, Fairview Park, OH, 2011.

[21]Jackson, J., *Classical Electrodynamics*, John Wiley & sons, 2001.

[22]Abramowitz, M. and Stegun, I., *Handbook of mathematical functions with formulas, graphs, and mathematical tables*, Dover publications, 1964.

Magnetic confinement of a high-density cylindrical plasma

Eduardo Ahedo *

E.T.S. Ingenieros Aeronáuticos, Universidad Politécnica de Madrid, 28040 Madrid, Spain

August 17, 2011

Abstract

The stationary structure of a weakly-collisional plasma column, confined by an axial magnetic field and a cylindrical vessel, is studied for the high-density case, when the diamagnetic azimuthal current is large enough to demagnetize partially the plasma. The plasma response is characterized mainly by two dimensionless parameters: the ratios of the electron gyroradius and the electron skin-depth to the plasma radius, and each of them measures the independent influence of the applied magnetic field and the plasma density on the plasma response. The strong magnetic confinement regime, characterized by very small wall losses, is limited to the small gyroradius and large skin-depth ranges. In the high-density case, when the electron skin-depth is smaller than the electron gyroradius, the skin-depth turns out to be the magnetic screening length, so that the bulk of the plasma behaves as unmagnetized.

PACS numbers: 52.25.Xz, 52.30.-q, 52.50.Dg, 52.75.Di

*Professor; e-mail: eduardo.ahedo@upm.es; website: www.fmetsia.upm.es/ep2

1 Introduction

A plasma contained in a cylindrical vessel and affected by an axial magnetic field is a classical confinement configuration. The first detailed analysis of the problem dates back to the radial diffusive model of Tonks[1], who showed the formation and central role of the azimuthal plasma current. Later, Forrest and Franklin[2] and Ewald et al.[3] included ion inertia effects for a weakly-collisional plasma. In the last years, the problem has been revisited by several authors. Sternberg et al.[4] have highlighted that, for a magnetized plasma, the electron force balance involves the expanding pressure gradient and the confining magnetic force caused by the plasma current, so that the Boltzmann relation does not apply to electrons. Our contribution[5] has been to carry out a detailed asymptotic and parametric analysis of the problem, which has shown that: (1) the inertial layer linking the bulk diffusive region to the Debye sheath is initiated by electron-inertia effects that tend to limit the growth of the electron azimuthal current; (2) ion-inertia effects are limited to a subregion within that layer; and (3) the change from the magnetic to the electric force as main confining force on electrons takes place *within* the ion-inertia sublayer, when the ion Mach number is about 0.7. In addition, we showed the existence of a second distinguished magnetized regime when electron collisionality is very small, and we provided simple scaling laws for particle and energy fluxes to the wall (which measure the magnetic confinement level of the plasma column).

In our analysis, the main magnetized regime is characterized by the distinguished limits

$$\lambda_{d0} \ll \ell_{e0} \ll R \sim c_s/\nu_e, \tag{1}$$

$$\beta_0 \ll 1, \tag{2}$$

where: R is the radius of the plasma column, $\lambda_{d0} = \sqrt{\epsilon_0 T_e/e^2 n_0}$ is the Debye length, with T_e the electron temperature and n_0 the plasma density at the axis; $\ell_{e0} = \sqrt{T_e m_e}/eB_0$ is the electron gyroradius, with B_0 the applied magnetic field; $c_s = \sqrt{T_e/m_e}$ is the plasma sound speed and ν_e is the electron collision frequency; and $\beta_0 = \mu_0 n_0 T_e/B_0^2$ is *half the* ratio between

thermal and magnetic pressures. Conditions (1)-(2) assure that the plasma is magnetized, weakly collisional, and quasineutral except in the thin Debye sheath adjacent to the wall.

It is well known –for instance from the MHD equilibrium of a θ-pinch [6]–, that the azimuthal plasma current is diamagnetic and induces a magnetic field that opposes the applied one. The induced field is negligible in the low-density or zero-beta limit, Eq. (2), but otherwise it makes the total magnetic field to have a minimum at the center of the plasma column[6, 7]. Nonzero-β_0 effects are of interest to high-density plasmas. For instance, helicon thrusters, in order to be competitive, require[8, 9, 10, 11, 12] a moderate magnetic field [$\sim 0.01 - 0.05$T], a high plasma temperature ($\sim 20 - 30$eV), and a relatively-high density($\sim 10^{19}\mathrm{m}^{-3}$), so that values of β_0 about 0.5 can be reached.

This paper attempts to characterize the nonzero-beta regime of a cylindrical plasma satisfying conditions (1). Specific goals of the study are, first, to determine the changes caused by β_0 in the radial plasma structure and in the magnetic confinement of the plasma column, and, second, the different parametric regimes of the plasma response. Interestingly, the collisionless electron skin-depth, generally related to time-dependent problems, such as inductive plasma discharges[13, 14] or hydromagnetic solitary waves[15], will turn out to be a characteristic length of both the plasma spatial profile and the confinement regime. Finally, the competition between the ambipolar electric field and the total magnetic field in confining the plasma column[4, 5, 7] is commented.

2 Model formulation

In order to tackle with nonzero-beta effects, the Ampere's law must be added to the zero-beta, cylindrical model of Ref.[5]. Neglecting terms that we already showed to be small, the

relevant set of equations for the quasineutral plasma column are

$$\frac{1}{r}\frac{d}{dr}(rn_e u_r) = n_e \nu_w, \tag{3}$$

$$0 = -\frac{1}{n_e}\frac{d}{dr}(T_e n_e) + e\frac{d\phi}{dr} - eu_{\theta e}B + m_e\frac{u_{\theta e}^2}{r}, \tag{4}$$

$$m_i u_r \frac{du_r}{dr} = -e\frac{d\phi}{dr} - m_i \nu_i u_r, \tag{5}$$

$$m_e u_r \frac{du_{\theta e}}{dr} = eu_r B - \nu_e m_e u_{\theta e} - m_e\frac{u_{\theta e}u_r}{r}, \tag{6}$$

$$\frac{dB}{dr} = \mu_0 e n_e u_{\theta e}. \tag{7}$$

where: n_e is the density of the quasineutral plasma; $u_r = u_{re} = u_{ri}$ is the radial velocity of both ions and electrons, consistent with a one-dimensional model and a dielectric wall; $u_{\theta e}$ is the electron azimuthal velocity; B is the local magnetic field; ϕ is the ambipolar electric potential; $\nu_i = \nu_{ion} + \nu_{in}$ is the ion total collision frequency, with contributions of the ionization frequency and the ion-neutral collision frequency; $\nu_e = \nu_{ion} + \nu_{en} + \nu_{ei}$ is the electron total collision frequency, with contributions of ν_{ion}, and the electron-neutral and electron-ion collision frequencies; and ν_w is the frequency for plasma losses at the wall. This loss frequency is indeed an eigenvalue of the problem and must satisfy the plasma balance condition[16]. This states that, in the stationary response, plasma losses at the wall are equal to the volumetric plasma production (i.e. $\propto \nu_{ion}$) plus any axial differential transport [$\propto (\nu_w - \nu_{ion})$ in this one-dimensional model]. Equations (3)-(7) do not include the ion azimuthal velocity, because it was shown to be negligible in practical cases,[5] $u_{\theta i}/u_{\theta e} \sim m_e\nu_i/(m_i\nu_e)$. Also the ion pressure has been neglected and hereafter we will take T_e, ν_e, and ν_i as known constants. These assumptions simplify the discussion without affecting the core and aims of the present study.

Manipulating Eqs. (3)-(5) allows us to solve for the derivatives of u_r and n_e,

$$m_i\left(\frac{c_s^2}{u_r}-u_r\right)\frac{du_r}{dr}=eu_{\theta e}B+m_i\left(\nu_i u_r+\nu_w\frac{c_s^2}{u_r}\right)-\frac{m_ic_s^2+m_eu_{\theta e}^2}{r}, \tag{8}$$

$$u_r\frac{dn_e}{dr}=n_e\left(\nu_w-\frac{u_r}{r}-\frac{du_r}{dr}\right), \tag{9}$$

and then to solve Eq. (5) for the derivative of ϕ. Now the set of Eqs.(5)-(9) constitute a standard first-order system of differential equations, which presents singularities at $r=0$, $u_r=0$, and $u_r=c_s$. The two first ones take place at the plasma axis and they are avoided by just eliminating unbounded modes there [see boundary condition (12) in Ref.[5]]. The third one is the classical sonic singularity and matches with the Bohm condition at the edge S of the Debye sheath. In the asymptotic analysis consistent with Eq. (1), the Debye sheath is a discontinuity between the quasineutral plasma and the wall W, so that we can take $r_S=R$ in the quasineutral scale. Therefore, the six boundary conditions for the five plasma equations *and* the eigenvalue ν_w are $n_e=n_0$, $u_r=0$, $u_{\theta e}=0$, and $\phi=0$ at the plasma axis ($r=0$), and $u_r=c_s$ and $B=B_0$ at the sheath edge S (i.e. $r\simeq R$).

Equations (5)-(9) are non-dimensionalized as in Ref.[5], and this process identifies the set of free parameters that determine the plasma response. Here, Eq. (7) introduces β_0 as a new free parameter and the dimensionless plasma balance equation takes the functional form

$$\frac{\nu_w R}{c_s}=\hat{\nu}_w\left(\frac{\ell_{e0}}{R},\frac{\bar{\lambda}_e}{R},\frac{R\nu_i}{c_s},\beta_0\right), \tag{10}$$

where $\bar{\lambda}_e=c_s/\nu_e$ is a *reduced* (by the square of the electron-to-ion-mass ratio) collisional mean-free path for electrons. It was shown in Ref. [5] that ion-collision parameter $R\nu_i/c_s$ has a minor role in the response and scaling laws for the magnetized regime, so discussions here will assume implicitly that $R\nu_i/c_s\ll 1$.

The electron skin-depth $d_{e0}=\sqrt{m_e/(e^2\mu_0 n_0)}$ satisfies $\beta_0=\ell_{e0}^2/d_{e0}^2$. Therefore d_{e0}/R can

be used as free parameter instead of β_0. Indeed, since

$$\ell_{e0} \propto B_0^{-1}, \qquad d_{e0} \propto n_0^{-1/2}, \tag{11}$$

the pair of parameters $(\ell_{e0}/R, d_{e0}/R)$ is clearly more appropriate than the pair $(\ell_{e0}/R, \beta_0)$ for studying the independent effects of the applied magnetic field and the density on the plasma response. Since n_0 is present only in β_0 (or in d_{e0}/R), the nonzero-beta case brings with it all the influence of the plasma density on the dimensionless response of the plasma column. Zimmerman et al.[7], who include Ampere's law and present particular solutions with the induced magnetic field, miss somehow β_0 among their model parameters (their β_0 and χ are comparable to ours R/ℓ_{e0} and $\bar{\lambda}_e/\ell_{e0}$, respectively, and none of them include the product $\mu_0 n_0$, present in β_0).

3 Plasma response

3.1 Zero-beta limit

We briefly summarize here results of Ref.[5] that are of interest for the nonzero-beta study. For $\beta_0 \to 0$, Eq. (7) yields $B(r) = B_0$. Then, the asymptotically exact solution of the diffusive bulk region is

$$\frac{n_e}{n_0} = J_0\left(a_0 \frac{r}{R}\right), \qquad \frac{n_e u_{\theta e}}{n_0 c_e} = \frac{\ell_{e0}}{R} a_0 J_1\left(a_0 \frac{r}{R}\right), \qquad \frac{u_r}{c_s} = \frac{u_{\theta e}}{c_e}\frac{\ell_{e0}}{\bar{\lambda}_e}, \tag{12}$$

with J_0 and J_1 Bessel functions and $a_0 \simeq 2.405$ the first zero of J_0. Notice that u_r is normalized with c_s and $u_{\theta e}$ with $c_e = \sqrt{T_e/m_e}$. The transition to the inertial layer takes place when $u_{\theta e} = O(c_e)$. Within this layer, of thickness $O(\ell_{e0})$ roughly, electron inertia hinders further increments of $u_{\theta e}$. Then, in a shorter sublayer [see Eq.(31) of Ref.[5]], ion inertia brings u_r/c_s from $O(\ell_{e0}/\bar{\lambda}_e)$ to 1, and the ambipolar electric force surpass the magnetic force at $u_r/c_s \simeq 2^{-1/2}$.

The plasma flux to the wall (also constant across the inertial and Debye layers) is $n_{eS} c_s$

with

$$\frac{n_{eS}}{n_0} \simeq 1.25 \frac{\ell_{e0}^2}{R\bar{\lambda}_e}. \tag{13}$$

This illustrates the excellent confinement provided by the applied magnetic field; for instance, experimental measurements by Tysk et al.[17] yield $n_{eS}/n_0 \sim 1\%$. Equation (13) has to be compared with

$$\frac{n_{eS}}{n_0} = \mathrm{e}^{-1/2} \simeq 0.61, \tag{14}$$

for an unmagnetized, weakly-collisional plasma, which is confined only electrostatically, by the ambipolar electric field set up by the presence of the wall.

3.2 Nonzero beta regimes

For $\beta_0 \ll 1$, the small induced magnetic field can be obtained by solving Eq. (7) with the zero-beta solution (12) on the right-hand side,

$$\frac{dB}{dr} \simeq \beta_0 B_0 \frac{a_0}{R} J_1\left(\frac{a_0 r}{R}\right). \tag{15}$$

Straightforward integration yields

$$1 - B(r)/B_0 \simeq \beta_0 J_0(a_0 r/R), \qquad (\beta_0 \ll 1) \tag{16}$$

and the minimum value of the magnetic field at the plasma center is $B(0) \simeq (1-\beta_0)B_0$.

When β_0 is no longer small, Eq. (7) must be solved together with the rest of plasma equations but Eq. (16) already suggests that the central part of the plasma column is demagnetized. Let us take the case of a plasma with $\ell_{e0}/R \ll 1$ and analyze the plasma response as its density at the axis is increased, that is as d_{e0}/R is decreased or β_0 is increased. Figure 1 plots the radial profiles of plasma magnitudes for $\ell_{e0}/R = 0.1$ and different values of β_0 in the range between 0 and 2.5, that is $\infty > d_{e0}/R > 0.032$. Figure 1(a) shows how the total magnetic field decreases as β_0 increases. The central plasma region becomes totally demag-

netized for $\beta_0 \sim 0.5$, and magnetization is limited to a thin layer near the wall when $\beta_0 > 1$. Figure 1(b) depicts the density profile, illustrating how magnetic confinement deteriorates as β_0 increases. Figure 1(c) plots u_r: the gentler profiles as β_0 increases are due to a larger electrostatic field in the central region. As the dashed lines of Figs. 1(b) and 1(c) corroborate, the behavior of a plasma with $\ell_{e0}/R \ll 1$ and β_0 large approaches that of the unmagnetized case $\ell_{e0}/R = \infty$, except in a thin demagnetization layer. The profiles of $u_{\theta e}$ in Fig. 1(d) are the consequence of two facts: (i) $u_{\theta e}$ provides the resistive force that opposes the azimuthal magnetic force, Eq. (6), (ii) the larger n_0 is, the lower is the value of $u_{\theta e}$ required to generate the current required to screen the applied magnetic field, Eq. (7). Figure 1(e) shows that the profiles of $j_{\theta e} = -en_e u_{\theta e}$ change significantly with β_0, and they reflect the fact that $j_{\theta e}$ is the product of variables with different trends as β_0 is varied.

Therefore, for $\beta \geq O(1)$, the magnetized plasma and $j_{\theta e}$ are limited to a thin quasineutral layer adjacent to the Debye sheath. The characteristic thickness of that layer is the electron skin-depth, d_{e0}, as the plots suggest and we confirm next with the plasma equations. For $\ell_{e0}/R \ll 1$ and $\beta_0 \geq O(1)$, the dominant form, *near the sheath edge* of Eq. (6) is $m_e du_{\theta e}/dr \simeq eB$. This yields $u_{\theta eS} \sim (eB_0/m_e)\Delta r$, with Δr the layer thickness. Then, Eq. (7) yields $\Delta r \sim d_{e0}$ and

$$u_{\theta eS} \sim c_e \beta_0^{1/2}. \tag{17}$$

A characterization of the combined effects of ℓ_{e0}/R and d_{e0}/R on the plasma response is provided by the parametric curves of Figs. 2 and 3. The normalized (or dimensionless) plasma flux to the wall is plotted in Fig. 2(a). Figures 2(b) and 2(c) plot the electron azimuthal velocity and current at the sheath edge, which are also a measure of the plasma magnetization level. There are three regions in the curves of Fig. 2(a): (1) for ℓ_{e0}/R small enough, the plasma is magnetically confined with $n_{eS}/n_0 \ll 1$; (2) for ℓ_{e0}/R large, the plasma is unmagnetized and confined only electrostatically, with $n_{eS}/n_0 \simeq 0.6$; (3) for intermediate values of ℓ_{e0}/R, the transition between those distinguished regimes takes place. As d_{e0}/R decreases from about 1, the range of ℓ_{e0}/R corresponding to magnetic confinement is reduced.

Figure 3(a) plots the normalized plasma flux to the wall versus $\ell_{e0}/d_{e0} \equiv \beta_0^{1/2}$, in the range $d_{e0}/R < 1$ of interest here. This figure shows that the magnetic confinement regime ends quite abruptly at $\ell_{e0}/d_{e0} \simeq 0.7$, i.e at $\beta_0 \simeq 0.5$. Figure 3(b) shows that this limit corresponds approximately to the case of the total magnetic field at the plasma axis becoming negligible. From $\beta_0 \simeq 0.5$ up there is a transition regime that ends around $\ell_{e0}/d_{e0} \approx 2$, i.e at $\beta_0 \approx 4$ when the plasma flux to the wall takes the value again of electrostatic confinement. For $\beta_0 > 4$, the plasma column is magnetized only in a thin layer around the wall, of thickness $\sim d_{e0}$, with no effect on plasma confinement. The location of magnetic and electrostatic confinement regimes in the parametric plane $(\ell_{e0}/R, d_{e0}/R)$ is illustrated in Fig. 4 , where constant flux-to-the-wall curves are plotted. The two selected curves, $n_{eS}/n_0 = 0.05$ and 0.5, could serve as approximate boundaries of the magnetic, electrostatic, and intermediate confinement regimes. Finally, notice that the above analysis has been centered in the weakly-collisional limit, when the Hall parameter, $\bar{\lambda}_e/\ell_{e0}$, is very large. Collisional effects, which tend to reduce magnetic confinement, were already discussed in Ref.[5].

3.3 Force balance

The sum of Eqs. (4) and (5), together with the Ampere's law (7) yields the radial momentum equation of the plasma in the form

$$m_i n_e u_r \frac{du_r}{dr} = -\frac{d}{dr}\left(T_e n_e + \frac{B^2}{2\mu_0}\right) - m_i n_e \nu_i u_r + m_e n_e \frac{u_{\theta e}^2}{r}, \tag{18}$$

where the magnetic pressure appears explicitly as complementing the thermal pressure. For $\ell_{e0}/R \ll 1$ and $0 < \beta_0 \ll 1$, the plasma response in the bulk region corresponds to the known θ-pinch equilibrium[6]

$$T_e n_e + B^2/(2\mu_0) = \text{const.} \tag{19}$$

Then, in the inertial layer, ion convection becomes significant, and, finally, the magnetic force is negligible in the Debye sheath. However, for $\beta_0 = O(1)$, when induced magnetic effects

are larger, the constant pressure balance of Eq. (19) holds nowhere because of the ion inertia term is relevant already in the bulk region. Apart from showing the similarity with the basic θ-pinch equilibrium, expressing the magnetic force term, $j_{\theta e}B$, as the gradient of the magnetic pressure does not present any advantage when solving the present problem. For β_0 small, most of the contribution to the magnetic pressure comes from the applied field, which is constant and has a zero contribution to the pressure gradient. Indeed, the magnetic pressure gradient term of Eq. (18), which is proportional to $(dB/dr)/\beta_0$, appears as a mathematically indeterminate expression of the form 0/0 in the asymptotic limit $\beta_0 \to 0$; therefore, the equivalent form $j_{\theta e}B$, which does not present that mathematical issue, is preferable.

The electron force balance, given by Eq. (4), can be expressed as

$$f_p + f_c = f_e + f_m \equiv f, \tag{20}$$

with $f_p = -T_e d\ln n_e/dr$, $f_c = m_e u_{\theta e}^2/r$, $f_e = -ed\phi/dr$, and $f_m = eu_{\theta e}B$. Each term in Eq. (20) is positive and represents a force contribution *on an 'average' electron*. The pressure gradient, f_p, and the centrifugal force, f_c, are the expanding forces, grouped in the left-hand side of Eq. (20); the electric force, f_e, and the magnetic force, f_m, confine the electrons. Notice from Eq. (5) that, when ion resistivity and ion pressure are negligible, f_e is the only force on an 'average' ion, and accelerates it towards the wall.

Figure 5 plots $f_c/f \equiv 1 - f_p/f$ and $f_m/f = 1 - f_e/f$ at different spatial locations and different values of β_0, for a plasma with $\ell_{e0}/R = 0.10$. This representation facilitates a quick assessment of the relevance of each of the four forces to the balance of Eq. (20). First, the thermal pressure gradient is by far the main contribution to the electron expansion, i.e. $f \simeq f_p$; the centrifugal contribution f_c/f is relevant only in the collisionless (i.e. $R \ll \bar{\lambda}_e$), intermediate-magnetization regime of Ref.[5]. Then, the solid lines of Fig. 5 illustrate on the competition between electric and magnetic forces in confining electrons, the dominant force changing both with the *radial* location and the *parametric* point in the plane $(\ell_{e0}/R, d_{e0}/R)$. Starting with the parametric influence, the magnetic force is stronger, on the average, the

lower are ℓ_{e0}/R and β_0, and it is marginal *at any* r for β_0 large, even when $\ell_{e0}/R \ll 1$. With respect to the dominant force at different radial locations, the electric force dominates *always* in the region $u_r/c_s \gtrsim 0.7$ independently of ℓ_{e0}/R and β_0. In addition, for $\ell_{e0}/R \ll 1$, the electric force becomes dominant in the central region for moderate values of β_0. At the sheath edge limit $u_r/c_s \to 1$, one has $f_m/f \to 0$, that is $f_m/f_e \to 0$. The magnetic force at the sheath edge is $f_{mS} = eu_{\theta eS}B_0$, with $u_{\theta eS}$ plotted in Fig. 2(b). Thus, the vanishing of the magnetic-to-electric force ratio is due to the known singular behavior of the ambipolar electric field there, i.e $f_{eS} \to \infty$.

4 Conclusions

The strong diamagnetic currents and the induced magnetic field that arise in a magnetized cylindrical plasma when the thermal-to-magnetic pressure ratio is not small cause important changes in the plasma behavior. For a zero-Debye-length and weakly-collisional plasma the problem is characterized by two dimensionless parameters, ℓ_{e0}/R and either d_{e0}/R or β_0. These parameters are based on the known values of the applied magnetic field and the plasma density at the axis. The strong magnetic confinement regime, characterized in a previous work, is found here to be limited to $\ell_{e0}/R \ll 1$ and $\beta_0 < 0.5$. For $\beta_0 > 0.5$, the central region of the column is demagnetized, which allows the development of the electric force and ion acceleration there, and increases the plasma flux to the wall. For $\beta_0 > 3 - 4$ roughly, the plasma is unmagnetized except in a thin layer near the wall, but this has no effect in confinement. Interestingly, the electron skin-depth is the *magnetic screening length* of this stationary, large-beta, plasma column.

To summarize, a magnetically confined plasma, crucial to have small recombination and energy losses at the vessel walls, requires the electron gyroradius, based on the applied magnetic field, be smaller than three typical lengths: the plasma radius, a (reduced) collisional mean free path for electrons, and the electron skin depth. The two last lengths depend on plasma density and temperature.

Acknowledgments

This work has been sponsored by the Air Force Office of Scientific Research, Air Force Material Command, USAF, under grant number FA8655-10-1 -3085. The U.S Government is authorized to reproduce and distribute reprints for Governmental purpose notwithstanding any copyright notation thereon. Additional support came from the Gobierno de España (Project AYA2010-16699). The author thanks Dr. Mitat Birkan for his support.

References

[1] L. Tonks, Physical Review **56**, 360 (1939).

[2] J. Forrest and R. Franklin, Brit. J. Appll. Phys. **17**, 1061 (1966).

[3] H. Ewald, F. Crawford, and S. Self, Journal of Applied Physics **38**, 2753 (1967).

[4] N. Sternberg, V. Godyak, and D. Hoffman, Physics of Plasmas **13**, 063511 (2006).

[5] E. Ahedo, Physics of Plasmas **16**, 113503 (2009).

[6] J. Freidberg, *Plasma Physics and Fusion Energy* , Cambridge University Press, Cambridge, 2007.

[7] T. Zimmermann, M. Coppins, and J. Allen, Physics of Plasmas **17**, 022301 (2010).

[8] R. Winglee, T. Ziemba, L. Giersch, J. Prager, J. Carscadden, and B. R. Roberson, Physics of Plasmas **14**, 063501 (2007).

[9] O. Batishchev, IEEE Transaction on Plasma Science **37**, 1563 (2009).

[10] D. Pavarin, F. Ferri, M. Manente, D. Curreli, Y. Guclu, D. Melazzi, D. Rondini, S. Suman, J. Carlsson, C. Bramanti, E. Ahedo, V. Lancellotti, K. Katsonis, and G. Markelov, Design of 50W Helicon Plasma Thruster, in *31th International Electric Propulsion Conference, Ann Arbor, Michigan, USA*, IEPC 2009-205, Electric Rocket Propulsion Society, Fairview Park, OH, 2009.

[11] E. Ahedo, Cylindrical model of a helicon-generated plasma, in *31th International Electric Propulsion Conference, Ann Arbor, Michigan, USA*, IEPC 2009-193, Electric Rocket Propulsion Society, Fairview Park, OH, 2009.

[12] E. Ahedo and M. Merino, Physics of Plasmas **17**, 073501 (2010).

[13] L. Spitzer, *Physics of fully ionized gases* , Wiley, New York, 1962.

[14] M. Lieberman and A. Lichtenberg, *Principles of plasma discharges and materials processing*, Wiley-Blackwell, 2005.

[15] J. Adlam and J. Allen, Philosophical Magazine **3**, 448 (1958).

[16] L. Tonks and I. Langmuir, Physical Review **34**, 876 (1929).

[17] S. Tysk, C. Denning, J. Scharer, and K. Akhtar, Physics of Plasmas **11**, 878 (2004).

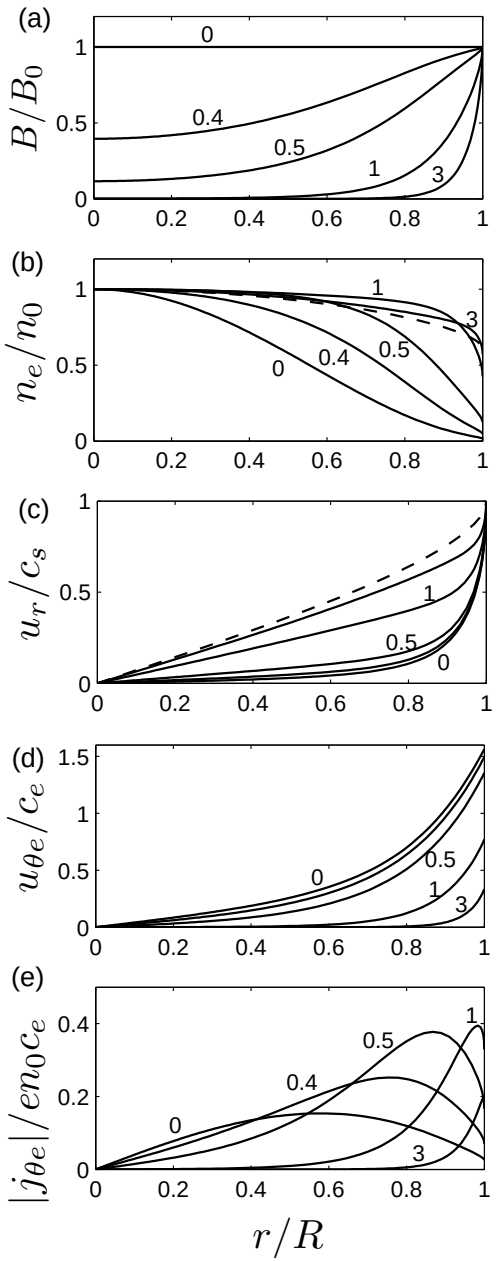

Figure 1: Plasma profiles for $\ell_{e0}/R = 0.1$, and $\beta_0 = 0$, 0.4, 0.5, 1, and 3 (solid lines), corresponding to $d_{e0}/R \simeq \infty$, 0.16, 0.14, 0.10 and 0.058. Dashed lines correspond to the unmagnetized case $\ell_{e0}/R = \infty$. Other parameters for all curves are $\bar{\lambda}_e/R = 1$ and $R\nu_i/c_s \to 0$.

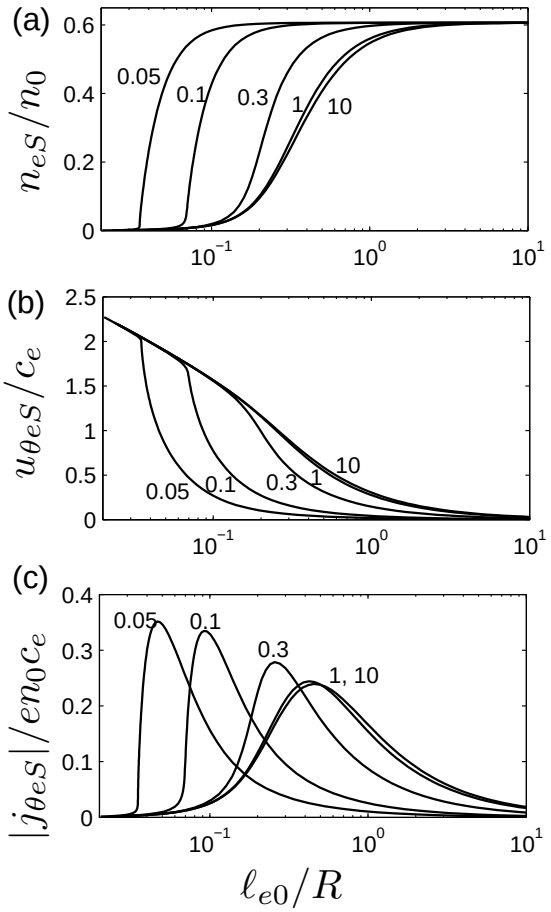

Figure 2: Plasma response versus ℓ_{e0}/R for d_{e0}/R =10, 1, 0.3, 0.1, 0.05; other parameters are $\bar{\lambda}_e/R = 1$ and $R\nu_i/c_s \to 0$. (a) Normalized plasma density at the sheath edge, which coincides with the normalized plasma flux to the wall. (b)-(c) Normalized azimuthal velocity and current of electrons at the edge of and within the Debye sheath.

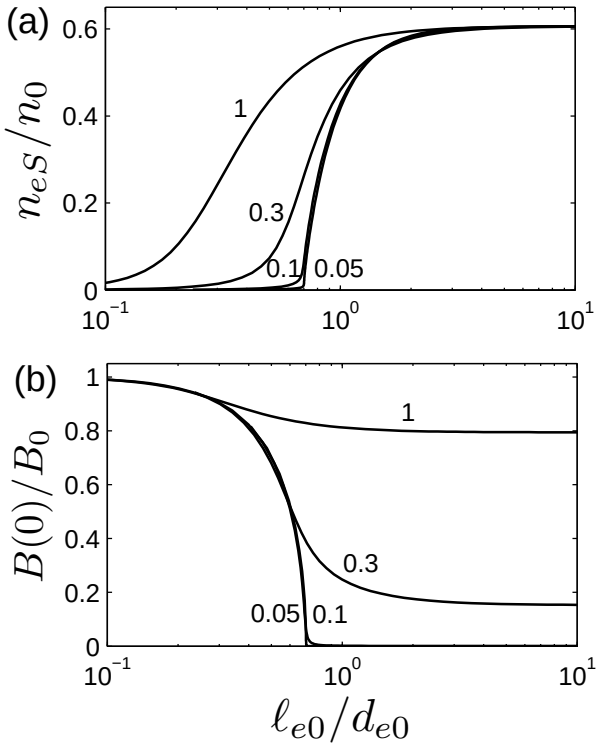

Figure 3: Plasma response versus $\ell_{e0}/d_{e0} \equiv \beta_0^{1/2}$ for $d_{e0}/R = 1, 0.3, 0.1, 0.05$; other parameters are $\bar{\lambda}_e/R = 1$ and $R\nu_i/c_s \to 0$. (a) Normalized plasma density at the sheath edge, which coincides with the normalized plasma flux to the wall. (b) Total magnetic field at the plasma axis relative to the applied magnetic field.

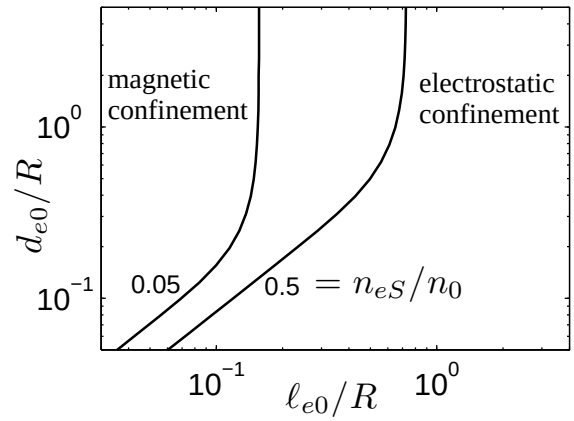

Figure 4: Curves of constant plasma flux to the wall: $n_{eS}/n_0 = 0.5$ and 0.05, in the parametric plane $(\ell_{e0}/R, d_{e0}/R)$. Other parameters are $\bar{\lambda}_e/R = 1$ and $R\nu_i/c_s \to 0$.

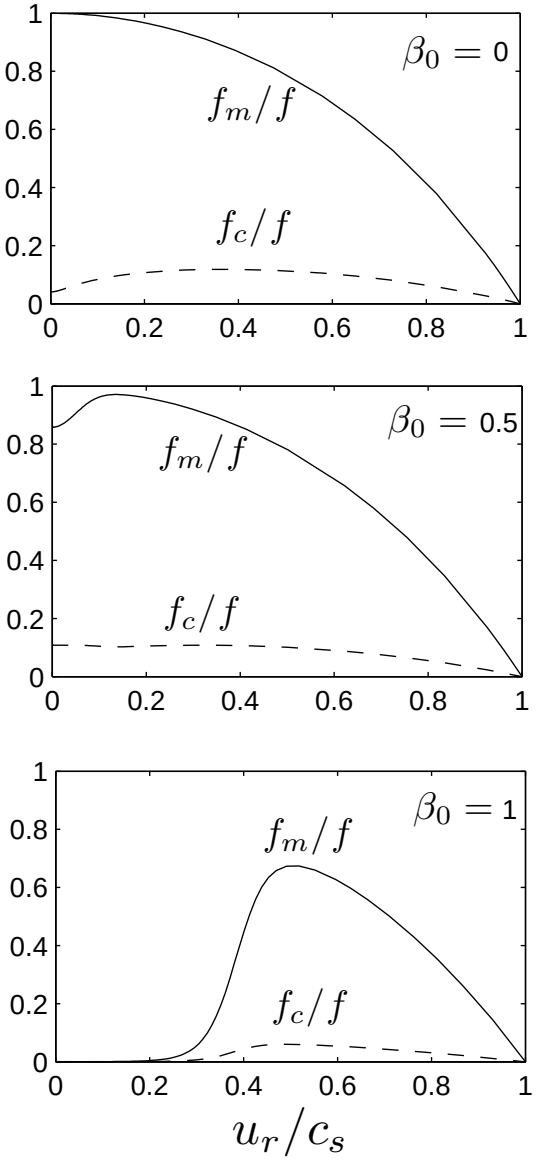

Figure 5: Relative strength of each force contribution to the electron force balance, Eq. (20), for three values of β_0. Other parameters are $\ell_{e0}/R = 0.10$, $\bar{\lambda}_e/R = 1$, $R\nu_i/c_s \to 0$. Notice that $f_p/f = 1 - f_c/f$, $f_e/f = 1 - f_m/f$, and u_r is used as abscissa instead of r.